On the benefit of the adjoint technique for inversion of the atmospheric transport employing carbon dioxide as an example of a passive tracer

Dissertation
zur Erlangung des Doktorgrades
der Naturwissenschaften im Fachbereich
Geowissenschaften
der
Universität Hamburg

vorgelegt
von
Thomas Kaminski
aus Berlin

Hamburg
1998

Contents

List of Tables

List of Figures

1 Introduction

The radiative balance of our atmosphere is sensitive to the concentrations of a number of trace gases. Enhanced concentrations of these greenhouse gases may thus lead to climate change. This sensitivity of climate to perturbations in the concentrations of greenhouse gases is being estimated by means of complex General Circulation Models [*Watson et al.*, 1995]. For predictions of climate change and its impacts, these models use the greenhouse gase's concentrations as boundary condition. To control the temporal development of these concentrations, in turn, the sources and sinks of the respective gases have to be predicted over the time period of interest. Hence, reliable models of the underlying source and sink processes are urgently needed to determine the feedbacks of future climate changes on the concentration of the gases. Improving our knowledge about the past and current source and sink magnitudes would help to improve and verify these process models.

At present, however, for many greenhouse gases such as carbon dioxide (CO_2), carbon monoxide (CO), methane (CH_4), or nitrous oxide (N_2O) not even the current magnitudes of the natural as well as the anthropogenic sources and sinks can be quantified with sufficient accuracy [*Houghton et al.*, 1995b]. Especially for CO_2 and CH_4 there have been considerable efforts to measure directly the exchange fluxes between the atmosphere and different source reservoirs (over oceans e.g by global ship campaigns or over land by means of eddy correlation methods). Although this "Bottom Up" approach locally yields important information on the relevant processes, large uncertainties are induced by the necessary assumptions for extrapolation to regional or global scales.

During the last decades, an observational network of increasing density is being established to monitor the relevant trace gases. Space borne observations are also becoming available, as well as measurements on board of ships and planes. In contrast to local flux measurements, if carefully selected, the atmospheric data are representative for the concentrations on larger spatial scales. Hence, these observations provide a means of estimating the sources and sinks on larger scales. Thereby the fluxes can be linked to atmospheric observations by a more or less sophisticated model of the atmospheric transport, if necessary complemented by a module of the relevant atmospheric chemistry. The systematic search for spatio-temporal flux fields that, in combination with an atmospheric transport model, yield modeled concentrations close to observations is called inverse modeling of the atmospheric transport.

In order to prevent future climate change, for several greenhouse gases, attempts are being made to reduce the anthropogenic emissions: On intergovernmental level, emission targets are being negotiated. In this context, another perspective for inverse modeling is to derive regional estimates of the fluxes to monitor the success of these attempts.

A number of groups have investigated the feasibility of inversion of the atmospheric transport. The challenge consists in employing the information from a spatially sparse observational network in an optimal way to derive regional flux estimates together with an estimated range of confidence. Technically, this constitutes an ill-posed or underdetermined inverse problem: A unique solution can only be derived by use of additional assumptions (regularization of the inverse problem). The validity of these assumptions as well as the reliability of the transport model are crucial for the quality of the resulting estimates. Recently, a number of studies have been carried out to quantify the magnitude of the sources and sinks of CO_2 [*Enting and Mansbridge*, 1989; *Enting et al.*, 1995; *Ciais et al.*, 1995; *Haas-Laursen*, 1997], CH_4 [*Brown*, 1993; *Hein and Heimann*, 1994; *Brown*, 1995;

Hein et al., 1996], and halocarbons [*Brown*, 1993; *Hartley and Prinn*, 1993]. From the conceptional point of view, differences among these studies mainly consist in the resolution of the transport models (two dimensional or three dimensional) and in the kind of assumptions for regularization, which is formally reflected by different inversion techniques.

Most of the relevant long lived trace gases are either not (CO_2) or only weakly (CH_4, N_2O, halocarbons) coupled to tropospheric chemistry and thus, in a good approximation, can be inverted with a linearized representation of the transport. The transport then can be taken into account in the following way: The surface flux field is decomposed into prescribed spatio-temporal patterns ("source" or "flux" components) with unknown scaling coefficients. The transport model is run separately with each of the source components, and the contributions to the concentration signal at each of the monitoring sites and times are recorded. These contributions can be interpreted as a discretized "impulse response" or "Greens function" that quantifies the response of the modeled concentration at the observational sites and time periods to unit changes in the magnitude of each source component.

Formally, this impulse response or Greens function is the Jacobian matrix representing the first derivative of the modeled concentration at the observational sites and dates with respect to the coefficients of the source components. Computationally, for n_f source components, n_f model runs (or a single run with n_f tracers) have to be performed to determine the n_f differential quotients constituting the columns of the Jacobian matrix. The complexity of the transport model thus essentially limits the number of source components that can be considered. The additional assumption that the flux fields can be represented by a few patterns is thus inherent in this approach and, in part, determines the result of the inversion. It is evident, though, that for many trace gases such a restricted representation does not take account of the spatial and temporal variability in an appropriate way. In combination with inhomogeneous sampling, this low resolution in the space of unknowns may lead to biased estimates as recently investigated by *Trampert and Snieder* [1996].

Here we present an alternative approach employing the adjoint of the three-dimensional transport model TM2. By means of the Tangent linear and Adjoint Model Compiler [TAMC *Giering*, 1996] this numerical module has been constructed automatically from the TM2 source code in the "reverse mode" of computational differentiation. The principles of adjoint code generation and the adjoint model are introduced in Sect. (3). By a single run of the adjoint model the exact Jacobian is efficiently computed row by row, for which the cost is proportional to the number of observations and nearly independent of the number of flux components. Hence, defining the flux patterns as the model grid cells, we are able to determine the Jacobian for the horizontal TM2 resolution of approximately 8^o by 10^o and monthly temporal resolution.

The Jacobian is computed for the simulation of the quasi-stationary seasonal cycle of CO_2, which is carried out in a cyclostationary setup of TM2 described in Sect. (2). The rows of the Jacobian quantify the sensitivity of the modeled concentration at a particular station and month to the fluxes into every surface layer grid cell at every month. A visualization results in instructive maps of the potential influence of the flux components for the respective months on a particular observable. Prescribing for each grid cell the relative distribution of the fluxes over the year (e.g. constant flux), the information on potential influence can be condensed to one map for each monthly mean concentration. On the other hand, it is possible to derive the sensitivity of any particular feature that can be computed from the monthly mean concentrations (e.g. the yearly mean concentration, or

the magnitude of the seasonal cycle). For linear combinations of the monthly mean concentrations, in addition to compute potential influence areas, it is possible to decompose the feature as modeled in a particular run according to the contributions resulting from the respective flux components. Besides these sensitivity studies, the Jacobian can be applied for tracer simulations instead of TM2 [*Knorr*, 1997], as long as the setup the matrix has been derived for is appropriate for the problem at hand.

As an example for an inversion on the TM2 grid, in Sect. (5) we combine the Jacobian with atmospheric CO_2 observations of the period from January 1981 to January 1987 from the NOAA/CMDL program [*Globalview–CO2*, 1996]. A Bayesian inversion enables us to include a priori information on the fluxes derived from output of high resolution models of both, the terrestrial biosphere (SDBM, [*Knorr and Heimann*, 1995]) and the ocean [*Six and Maier-Reimer*, 1996] as well as fossil fuel burning statistics [*Andres et al.*, 1997] and estimates of land use change [*Houghton et al.*, 1987]. Technically, our inversion procedure is based on a Singular Value Decomposition (SVD) of the Jacobian. Besides the seasonal cycle and mean annual source and sink distribution of the surface fluxes on the approximately 8^o by 10^o horizontal TM2 grid, for these flux components, the Bayesian inversion allows to derive a posteriori estimates of the uncertainties and their correlations.

To explore the extend to which the observations of a sparse network can improve our knowledge about the processes controlling the surface fluxes, we discuss flux estimates for several oceanic regions. Contrasting conclusions of a study of *Tans et al.* [1990] we infer an oceanic sink of 1.5 ± 0.4 gigatons of carbon (GtC), which is lower than the *Houghton et al.* [1995a] estimate of 2.0 ± 0.5 GtC for the 1980s or the value of 2.3 GtC for 1984 found by *Keeling et al.* [1989b]. We investigate the capacity of the observations to monitor trace gas emissions on a regional scale by estimating the mean biospheric fluxes for a few countries and continents.

In summary, the outline is as follows: In Sect. (2) we give a description of the transport model and the setup for which we derive the matrix representation. The principles of adjoint code generation and the adjoint model are introduced in Sect. (3). Sect. (4) discusses the Jacobian and its use to compute sensitivities of particular features. Sect. (5) presents an inversion of the atmospheric transport of CO_2: We describe the preparation of the atmospheric observations as well as the a priori estimates of the fluxes, followed by a discussion of the resulting fluxes and their uncertainties. Eventually, in Sect. (6) we draw conclusions and discuss some perspectives of the adjoint approach for inversion of the atmospheric transport.

2 Model of the Quasi–Stationary Seasonal Cycle

A statistical analysis of the observed atmospheric CO_2 concentrations as performed e.g. by *Keeling et al.* [1989a] points out that, on time scales of a few years, the concept of a quasi-stationary seasonal cycle is appropriate to describe the prevailing features in the records. This quasi-stationary seasonal cycle component in the concentration, which essentially is composed of a global trend and a spatially varying seasonal cycle, can be extracted from the observations as well as be simulated by atmospheric transport models. Since these transport models use CO_2 surface exchange flux fields as boundary condition, comparison of the observed and the simulated quasi-stationary seasonal cycles provides a way to constrain these fluxes. In this section we briefly introduce our transport model TM2, give a formal definition of the quasi-stationary seasonal cycle, and describe an appropriate setup of TM2 for simulation of the quasi-stationary seasonal cycle. Comparison of simulated concentrations to observations is deferred to Sect. (5).

TM2 is a three-dimensional atmospheric transport model, which solves the continuity equation for an arbitrary number of atmospheric tracers on an Eulerian grid spanning the entire globe [*Heimann*, 1995]. It is driven by stored meteorological fields derived from analyses of a weather forecast model or from output of an atmospheric general circulation model. Tracer advection is calculated using the "slopes scheme" of *Russel and Lerner* [1981]. Vertical transport due to convective clouds is computed using the cloud mass flux scheme of *Tiedtke* [1989]. Turbulent vertical transport is calculated by stability dependent vertical diffusion according to the scheme by *Louis* [1979]. Numerically, in each base time step the model calculates the source and sink processes affecting each tracer, followed by the calculation of the transport processes.

The spatial structure of the model is a regular latitude-longitude grid and a sigma coordinate system in the vertical. The base "coarse grid" version of the model uses a horizontal resolution of approximately 8^o latitude by 10^o longitude (the horizontal dimension of the grid is $n_g = 36 \times 24$) and 9 layers in the vertical dimension. The numerical time step of this model version is four hours.

We apply TM2 to simulate the quasi-stationary seasonal cycle component in the CO_2 concentration at particular observational sites. Therefore, prescribing the same monthly mean surface exchange flux fields f each year (cyclostationarity), and starting from zero initial concentration, TM2 is run by repeatedly cycling through the same meteorological fields of the year 1987 derived from analyses of the European Center for Medium Range Weather Forecast (ECMWF), which are available to the model every 12 hours. Thereby the meteorological fields have been adjusted in order to guarantee air mass conservation. This adjustment is also applied when switching from the fields of December 31 to January 1 [*Heimann*, 1995]. Since we do not resolve any interannual variability, for comparison with observations monthly resolution is appropriate to extract time series of concentrations c_S at particular sites S: First monthly means are computed, and then a bilinear interpolation in the horizontal from the TM2 grid to the exact location of S is performed.

With periodic boundary conditions and periodic transport, at every site, the simulated concentration as well tends towards a periodic state c_p. For a flux field with nonzero global annual mean, however, a linear trend is superimposed on the cyclostationary concentrations. The spatial variation of the magnitude of the annual mean flux as well as the effect of covarying seasonal cycles of fluxes and transport (rectifier effect) described e.g. by *Pearman and Hyson* [1980], *Heimann et al.* [1986], *Heimann and Keeling* [1989], *Denning et al.* [1995] result in a spatially varying offset

in c_p. Formally, at the $i-$th month, the simulated concentration $c_{S,i}$ can be composed as:

$$c_{S,i} \quad = \quad S_{S,i} + b \cdot t_i + a_S + R_{S,i} \qquad , \tag{1}$$

where the single terms have the following meaning: The periodic component has been split up into a function $S_{S,i}$ with yearly period ($S_{S,i+12} = S_{S,i}$) and zero annual mean denoting the seasonal cycle as well as the spatial gradient contribution a_S. The long term global linear trend b is related to the global annual mean flux $\bar{f}$ by

$$b = \alpha \cdot \bar{f} \quad , \tag{2}$$

where $\alpha = 0.476$ ppmv/GtC is the conversion factor from mass to concentration for instantaneous global mixing as used by the transport model. The length of the time interval from the beginning of the simulation to the middle of the $i-$th month t_i is given by

$$t_i := \frac{(i - {}^1\!/_2)}{12} \text{ years} \quad . \tag{3}$$

The residuum $R_{S,i}$ tends to zero as the length of the time series increases.

We define the quasi-stationary seasonal cycle as

$$c_{S,i} - R_{S,i} = S_{S,i} + b \cdot t_i + a_S = c_{p,S,i} + b \cdot t_i \qquad . \tag{4}$$

To represent the quasi-stationary seasonal cycle, in addition to the global linear trend, 12 numbers per site are needed to quantify c_p: 11 numbers for S_S and 1 number for a_S. As soon as $R_{S,i}$ is close enough to zero to be neglected, the quasi-stationary seasonal cycle can be extracted from our modeled time series. *Heimann and Keeling* [1989] found that for tropospheric sites a spin up period of 3 years is sufficient to achieve an appropriate degree of convergence in Eq. (4). The rate of convergence reflects the model's time scales of mixing. These time scales are commonly quantified in terms of exchange times [*Rayner and Law*, 1995], a concept applied in the context of box diffusion models. More precisely, the rate of convergence is determined by the longest exchange time, which, in the troposphere, is associated to the interhemispheric transport. Employing the radioactive tracer ^{85}Kr, *Jacob et al.* [1987] found an interhemispheric exchange time of 1.1 years for a similar transport model, and *Heimann and Keeling* [1989] found 1.3 years for TM2. Similar to *Heimann and Keeling* [1989] as "standard setup" of TM2, we choose to perform a four year run, of which we extract the monthly mean concentrations in the last year. Together with the global annual mean flux, these 12 values per site determine the trend and the periodic component representing the quasi-stationary seasonal cycle :

$$\begin{aligned} b \quad &= \quad \alpha \cdot \bar{f} \\ c_{p,S,i} \quad &= \quad c_{S,i+3\cdot 12} - t_{i+3\cdot 12} \cdot \alpha \cdot \bar{f} \qquad (i = 1, 12). \end{aligned} \tag{5}$$

In the terminology of linear algebra, the standard setup includes the choice of a basis (and its order) for the space of fluxes, i.e. a set of $n_f = 12 \times n_g$ vectors spanning the space, and $f \in I\!R^{n_f}$ is a representation of a particular flux vector by its components with respect to that basis. The components of f quantify the 12 monthly mean fluxes into each surface grid cell. In particular, the basis defines the physical units of the fluxes. Similarly, with respect to a basis in the space of concentrations, the output $c \in I\!R^{n_c}$ is a vector of $n_c = 12 \times n_s$ components for the modeled monthly mean concentration at n_s observational sites. Since, in addition, every step in the simulation is

linear, in the standard setup TM2 can be represented by a real $n_c \times n_f$ matrix T, and the application of the model to a flux field f can be written as

$$c = Tf \quad . \tag{6}$$

Using this matrix notation, the model of the quasi-stationary seasonal cycle in Eq. (5) reads

$$b = \alpha \cdot \bar{f} \tag{7}$$

$$c_p = Tf - t \cdot \alpha \cdot \bar{f} \quad , \tag{8}$$

where the vector t contains the values of t_i.

Concatenating b and c_p to one vector c_{qsc}, these equations define a single matrix M:

$$c_{qsc} =: Mf \quad . \tag{9}$$

Since our model neglects interannual variations in the transport as well as in the fluxes, a careful interpretation of c_{qsc} is necessary: If it was interpreted as the quasi-stationary seasonal cycle of 1987, the year of the meteorological data, c_{qsc} would be subject to both sources of error: For the spin up years the difference in the meteorologies to 1987 as well as the differences in the fluxes to 1987 would be neglected. Instead, as in the study of *Hein et al.* [1996], c_{qsc} should be interpreted as a mean quasi-stationary seasonal cycle over a target period of a few years: Prescribing the mean flux over the whole target period, the error caused by the cyclostationary flux assumption decreases with increasing length of the target period. The error induced by using the meteorology of a particular year to simulate the whole target period still remains. One might argue that a climatology, i.e. the meteorology of a mean year, should be employed instead. In order not to underestimate the transport, however, TM2 needs the synoptic scale variation, which is partly removed by the averaging procedure yielding the climatology. Hence, instead of using a mean meteorology, c_{qsc} is interpreted as one particular element of the ensemble of modeled concentrations that would result from using the same mean fluxes but the meteorologies from the particular years of the target period. This model error has to be taken into account, when comparing c_{qsc} to the mean quasi-stationary seasonal cycle extracted from observations. Recent studies indicate that this error is not too large: *Knorr and Heimann* [1995] investigated the impact of the meteorological data by comparing the seasonal cycle of the monthly mean concentration simulated with TM2 in the standard setup driven by the meteorology either of 1986 or 1987. In their study they obtain only a minor difference. With a different model *Law and Simmonds* [1996] explored the sensitivity of fluxes resulting from an inversion to the year of the meteorological fields. They also found small differences. In Sect. (5.8) these results are confirmed by a comparison of the flux fields inferred from two inversions that we perform on the basis of meteorological data from 1986 and 1987.

3 The Adjoint Model

As explained in Sect. (2), for the standard setup, TM2 can be represented by a $n_c \times n_f$ matrix T. For given surface fluxes f, by a model run, we are able to compute the resulting concentrations at the station locations $c_{mod} = Tf$. The matrix T itself is yet to be determined.

Following e.g. *Enting et al.* [1995], by applying TM2 subsequently to the n_f standard basis vectors $e_1 = (1, 0, ..., 0), ..., e_{n_f} = (0, ..., 0, 1)$ spanning $\mathbb{R}^{n_f}$, the matrix T could be computed column by column. This can be looked upon as a special case of approximating the Jacobian matrix that represents the first derivative of a function by differential quotients: Due to linearity of the model (i) differential quotients are not merely an approximation of the Jacobian, and (ii) the Jacobian of T is equal to T. A disadvantage of this approach is that it requires n_f runs of TM2 and thus is only feasible for a small number of flux components. In this section we introduce an alternative and for our matrix much more efficient approach: By the model adjoint to TM2 in the standard setup the Jacobian matrix is computed row by row in reverse mode. Here the computational cost depends on the number of rows, i.e. on n_c, rather than on the number of columns, i.e. on n_f. This kind of an adjoint model is uncommon in geosciences: Usually, rather than vector valued functions, scalar valued functions are being differentiated.

As will be sketched in Sect. (3.1), for the implementation of an adjoint model there are alternative strategies. The adjoint of TM2 has been derived directly from the model code, following the concept of differentiation of algorithms. Thereby the Tangent linear and Adjoint Model Compiler [TAMC *Giering*, 1996] has been applied to generate automatically the adjoint code. Briefly summarizing earlier work [*Giering and Kaminski*, in press], Sect. (3.2) introduces the concept of differentiation of algorithms. Finally, Sect. (3.3) describes how TM2's adjoint has been generated.

3.1 Adjoint Code Construction

In the following we briefly sketch 3 approaches to adjoint code construction whose essential difference is the level on which the adjoint operators are constructed. Traditionally, as demonstrated e.g. by *Marchuk* [1995] for various dynamical systems, adjoint models have been derived from the description of the system by a state function of space and time, being the solution of what Marchuk refers to as the main problem. Typically, the main problem consists of a set of differential equations together with initial and boundary conditions that, in the terminology of functional analysis, define a differential operator T in an appropriate space of functions H. Spaces of this type are examples of Hilbert spaces, vector spaces furnished with an inner product $\langle \cdot, \cdot \rangle$. For the atmospheric transport of a passive tracer, the main problem consists of the continuity equation, together with a prescribed initial concentration field and a prescribed source sink distribution. Each observable quantity is represented by a linear functional on the Hilbert space. The control variables, i.e. functions that characterize the system such as initial or boundary conditions or parameters in the formulation of T, are also elements of appropriate Hilbert spaces. The sensitivity of a quantity to a change in the control variables is then the Hilbert space or continuous analogue of the familiar first derivative in finite dimensional spaces, which will be discussed in Sect. (3.2). Applying first order perturbation theory to the particular problem at hand, a Hilbert space analogue of the chain rule is derived: The sensitivity of the functional's value to a change in the control variables can be composed of

the sensitivity of the functional's value to a change in the state function and the sensitivity of the state function to a change in the control variables. Thereby it can be shown, that the sensitivity of the state function with respect to a change in the control variables can be obtained as the solution of the adjoint problem, being defined by the adjoint T^* of the differential operator T. The adjoint operator can be defined by

$$\langle T\phi\,,\,\psi\rangle = \langle\,\phi\,,\,T^*\psi\,\rangle \tag{10}$$

for each $\psi \in D(T^*) \subset H$ and $\phi \in D(T) \subset H$, whenever the domain $D(T)$ of T is 'large enough'.

In most practical applications the main problem is so complex that it has to be tackled numerically: First a discretization scheme for the main equations is chosen, and then a numerical model for integration of the discrete equations is coded. Since, in general, the adjoint problem is as complex as the main problem, it is solved numerically as well. The resulting implementation is called adjoint model. The solution of the adjoint problem is then used to evaluate the discretized expression of the sensitivity. Besides the cumbersome analysis that for a particular problem is necessary to rigorously define T and T^* and to derive an expression for the sensitivity, this approach has a distinct disadvantage: There is no unique choice of a discretization scheme for the adjoint problem, and a priori it is not clear which choice will result in a discrete version that is adjoint to the discretization of the main problem. In particular, the appropriate discretization scheme for the adjoint problem can be different from that for the main problem, i.e., as operators, building the adjoint and discretization do not interchange [*Griewank*, 1989]. Due to inappropriate discretization, thus, the sensitivity computed by the adjoint model differs from the sensitivity of the numerical model of the main problem. As is examined by e.g. *Shah* [1991] and remarked by *Talagrand and Courtier* [1987], therefore it is favorable to develop the adjoint model from the discretization of the main problem: The adjoint operator is derived for the discretized form of T, operating in a finite dimensional space. Implicitly, this adjoint operator also defines the discretization scheme for the adjoint problem. As in the traditional approach, eventually an adjoint model solving the discrete adjoint problem has to be implemented, and the solution is used to evaluate the discretized expression of the sensitivity. This approach has been applied to weather forecast models e.g. by *Talagrand and Courtier* [1987], *Courtier and Talagrand* [1987] or to ocean circulation models e.g. by *Thacker and Long* [1988].

A more direct approach for adjoint code generation uses the code of the main model as starting point: The composition of the main model with some functionals characterizing the quantities of interest is considered as an algorithm mapping a finite representation of the control variables onto the values of the functionals. As described below, by applying systematically the chain rule of differentiation to every single step in the model code in reverse mode, a model for the sensitivity is constructed. In the terminology introduced above, this model is the composition of the adjoint model with the implementation of the functional's first derivative. Using the model code as starting point for adjoint code construction, however, this distinction is no longer important, so that we slightly change our terminology and refer to this composition as adjoint model in the following. In Sect. (3.2) we demonstrate that, essentially, the adjoint model performs subsequent multiplications in reverse order of the adjoints of the Jacobians corresponding to the single steps in the model code. The main advantage of this approach is that, on the level of the single steps in the model code, the adjoints can be constructed according to simple rules [*Giering and Kaminski*, in press]. Thus this task can be handled automatically [*Giering*, 1996; *Juedes*, 1991] without any knowledge of the

nature of the main problem and the system that is integrated by the model. For applications to geosciences see e.g. *Talagrand* [1991] and *Thacker* [1991]. The concept of applying systematically the chain rule to differentiate a numerical code is known as 'differentiation of algorithms', 'computational differentiation', or 'automatic differentiation', and adjoint code construction is merely one of its applications. For an overview see e.g. *Iri* [1991] or *Corliss and Rall* [1996].

3.2 Differentiation of Algorithms

In the following we describe how a function that is composed of elementary functions can be differentiated by use of the chain rule. When talking about elementary functions the reader should have in mind the single statements of the TM2 code, although the same mathematical formalism can be applied, if the elementary functions are considered to be related e.g. to basic physical processes such as advection or diffusion. For automatic generation of derivative computing code, however, it is crucial that the Jacobians of the single steps can be constructed according to simple rules. Let

$$\begin{array}{rccc} \mathcal{H} : & I\!R^n & \rightarrow & I\!R^m \\ & X & \mapsto & Y \end{array}$$

be a function that is composed

$$\mathcal{H} \;=\; \mathcal{H}^K \circ \ldots \circ \mathcal{H}^1 \;=:\; \bigodot_{l=1}^{K} \mathcal{H}^l \tag{11}$$

of K differentiable elementary functions:

$$\begin{array}{rccc} \mathcal{H}^l : & I\!R^{n_{l-1}} & \rightarrow & I\!R^{n_l} \qquad (l = 1, ..., K) \\ & Z^{l-1} & \mapsto & Z^l \;. \end{array}$$

Even if $\mathcal{H}$ is not given symbolically, i.e. by a formula, but by a numerical algorithm such as TM2, the Jacobian matrix representing the first derivative of $\mathcal{H}$

$$\frac{\partial \mathcal{H}(X)}{\partial X} := \begin{pmatrix} \frac{\partial \mathcal{H}_1(X)}{\partial X_1} & \cdots & \frac{\partial \mathcal{H}_1(X)}{\partial X_n} \\ \vdots & & \vdots \\ \frac{\partial \mathcal{H}_m(X)}{\partial X_1} & \cdots & \frac{\partial \mathcal{H}_m(X)}{\partial X_n} \end{pmatrix}$$

can be computed using the chain rule of differentiation from the Jacobians of the elementary functions

$$\left.\frac{\partial \mathcal{H}(X)}{\partial X}\right|_{X=X_0} = \left.\frac{\partial \mathcal{H}^K}{\partial Z^{K-1}}\right|_{Z^{K-1}=Z_0^{K-1}} \cdot \ldots \cdot \left.\frac{\partial \mathcal{H}^1}{\partial Z^0}\right|_{Z^0=X_0} \;. \tag{12}$$

Thereby

$$Z_0^l \;:=\; \mathcal{H}^l \circ \ldots \circ \mathcal{H}^1(X_0) \qquad (1 \leq l \leq K)$$

denote the intermediate results, through which the derivatives of the elementary functions depend on X_0.

For evaluating the multiple matrix product in Eq. (12) there are many possibilities. Depending on the size of the elementary matrices they differ in the number of operations that have to be

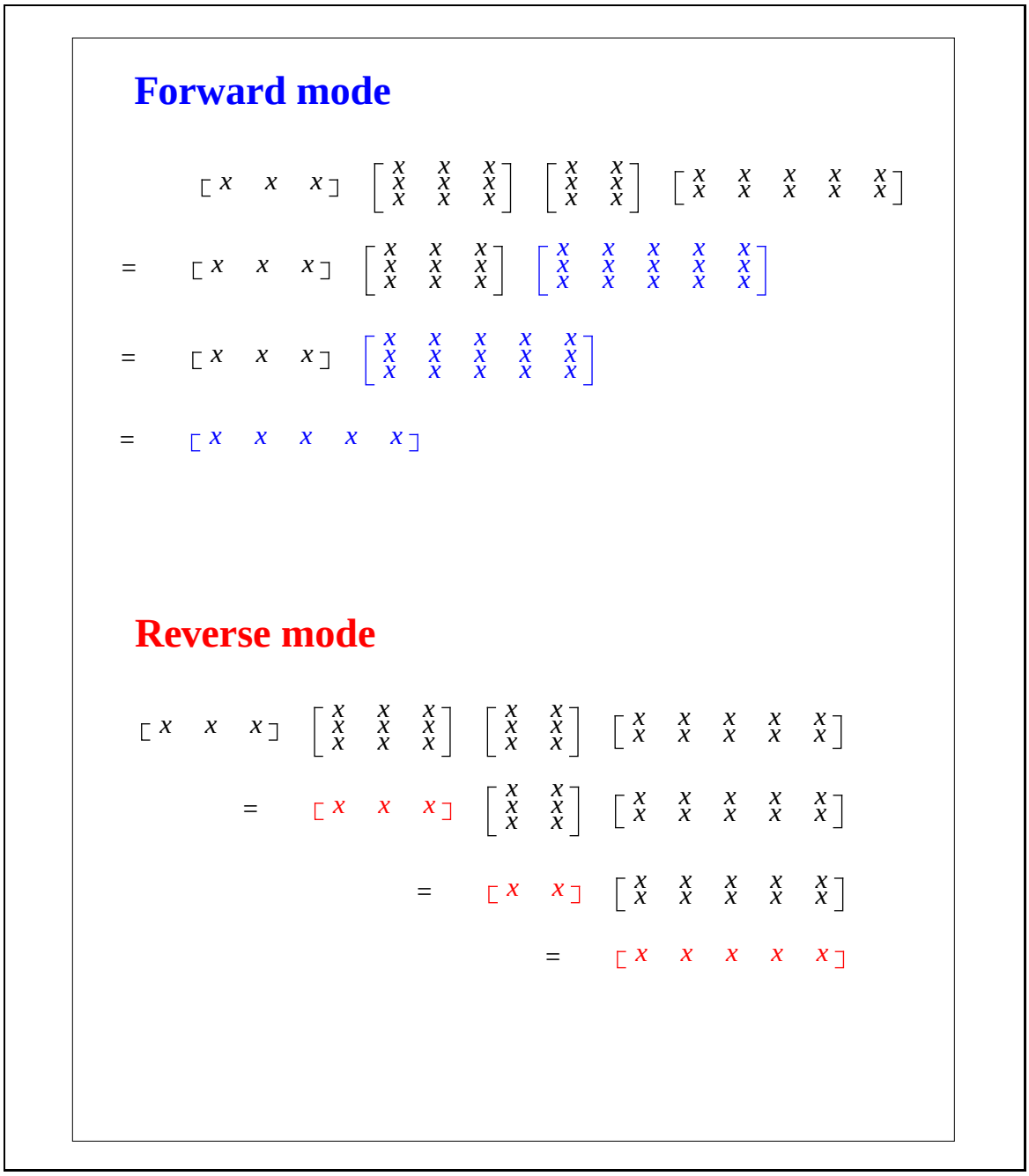

Figure 1: *Example of forward and reverse mode illustrating the differences in the storage requirements and in the number of operations: The same matrix product, whose result has 1 row and 5 columns, is evaluated in forward mode, i.e. from right to left (top), and in reverse mode, i.e. from left to right (bottom). In forward mode the matrices holding the intermediate results have 5 columns, while in reverse mode they have 1 row.*

performed and in the size of the matrices containing the intermediate derivatives as illustrated by Fig. (1). For an algorithm tackling the evaluation of this multiple matrix product, the most obvious strategies are the forward and the reverse mode, where forward and reverse refer to the

order of operations imposed by the composition (11): Operating in forward mode, the product is evaluated from the right to the left, which means that the product is computed in the same order as for evaluation of $\mathcal{H}$ in Eq. (11). Alternatively, the product can be evaluated from the left to the right, which is denoted as reverse mode, because the order is opposite to the order for evaluation of $\mathcal{H}$ in Eq. (11). Thereby the intermediate matrices at the l-th step of this procedure contain $\frac{\partial(\mathcal{H}^l \circ \ldots \circ \mathcal{H}^1)(X)}{\partial X}\Big|_{X=X_0}$ in forward mode and $\frac{\partial(\mathcal{H}^K \circ \ldots \circ \mathcal{H}^{l+1})(Z^l)}{\partial Z^l}\Big|_{Z^l=Z_0^l}$ in reverse mode. Thus forward and reverse refer to the directions in which the intermediate derivatives are propagated by the respective algorithm for evaluation of Eq. (12). According to Eq. (12) the forward mode step corresponding to the l-th step of the composition (11) is:

$$\frac{\partial(\mathcal{H}^l \circ \ldots \circ \mathcal{H}^1)(X)}{\partial X}\Big|_{X=X_0} = \frac{\partial \mathcal{H}^l}{\partial Z^{l-1}}\Big|_{Z^{l-1}=Z_0^{l-1}} \cdot \frac{\partial(\mathcal{H}^{l-1} \circ \ldots \circ \mathcal{H}^1)(X)}{\partial X}\Big|_{X=X_0} \quad . \tag{13}$$

With respect to the standard inner product the adjoint matrix of $\frac{\partial \mathcal{H}(X)}{\partial X}$ is simply the transposed matrix. Thus Eq. (12) can be written in the form

$$\frac{\partial \mathcal{H}(X)}{\partial X}\Big|_{X=X_0}^{*} = \frac{\partial \mathcal{H}^1}{\partial Z^0}\Big|_{Z^0=X_0}^{*} \cdot \ldots \cdot \frac{\partial \mathcal{H}^K}{\partial Z^{K-1}}\Big|_{Z^{K-1}=Z_0^{K-1}}^{*} \quad . \tag{14}$$

This means, the reverse mode step corresponding to the l-th step of the composition (11) is performed by multiplying the intermediate matrix $\frac{\partial(\mathcal{H}^K \circ \ldots \circ \mathcal{H}^{l+1})(Z^l)}{\partial Z^l}\Big|_{Z^l=Z_0^l}$ by the adjoint of $\frac{\partial \mathcal{H}^l}{\partial Z^{l-1}}\Big|_{Z^{l-1}=Z_0^{l-1}}$:

$$\frac{\partial(\mathcal{H}^K \circ \ldots \circ \mathcal{H}^l)(Z^{l-1})}{\partial Z^{l-1}}\Big|_{Z^{l-1}=Z_0^{l-1}}^{*} = \frac{\partial \mathcal{H}^l}{\partial Z^{l-1}}\Big|_{Z^{l-1}=Z_0^{l-1}}^{*} \cdot \frac{\partial(\mathcal{H}^K \circ \ldots \circ \mathcal{H}^{l+1})(Z^l)}{\partial Z^l}\Big|_{Z^l=Z_0^l}^{*} \quad . \tag{15}$$

Therefore the reverse mode is also called adjoint mode.

As illustrated by Fig. (1), in the forward mode all matrices containing intermediate derivatives have n columns, whereas in the reverse mode they have m rows. Therefore in forward mode the number of operations as well as the storage requirements are proportional to n, whereas in reverse mode both is proportional to m.

In general, the intermediate results Z_0^l of the preceding step are required for the evaluation of the derivatives of the elementary functions (see Eq. 12). While in the forward mode the intermediate results are required in the same order as computed, in the reverse mode they are required in reverse order. Thus providing of the intermediate results is more complicated in reverse mode and in general causes extra operations or extra storage requirements [*Giering and Kaminski*, in press], which has to be taken into account when comparing the efficiency of reverse and forward mode for a particular function $\mathcal{H}$ (see Sect. (3.3)).

The Tangent linear and Adjoint Model Compiler [TAMC *Giering*, 1996] is a tool that automatically generates code for evaluation of first derivatives. The TAMC is a precompiler that accepts essentially FORTRAN 77 code for the evaluation of a function and generates code for evaluation of its Jacobian. As requested by the user, the generated code operates either in forward or reverse mode. The schemes for forward or reverse mode are practically implementations of the general rules (13) and (15) respectively. Of course, this implementation is not unique: The scheme chosen for the TAMC is based on a few principles [*Giering and Kaminski*, in press], which essentially have been suggested by *Talagrand* [1991]. Rigorous application of these principles yields rules for differentiating the single statements a code is composed of. These simple rules can be applied automatically by precompilers like TAMC or Odyssée [*Rostaing et al.*, 1993].

Table 1: *Comparison of efficiency in the computation of the Jacobian between adjoint model and differential quotients for a Cray C90; columns: no. and description of run, CPU time in seconds and multiples of the CPU time for a simple forward run, Memory requirements in MW and in multiples of the memory required by a simple forward run.*

Run		CPU time in			Memory in	
		s	h/d	Relative	MW	Relative
1	Adjoint, n_c =1	660		3.5	1.092	1.2
2	Adjoint, n_c =24 (2 Stations)	3045		16.4	3.999	4.3
3	Adjoint, n_c =108 (9 Stations)	5560		30	15.797	16.9
4	Adjoint, n_c =216 (18 Stations)	10260		55	30.962	33.2
	Sum of 3 and 4	15820	4.4 h	85		
5	Forward 1 Tracer	186		1	0.933	1
6	Forward 2 Tracers	320		1.72	0.974	1.04
	10368 Tracers (from 5 and 6)	1389364	16 d	7460	429.090	460
	10368 $\times$ 1 Tracer	1928448	22 d	10368	0.933	1

3.3 Generation of the Adjoint Model

By the TAMC the model adjoint to TM2 in the standard setup has been generated automatically. To ensure an accurate interpretation by the TAMC the structure of the model code had to be slightly rearranged.

As is obvious from Eq. (15), the intermediate results Z_0^l (required variables) have to be provided for the adjoint run. Unlike many other adjoint applications in meteorology and oceanography, in transport models many of the required variables quantify the dynamic state of the atmosphere. These required variables do not depend on the control variables, i.e. the sources and sinks. In the terminology of adjoint code construction they are called passive variables. Hence, in principle, they could be computed and stored once and then be read during each adjoint run. Since this would require disk space of about 1.3 gigawords (GW), (at least on a Cray C90) it is more efficient to recompute the required values during every adjoint run. In order to reduce these storage requirements during the adjoint run it is favorable to include a so-called checkpointing scheme [*Griewank*, 1991] in the adjoint model: In a first integration of TM2 the state of the model is saved at checkpoints in weekly intervals on disk. During the adjoint run the checkpoints are used as starting points for recomputation and storing of required values for the whole week in a second file. Finally, for the adjoint computations these stored values are read. The storage requirements are reduced considerably at the cost of an additional model integration. This checkpointing scheme also is implemented automatically by the TAMC.

In Table (1) the adjoint model's CPU and memory requirements are compared to computation of the Jacobian by differential quotients. The numbers refer to a Cray C90 supercomputer. For the standard setup with $n_c = 1$, the adjoint model needs the CPU time of about 3.5 TM2 runs and about the same amount of memory as TM2. The Jacobian for 27 stations, including the stations in Fig. (2), has been computed in two separate runs in order not to allocate more memory than 32 Megawords (MW). In total, the CPU time of about 85 TM2 runs has been used. While the memory requirements are proportional to the number of output values n_c, the CPU time per value

decreases with increasing n_c for two reasons: First, for our function T, the cost of providing the required variables is independent of n_c. Thus, for higher n_c there is no additional cost. Second, by the TAMC the adjoint code is arranged to achieve a vector lengths of n_c; for vectorized loops of the transport model, advanced compilers are even capable to enlarge vector dimensions by a factor of n_c. On a vector machine like the C90, this yields a considerable speedup, because the computations for the individual vector components are independent of each other. For the same reason, a similar speedup could be achieved on a parallel machine. In contrast, from the difference of runs with one and two tracers, one can estimate a CPU time of 7460 TM2 runs for the computation of the full Jacobian by an n_f tracer run. By rearranging the TM2 code, so that the tracer dimension n_f is used for vectorization instead of the dimension of the zonal grid (36), a speedup could be achieved, too. Yet this speedup is limited by the maximum vector length, which is 128 on the C90. In addition, this multitracer run would need more memory than is available on most machines (429 MW), so that it had to be split up to a couple of runs with less tracers. For a linear function like T, the Jacobian that is computed by differential quotients is free from truncation error. In that respect, the forward mode is not superior to differential quotients. Nor is the forward mode superior in terms of computational efficiency: For small n_f the forward mode would be slightly slower, and for large n_f the efficiency would be comparable to differential quotients. Hence, there is no need to include explicit numbers for the forward mode in this comparison.

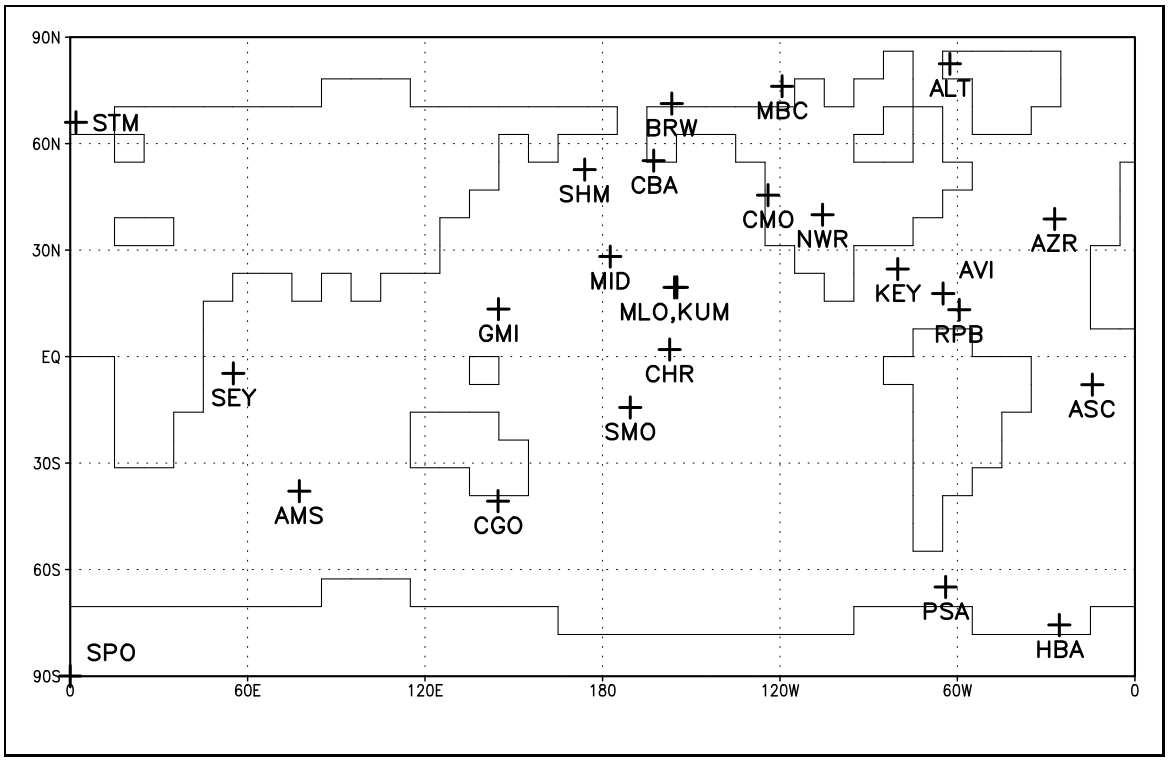

Figure 2: *25 NOAA/CMDL monitoring stations whose observational data we use in our inversion example.*

4 The Matrix Representation

In Sect. (2) we have defined a standard setup of our transport model to simulate the quasi-stationary seasonal cycle at particular observational sites. Sect. (3) then has introduced the adjoint of the transport model and has discussed the computational benefit of applying the adjoint to derive a representation of the model by its Jacobian matrix T, which in Sect. (5) is employed for an inversion of the atmospheric transport of CO_2. Besides its use for inversions, the Jacobian by itself is an interesting object to study, because it entirely quantifies how the transport mediates between a given flux field and the quasi-stationary seasonal cycle at the observational sites. In this section, we first visualize and discuss parts of the full Jacobian and then give examples of collapsing the matrix to compress or summarize its information.

In the following we discuss the Jacobian matrix T derived for $n_s = 25$ locations of stations from the NOAA/CMDL global observational network (see Fig. (2) and Table (2)), whose data we use for our inversion example of Sect. (5). A row of T consists of the sensitivity of the modeled concentration at a particular station and month to the fluxes into each of the $n_g = 36 \times 24$ TM2 surface layer grid cells at each month. The columns of T quantify the impact of a particular flux component on the modeled concentration at each station and month. Thereby the sensitivity or the impact are defined as the change in the concentration resulting from a change in the flux, which formally is represented by the derivative of the concentration with respect to the flux and has the unit of a concentration divided by a flux.

Table 2: *25 NOAA/CMDL monitoring stations whose observational data we use in our inversion example.*

Identifier	Description	Country	Latitude	Longitude	Elevation
ALT	Alert, N.W.T.	Canada	82 27'N	62 31'W	210
MBC	Mould Bay, N.W.T.	Canada	76 14'N	119 20'W	15
BRW	Point Barrow, Alaska	U.S.	71 19'N	156 36'W	11
STM	Ocean Station "M"	Norway	66 00'N	2 00'E	6
CBA	Cold Bay, Alaska	U.S.	55 12'N	162 43'W	25
SHM	Shemya Island	U.S.	52 43'N	174 06'E	40
CMO	Cape Meares, Oregon	U.S.	45 29'N	124 00'W	30
AZR	Azores (Terceira Is.)	Portugal	38 45'N	27 05'W	30
NWR	Niwot Ridge, Colorado	U.S.	40 03'N	105 38'W	3749
MID	Sand Island, Midway	U.S.	28 13'N	177 22'W	4
KEY	Key Biscayne, Florida	U.S.	24 40'N	80 12'W	3
MLO	Mauna Loa, Hawaii	U.S.	19 32'N	155 35'W	3397
KUM	Cape Kumukahi, Hawaii	U.S.	19 31'N	154 49'W	3
GMI	Guam	U.S. Territory	13 26'N	144 47'E	2
AVI	St. Croix, Virgin Islands	U.S.	17 45'N	64 45 W	3
RPB	Ragged Point	Barbados	13 10'N	59 26'W	3
CHR	Christmas Island	Kiribati	2 00'N	157 19'W	3
SEY	Seychelles (Mahe Is.)	Seychelles	4 40'S	55 10'E	3
ASC	Ascension Island	U.K.	7 55'S	14 25'W	54
SMO	American Samoa	U.S. Territory	14 15'S	170 34'W	30
AMS	Amsterdam Island	France	37 57'S	77 32'E	150
CGO	Cape Grim, Tasmania	Australia	40 41'S	144 41'E	94
PSA	Palmer Station (Anvers Is.)	Antarctica	64 55'S	64 00'W	10
HBA	Halley Bay	Antarctica	75 40'S	25 30'W	10
SPO	Amundsen Scott (South Pole)	Antarctica	89 59'S	24 48'W	2810

For comparison of the respective entries, direct visualization of the Jacobian is not very instructive: According to the definition of our standard setup, the single entries quantify the concentration change that results from switching on a uniform flux for a particular month in a particular grid cell in every year of the four year simulation period. Hence, in addition to the properties of the atmospheric transport model, the matrix also reflects features determined by our setup, such as (i) the lengths of the spin up period, (ii) whether the month the concentration refers to is earlier than the month the flux refers to, and (iii) the lengths of the month the flux refers to. Feature (iii) can be easily removed from the Jacobian by changing units from concentration per flux to concentration per yearly mean emission rate. To get rid of features (i) and (ii), rather than the Jacobian itself, we plot its difference from an appropriate reference matrix. In Eq. (7), we already made use of such a reference matrix, namely the matrix whose entries quantify the changes in the global linear trend contributions to the respective concentration components that result from changes of the respective flux components. With this reference matrix, we get rid of feature (i) but not of feature (ii), because the entries do not vary from flux component to flux component. Yet this choice of a

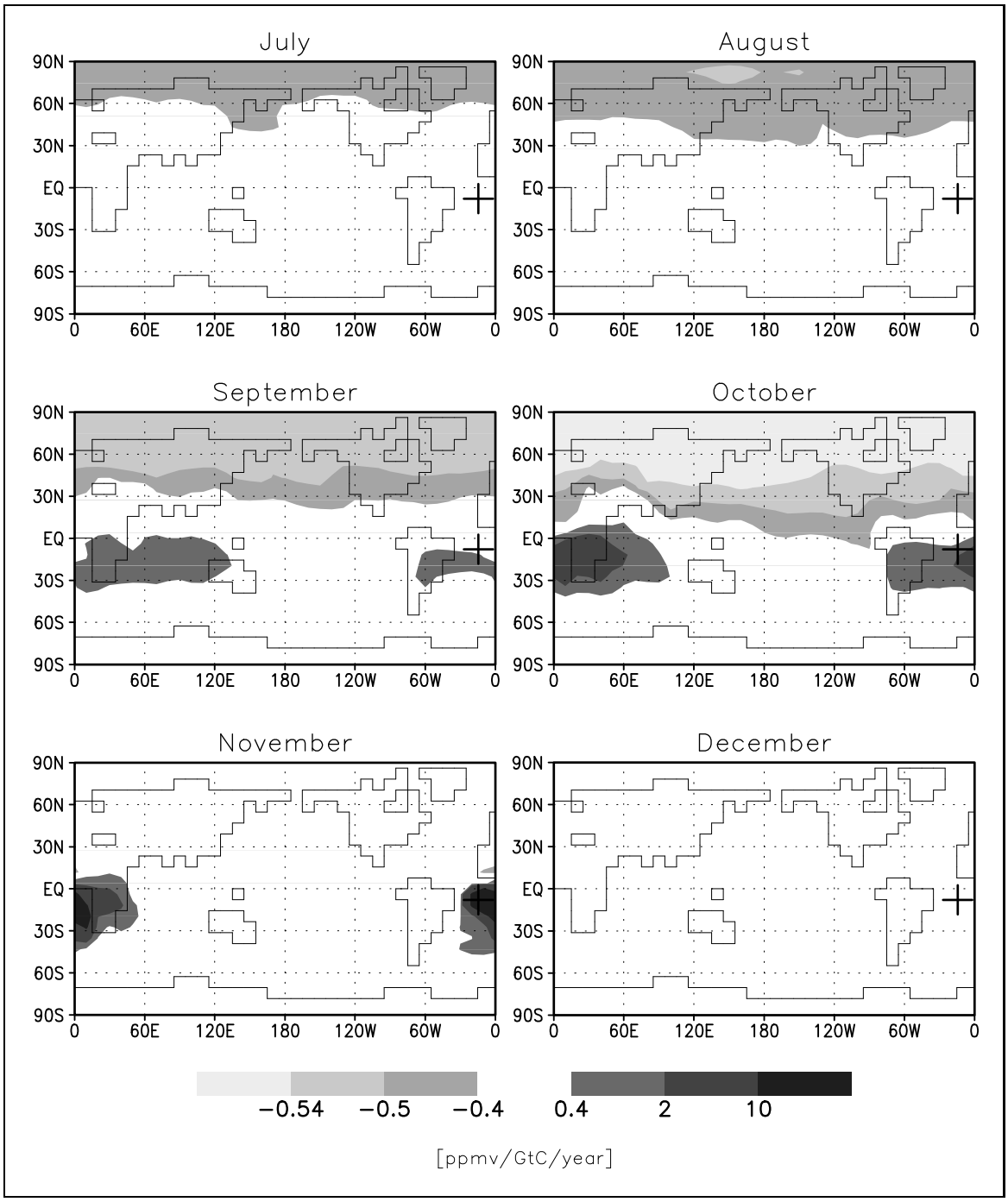

Figure 3: *The second half of the Jacobian's row corresponding to the November mean concentration at the station on Ascension Island (ASC: 7°55'S, 14°25'W, 54 m). For our cyclostationary model setup, each global map shows the concentration's sensitivity to a periodical yearly emission, which is uniformly distributed over a particular month. Reference is instantaneous global mixing, i.e. negative numbers quantify sensitivities that are reduced due to transport. The cross indicates the station location.*

reference matrix is appropriate to visualize a column of the Jacobian, because within one column of T all entries refer to the same flux component, and its impact on all the concentration components can be compared. With respect to this reference matrix, plots of the columns, according to Eq. (7), show the impact of a particular flux component on the periodic contributions to each of the concentration components.

For visualization of the Jacobian's rows as in Figs (3) – (5) discussed below, in contrast, we choose a reference matrix that removes features (i) and (ii), namely the Jacobian that our standard setup would yield, if global mixing was instantaneous. In other words, the reference matrix is derived from a one box model that behaves like TM2 with infinite diffusion, i.e. it also uses $\alpha = 0.476$ ppmv/GtC to convert mass into concentrations. Since a row corresponds to the concentration at a particular station and month, it yields 12 global maps, each of which is quantifying this concentration's sensitivity to the mean surface exchange fluxes in particular month at any location on the globe. A positive value on the map for any month quantifies a sensitivity to an emission at the corresponding grid cell and the respective months that is enhanced compared to instantaneous global mixing: a value of x ppmv/GtC/year means that a yearly emission of 1 GtC, which is uniformly distributed over the respective grid cell and month, in a TM2 run yields a monthly mean concentration at the station and month that is enhanced by x ppmv. Note that the average of these sensitivities with respect to all flux components, in general, will be higher than zero, because both the fluxes and the station are located in the troposphere (or even in the lowest model layer), while our reference is derived for a homogeneous distribution in the *entire* atmosphere.

As an example, in Fig. (3) the second half of the matrix row corresponding to the November mean concentration at the station on Ascension Island (ASC: 7°55'S, 14°25'W, 54 m) is displayed. November emissions in the ocean region ranging from the south of Africa (30° south) to the equator at the longitude of ASC would have the highest impact (more than 10 ppmv/GtC). Going one month back to October emissions, the area of highest impact is shifting to the east, now covering the southern half of Africa. Still the impact of this region is at least as high as for November emissions. Interestingly, at the latitude of ASC in the Pacific Ocean and part of the Indian Ocean, the impact of emissions in November or even in October is smaller than for instantaneous global mixing. This demonstrates the disadvantages of using the mean concentration at a monitoring station in a two-dimensional inversion to constrain the fluxes at a latitude band around the respective station on a monthly time scale. In the maps quantifying the impact of emissions earlier in the year, the predominant structure is a division of both hemispheres. Compared to instantaneous global mixing the impact of the northern hemisphere is about 0.5 ppmv/GtC smaller, whereas the impact of the southern hemisphere is larger by the same amount. This feature is clearly caused by the slow interhemispheric mixing across the Hadley cell. Quantitatively, the fact that the impact of October emissions north of 30° is more than 0.5 ppmv/GtC smaller as compared to instantaneous global mixing shows that not even the emissions of the previous year have been transported to ASC at an amount comparable to instantaneous global mixing (0.476 ppmv/GtC). This reflects the fact that in TM2 the transport needs more than one year to achieve a globally well mixed atmosphere (see Sect. (2)). We only display the second half of this matrix row, because the first half does not contain much structure.

For comparison, maps for two stations and months are displayed, where the shape of the areas with high potential impact compared to instantaneous global mixing is more zonal than for ASC.

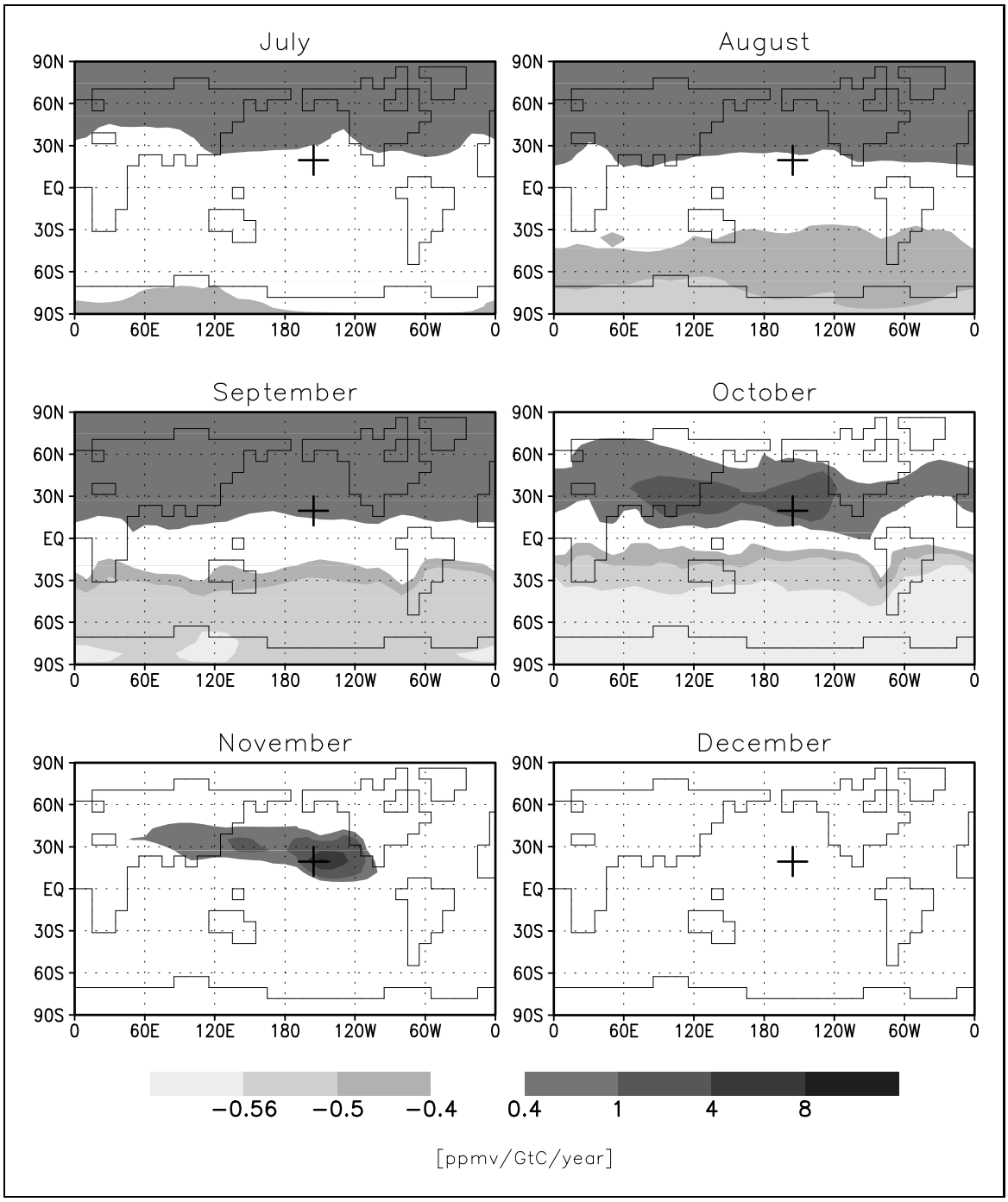

Figure 4: *The first half of the Jacobian's row corresponding to the May mean concentration at the station on the mountain Mauna Loa, Hawaii (MLO: 19°32'N, 155°35'W, 3397 m). For our cyclostationary model setup, each global map shows the concentration's sensitivity to a periodical yearly emission, which is uniformly distributed over a particular month. Reference is instantaneous global mixing, i.e. negative numbers quantify sensitivities that are reduced due to transport. The cross indicates the station location.*

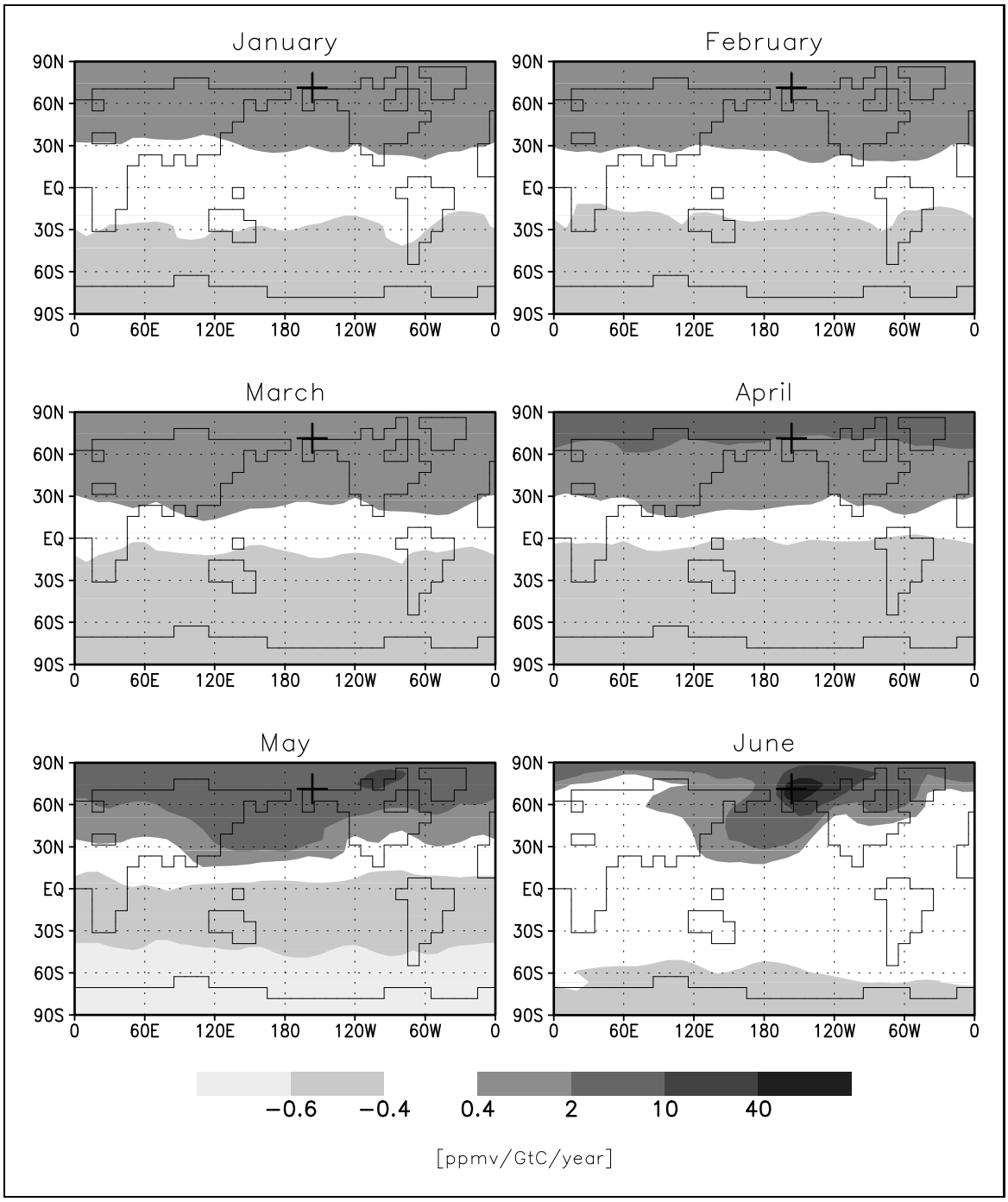

Figure 5: *The first half of the Jacobian's row corresponding to the June mean concentration at the Point Barrow station in Alaska (BRW: 66°00'N, 2°00'E, 6 m). For our cyclostationary model setup, each global map shows the concentration's sensitivity to a periodical yearly emission, which is uniformly distributed over a particular month. Reference is instantaneous global mixing, i.e. negative numbers quantify sensitivities that are reduced due to transport. The cross indicates the station location.*

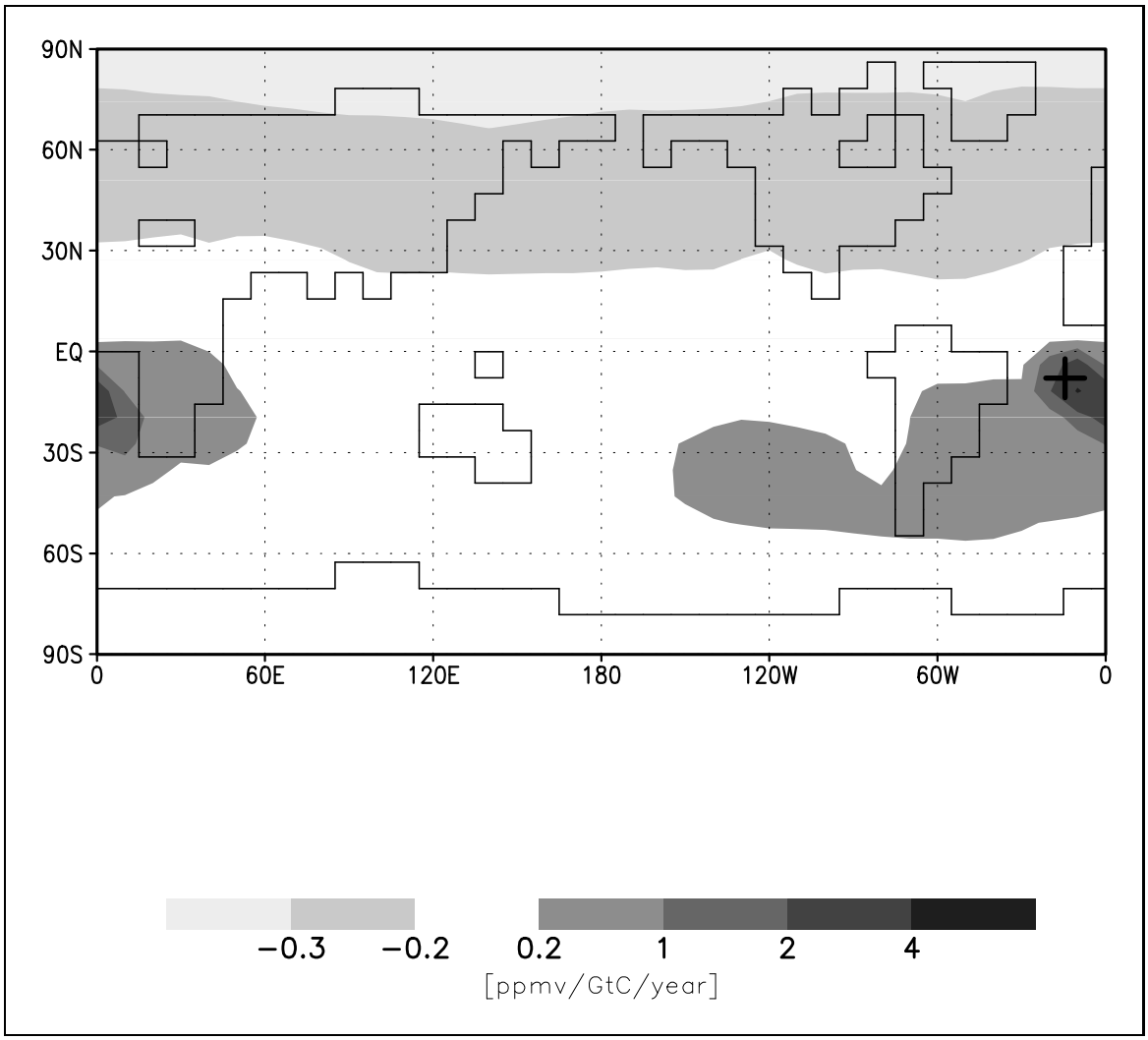

Figure 6: *Collapsed Jacobian's rows corresponding to the 12 monthly mean concentrations at the station on Ascension Island (ASC: 7°55'S, 14°25'W, 54 m). The annual mean concentration's sensitivity to a periodical yearly emission, which is constant in time, in our cyclostationary model setup. Reference is instantaneous global mixing, i.e. negative numbers quantify sensitivities that are reduced due to transport. The cross indicates the station location.*

Fig. (4) shows the potential impact of emissions in the second half of the year to the November mean concentration at the station on the mountain Mauna Loa, Hawaii (MLO: 19°32'N, 155°35'W, 3397 m). The potential impact is highest for December emissions eastward of the station. The corresponding relatively low absolute peak values (less than 10 ppmv/GtC) are due to dilution before reaching the mountain location. As another example, in Fig. (5) we display the impact of emissions in the first half of the year on the June mean concentration at the Point Barrow station in Alaska (BRW: 66°00'N, 2°00'E, 6 m). Here the area of highest impact is well focussed near the station with high peak values of up to 70 ppmv/GtC.

The information on potential impact can be compressed on the flux side, or on the concentration

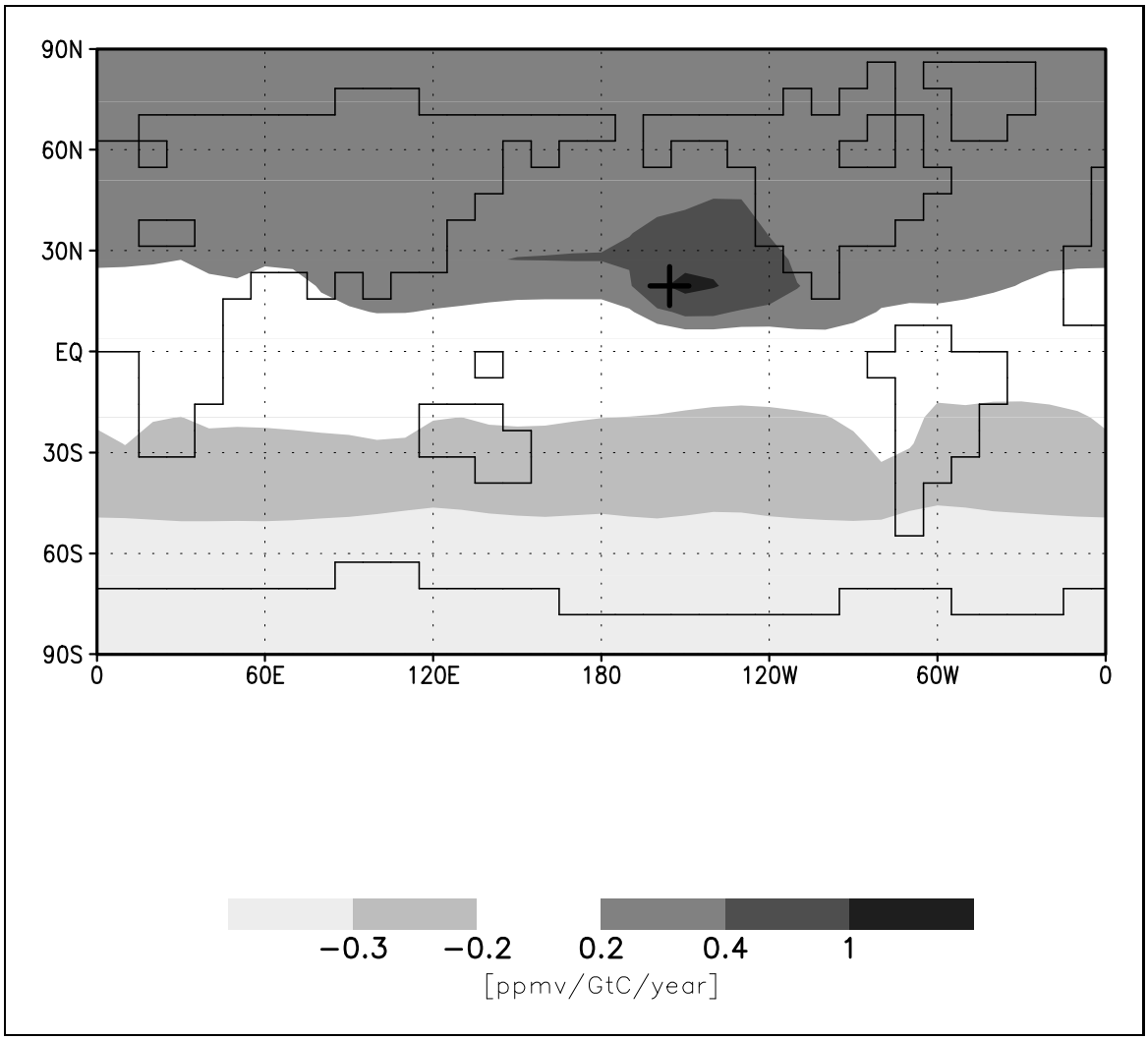

Figure 7: *Collapsed Jacobian's rows corresponding to the 12 monthly mean concentrations at the station on the mountain Mauna Loa, Hawaii (MLO: 19°32'N, 155°35'W, 3397 m). The annual mean concentration's sensitivity to a periodical yearly emission, which is constant in time, in our cyclostationary model setup. Reference is instantaneous global mixing, i.e. negative numbers quantify sensitivities that are reduced due to transport. The cross indicates the station location.*

side, or both: Prescribing the shape of the seasonal cycle of the emissions into every surface grid cell, each matrix row can be projected to a single map of the potential impact of a yearly flux on the respective monthly mean concentration. On the concentration side, for all features that can be derived from the monthly mean concentrations at the stations, the sensitivities with respect to monthly or yearly emissions (in combination with prescribed temporal shape) can be easily computed from the matrix. As an example, in Figs. (6), (7), and (8) we show the sensitivity of the annual mean concentration at ASC, MLO, and BRW, respectively, to fluxes that are constant in time over the whole year. Compared to the monthly maps the peak of the potential impact is lower, slightly more widespread but still in the same regions. This indicates that, for uniform emissions throughout the year, at these stations the modeled concentration is not very sensitive to

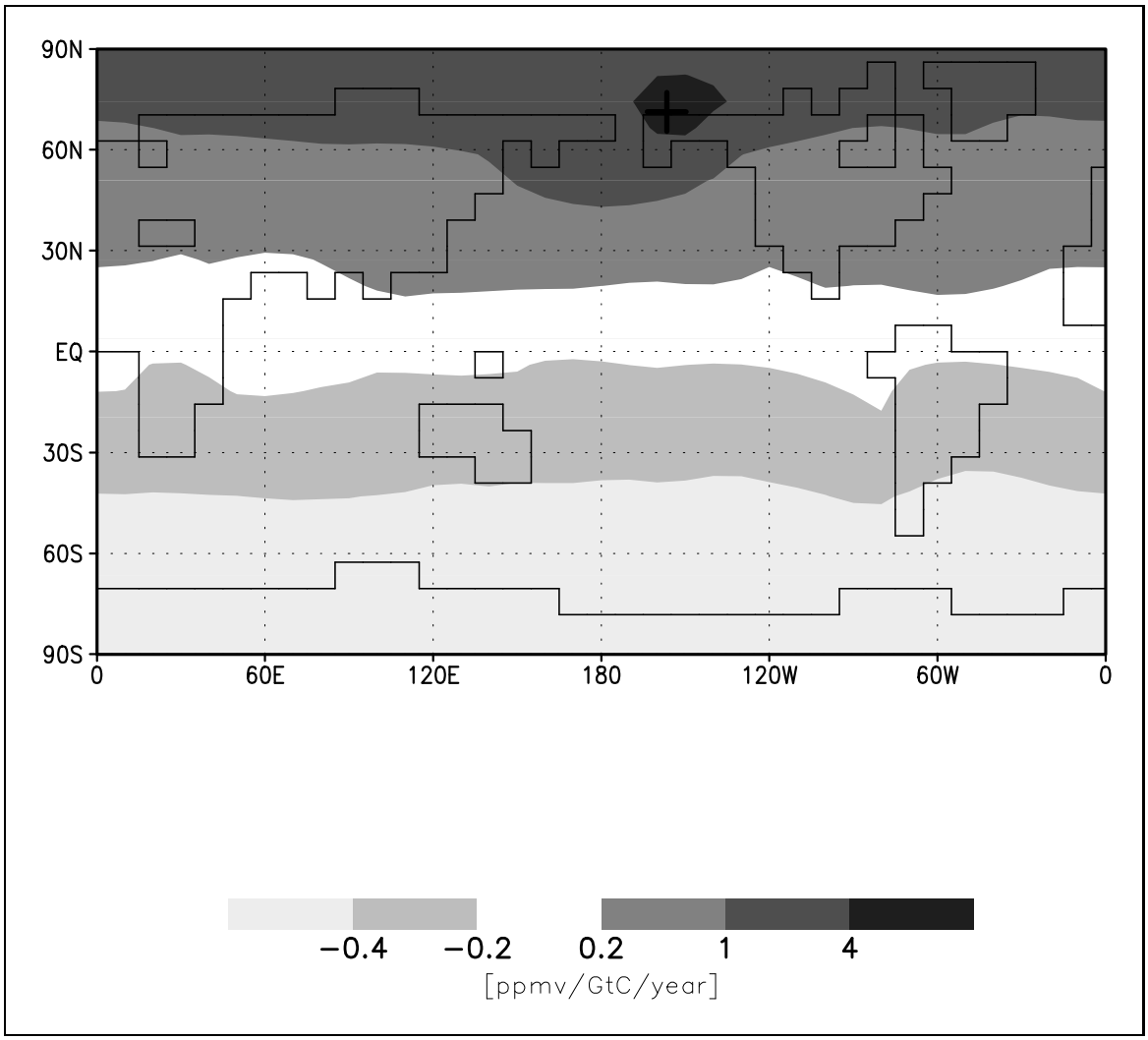

Figure 8: *Collapsed Jacobian's rows corresponding to the 12 monthly mean concentrations at the Point Barrow station in Alaska (BRW: 66°00'N, 2°00'E, 6 m). The annual mean concentration's sensitivity to a periodical yearly emission, which is constant in time, in our cyclostationary model setup. Reference is instantaneous global mixing, i.e. negative numbers quantify sensitivities that are reduced due to transport. The cross indicates the station location.*

the seasonality of the transport.

Another way of looking at the maps is in terms of the size of surface areas that are 'observed' by the respective stations: On the monthly time scale all three stations are most influenced by an area of only a few grid cells. On the annual time scale there are differences among the stations: While ASC still observes only a small area, BRW is representative for the northern high latitudes, and MLO is strongly influenced by the entire northern hemisphere. Of course, in addition to the transport considered here, the value of a monitoring location depends on many other features such as the specific source/sink characteristics of the particular tracer being observed.

We discussed the potential impact quantified by the Jacobian. If a particular flux field f is

prescribed, according to Eq. (6) by a matrix multiplication with the Jacobian this potential impact can be used to simulate the resulting concentrations c at the station locations. Hence, the Jacobian is an extremely efficient transport model by itself. Once the Jacobian has been computed, for the simulation of the quasi-stationary seasonal cycle at the stations, there is no need to run TM2 again, as long as the setup (including the location of the stations) is still appropriate for the tracer of interest. Using the matrix does not only reduce the computational cost of a simulation to the cost of a simple matrix multiplication but also the amount of required disk space. While the meteorological fields to drive TM2 for one year occupy about 30 MW, the matrix just needs $36 \times 24 \times 12 \times 27 \times 12$ W ≈ 3 MW. Thus, among other applications, as transport model the Jacobian represents a valuable tool for sensitivity tests: *Knorr* [1997] investigated the response of the atmospheric CO_2 concentration at the NOAA/CMDL stations to exchange flux fields computed by a large number of different formulations of his terrestrial biosphere model.

In addition to quantifying *potential* impact and to perform transport simulations, by means of the Jacobian it is easy to analyze the simulation in terms of the *simulated* impact of each flux component: Writing Eq. (6) in the form

$$c_i = \sum_{j=1}^{n_f} T_{i,j} f_j \quad , \tag{16}$$

each concentration component c_i is decomposed into the contributions $c_{i,j} := T_{i,j} f_j$ by the respective flux component f_j. The quantity $c_{i,j}/c_i$ is then the portion of c_i resulting from the flux component j in the simulation and like the potential impact can be conveniently displayed on 12 maps per concentration component.

Again, the information can be compressed on the flux side, the concentration side, or both sides. For example in *Kaminski et al.* [1996] we analyzed a TM2 run employing the fluxes derived by a biosphere model [SDBM, *Knorr and Heimann*, 1995]: On the flux side we prescribed the shape of the SDBM fluxes, and on the concentration side we projected on the simulated seasonal cycle. We thus decomposed the magnitude of the modeled seasonal cycle at particular observational sites with respect to the contributions by the respective grid cells, which yields one map per station. For this study we had to run the adjoint model once per station. By means of the Jacobian this kind of decomposition is easily performed without the adjoint model.

5 The Inverse Problem

5.1 Introduction to the Inverse Problem

The previous sections were concerned with a representation of our transport model TM2 by its Jacobian matrix. In this section we present an inversion of the atmospheric transport, which combines this Jacobian matrix to observations of atmospheric CO_2. The goals of this subsection are to introduce our approach to this inverse problem and to give an outline for the remainder of this section. There are a number of excellent introductions to the global carbon cycle and its perturbation by men [e.g. *Broecker and Peng*, 1993; *Heimann*, 1993; *Houghton et al.*, 1995a]. We begin with a brief summary of this topic to introduce our tracer.

Due to human activities such as fossil fuel burning and changes in land use, the atmospheric CO_2 concentration has rised by about 25% since preindustrial times. Observations of the atmospheric CO_2 concentrations indicate that during the 1980s about 3 GtC/year of the estimated anthropogenic emissions of about 7 CtC/year remained in the atmosphere. On decadal time scales, the most important processes that can remove CO_2 from the atmosphere are uptake by the ocean and by the terrestrial biosphere. The net exchange flux with the ocean is driven by the difference between oceanic and atmospheric partial pressures of CO_2, while the net exchange flux with the terrestrial biosphere is the difference between Net Primary Productivity (NPP) and soil respiration fluxes. NPP is the amount of carbon transformed to organic material and is defined as the difference between CO_2 absorbed by photosynthesis and CO_2 respired by the plant. By soil respiration flux we denote the return flux from soil and plant litter to the atmosphere. A number of terrestrial sink processes such as regrowth of forest following harvest, fertilization by an increased atmospheric CO_2 concentration, or fertilization by nitrogen have been identified, but their magnitude is difficult to quantify. The reports of the Intergovernmental Panel on Climate Change (IPCC) contain summaries of the current insight in the global budget of CO_2. For the 1980s, the IPCC estimates an oceanic uptake of 2 ± 0.5 GtC based on a number of studies running models of the oceanic carbon cycle [*Houghton et al.*, 1995a]. Uptake by the terrestrial biosphere is computed as the residuum in the budget equation of atmospheric CO_2.

Spatial differences in the atmospheric concentrations of CO_2, which are being measured at global networks of monitoring stations, reflect the spatial and temporal structure of the exchange flux fields. Feeding prescribed surface flux fields into atmospheric transport models, the atmospheric CO_2 concentration at observational sites can be simulated. Consistency of simulated concentrations with observations has the potential to constrain flux fields. Investigating the consistency of a number of reasonable flux scenarios with atmospheric observations, *Keeling et al.* [1989b] and *Tans et al.* [1990] inferred a sink in the midlatitudes of the northern hemisphere, but both studies differ in their interpretation of this sink. While *Keeling et al.* attributed much of this sink to an oceanic southward transport of carbon by the global thermohaline oceanic circulation (global ocean uptake of more than 2 GtC), *Tans et al.* found only a marginal oceanic uptake (less than 1 GtC) and concluded a major terrestrial sink. One reason for this disagreement is that in both studies the information from the atmospheric CO_2 observations is complemented by different pieces of additional information: while *Keeling et al.* use atmospheric measurements of the isotopic composition of CO_2, *Tans et al.* employed data of air–sea partial pressure differences of CO_2 .

Inversion of the atmospheric transport is an alternative to subjectively choose flux fields and compare the simulated atmospheric responses with observations. For an inert tracer such as CO_2, the inverse problem consists in the algorithmic determination of a flux field f, that, for prescribed concentrations c, satisfies Eq. (9). For our matrix M the problem consists of $n_c = 300$ equations for $n_f \approx 10000$ unknowns and thus is highly underdetermined, i.e. there are many flux fields yielding the same modeled concentration.

To obtain a unique solution additional information has to be included in the inversion procedure. One way to do so consists in introducing further equations (hard constraints) for the components of the flux vector. The usual approach is to compose the flux field of spatio-temporal patterns with n_x unknown coefficients. Spatial patterns such as latitude bands [*Brown*, 1993, 1995; *Ciais et al.*, 1995] or spherical harmonics in space [*Enting and Mansbridge*, 1989] can be derived from the geometry of the earth and then be combined e.g. with harmonics in time. Alternatively, a partitioning of the earths surface characterized by relevant processes can be constructed [*Hartley and Prinn*, 1993; *Hein and Heimann*, 1994; *Enting et al.*, 1995; *Hein et al.*, 1996; *Rayner et al.*, 1996], or statistically motivated patterns like Empirical Orthogonal Functions (EOFs) of the fluxes can be derived. Provided that n_x is small enough to yield an overdetermined inverse problem, the coefficients can be determined by a regression (More precisely, n_x has to be smaller than the number of linear independent equations). To yield an even-determined inverse problem often n_c is made equal to n_x by interpolation of the observed concentrations.

An alternative to handle the underdetermined problem without reducing the number of unknowns is the so-called Bayesian approach, which allows to include a priori information on the fluxes in the inversion: Both atmospheric observations and a priori information are described in terms of probability densities. Employing the transport as constraint, consistent probability densities are derived, as illustrated by Fig. (9). The a priori information regularizes the underdetermined inverse problem. Often the observations as well as the a priori information about the fluxes are described in terms of Gaussian probability distributions. In combination with linearized transport simple formulas for the posterior estimate of the fluxes and its uncertainty can be derived. A brief overview of the technical details is given in appendix A. Typical algorithms for evaluation of these formulas are the Kalman filter and the Singular Value Decomposition (SVD).

In many recent studies [*Hartley and Prinn*, 1993; *Hein and Heimann*, 1994; *Enting et al.*, 1995; *Hein et al.*, 1996; *Rayner et al.*, 1996], both approaches are applied: First flux patterns are defined, and then a priori information on the unknown scaling coefficients is included. The respective transport model is run separately with each of the flux components, and the contributions to the concentration signal at each of the monitoring sites and times are recorded. In this manner, a transport matrix mapping scaling coefficients onto concentrations is derived. Due to the considerable computational cost of the necessary transport model runs the number of source components remains low; in the abovementioned studies the spatial resolution ranges from 5 to about 30 regions.

For the present study we also apply the Bayesian approach. As described in Sect. (4), for TM2 in our standard setup (see Sect. (2)) a matrix representation on the entire model grid is available. In contrast to the abovementioned studies, we are in a situation to perform an inversion for the model's spatial resolution of approximately 8^o latitude by 10^o longitude and monthly time scale in the flux space. Compared to a few prescribed patterns this high resolution enables us to capture much more of the variability of the fluxes, which allows a more realistic simulation of the

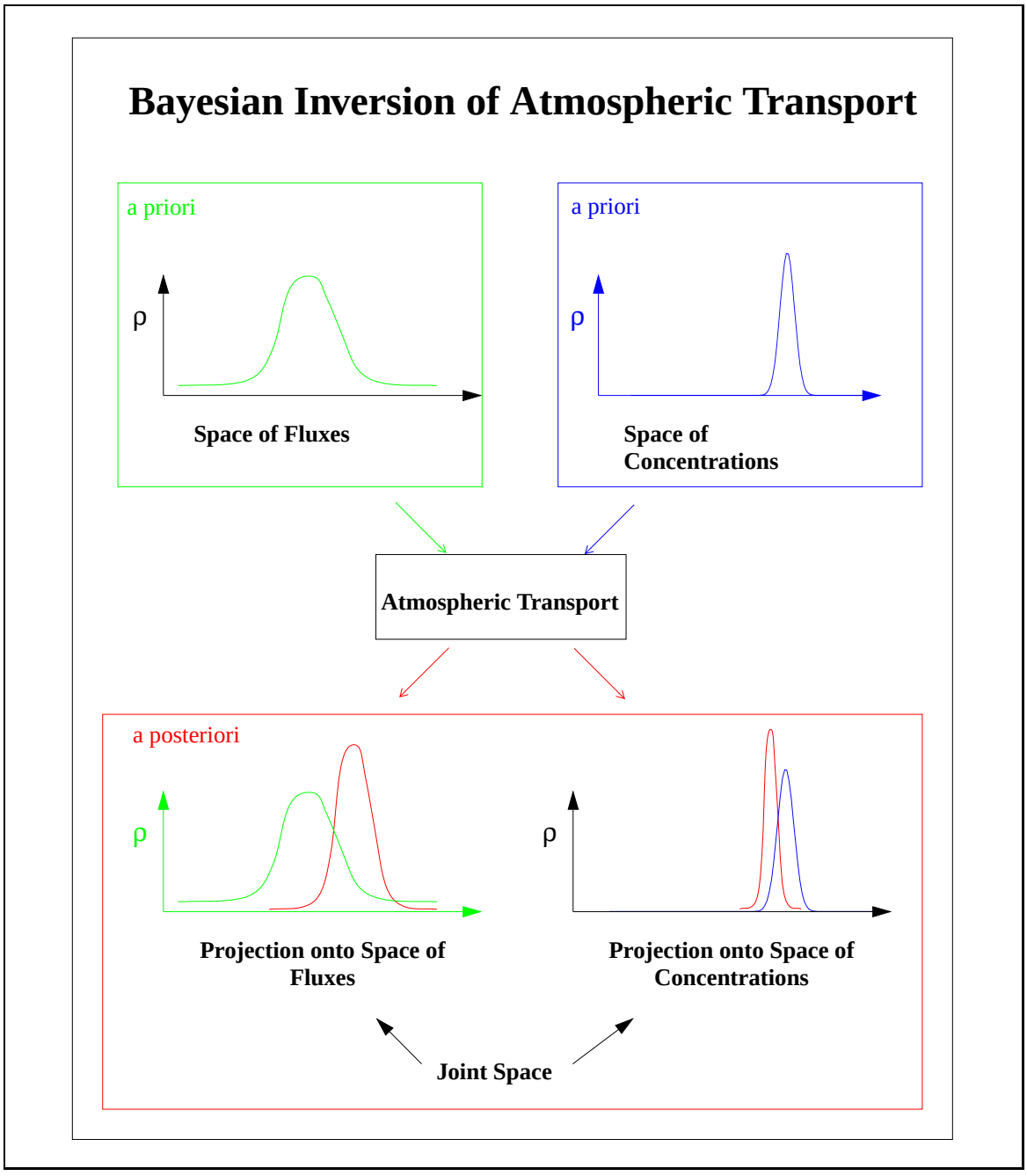

Figure 9: *A schematic illustration of the Bayesian approach: The a priori state of information is represented by independent probability densities for fluxes and concentrations. Combining this information to the information about the atmospheric transport, represented by our numerical model, yields a consistent a posteriori state of information, represented by a probability density in the joint space of fluxes and concentrations; projections to the individual spaces, in general, are sharper than the a priori densities.*

concentrations. Evidently, with increasing number of unknowns, the gain of information about the particular unknowns from the atmospheric observations gets smaller: The higher the resolution in the space of fluxes, the lower the reduction of uncertainty for a particular flux component by the inversion. Yet for sums of flux components representing large scale quantities such as e.g. the scaling coefficients of prescribed patterns, the gain of information is much higher. Sect. (5.5) gives examples. Another important advantage of a higher resolution has been pointed out by *Trampert and Snieder* [1996]: In combination with inhomogeneous sampling of the observations, insufficient resolution in the space of unknowns causes the inversion to yield biased estimates. Our network (see Fig. (2)) indeed seems to be characterized by an inhomogeneous spatial distribution of the observational sites. Hence, a high resolution appears favorable to reduce a possible bias, especially in sums of estimated fluxes.

For our inversion of the transport of CO_2, we use a priori information on the surface fluxes derived from output of high resolution models of both the terrestrial biosphere and the ocean, combined with statistics of fossil fuel burning and land use change. For these flux fields, however, uncertainties that would enable us to define a probability distribution are not available. For computational convenience, we assume fluxes to have a Gaussian distribution centered around those flux fields with a simple diagonal covariance matrix, thereby avoiding the definition of correlations among the uncertainties of different flux components. Due to the high spatial resolution in the space of fluxes, especially in the process model derived flux fields, correlated uncertainties seem more appropriate to express our a priori state of information, though.

The layout of the remainder of this section is as follows: Sect. (5.2) describes the a priori information on the fluxes. Sect. (5.3) deals with the atmospheric observations, followed by a description of our inversion technique and a discussion of the singular value spectrum in Sect. (5.4). The inferred flux fields as well as spatial and temporal means are presented in Sect. (5.5) together with their uncertainties. Sect. (5.6) discusses the concentrations at observational sites simulated with the optimal flux field. Sect. (5.7) discusses the total fluxes for some oceanic regions and countries. Finally, Sect. (5.7) makes an attempt to assess the reliability of the posterior flux estimate derived by our inversion.

5.2 A Priori Fluxes

We compose our a priori estimate of the net surface exchange fluxes into the atmosphere of the contributions from four components: the terrestrial biosphere in equilibrium, a correction for land use change, the ocean, and fossil fuel burning.

For the biospheric component the seasonal net exchange fluxes derived by the Simple Diagnostic Biosphere Model (SDBM, [*Knorr and Heimann*, 1995]) were interpolated from the models 0.5^o grid to the TM2 grid. The SDBM is driven by climate data, observed greenness from satellite derived global vegetation index data, and a drought stress indicator calculated with a one layer bucket model. NPP is the product of a globally constant photosynthetic light use efficiency, the observed greenness and the drought stress factor. Soil respiration is proportional to the drought stress factor and an exponential function of the soil temperature that is characterized by one global parameter Q_{10}; in each grid cell, the proportionality factor is chosen to achieve a locally balanced yearly net flux. Two global model parameters, the light use efficiency and Q_{10}, have been tuned by minimization of the misfit between observations of the seasonal cycle of atmospheric CO_2 and the seasonal cycle simulated by feeding the modeled fluxes into TM2. For this procedure the observations at the northern hemisphere stations BRW, CBA, AZR, KUM from 1980 to 1990 and STM from 1982 to 1990 were used (see station map in Fig. (2)). Through this parameter fit at least a part of the atmospheric observations that are used in our inversion have already influenced our a priori estimate of the fluxes. Here we make an error, because the inversion procedure is based on the assumption of independent information about fluxes and atmospheric observations. Yet we do not expect the flux field to change much, if instead the atmospheric observations from a period excluding our target period were chosen for the fit. In addition, since only two global parameters have been tuned, most details of the flux field's structure are imposed by the climate and satellite data. Of course, alternatively, fluxes computed from models that are not based on atmospheric observations can be used; for our standard case, nevertheless, we decided in favor of the SDBM, because the model performed well in intercomparison studies [*Heimann et al.*, in press].

Since the fluxes computed by the SDMB represent a terrestrial biosphere in local equilibrium, i.e. the local annual mean flux is zero, perturbations of this equilibrium have to be quantified separately. The only perturbation for which we explicitly specify an a priori flux is land use change. On the basis of regional estimates by *Houghton et al.* [1987], an annual mean field of fluxes due to land use change (see Fig. (10)) has been compiled by *Heimann and Keeling* [1989]. Within each region, they distributed the source component in proportion to NPP as described in detail in *Heimann and Keeling* [1989]. The global annual mean source is 1.7 GtC.

For the oceanic component the seasonal net exchange fluxes computed by a simple plankton model [*Six and Maier-Reimer*, 1996] embedded in the Hamburg model of the oceanic carbon cycle [*Maier-Reimer*, 1993] were interpolated from the models 3.5^o grid to the TM2 grid. The fluxes for the 1980s were taken from a transient run with prescribed observed atmospheric CO_2 concentrations, starting in 1756 from the models equilibrium for the preindustrial CO_2 concentration [*Enting et al.*, 1994]. Hence, in contrast to the biospheric component, the oceanic net exchange fluxes are not balanced; the global annual mean ocean uptake is 1.7 GtC.

From fossil fuel burning statistics of *Andres et al.* [1997] on a 1^o grid, annual mean fluxes on the TM2 grid have been interpolated (see Fig. (11)). The global annual net source is 5.3 GtC.

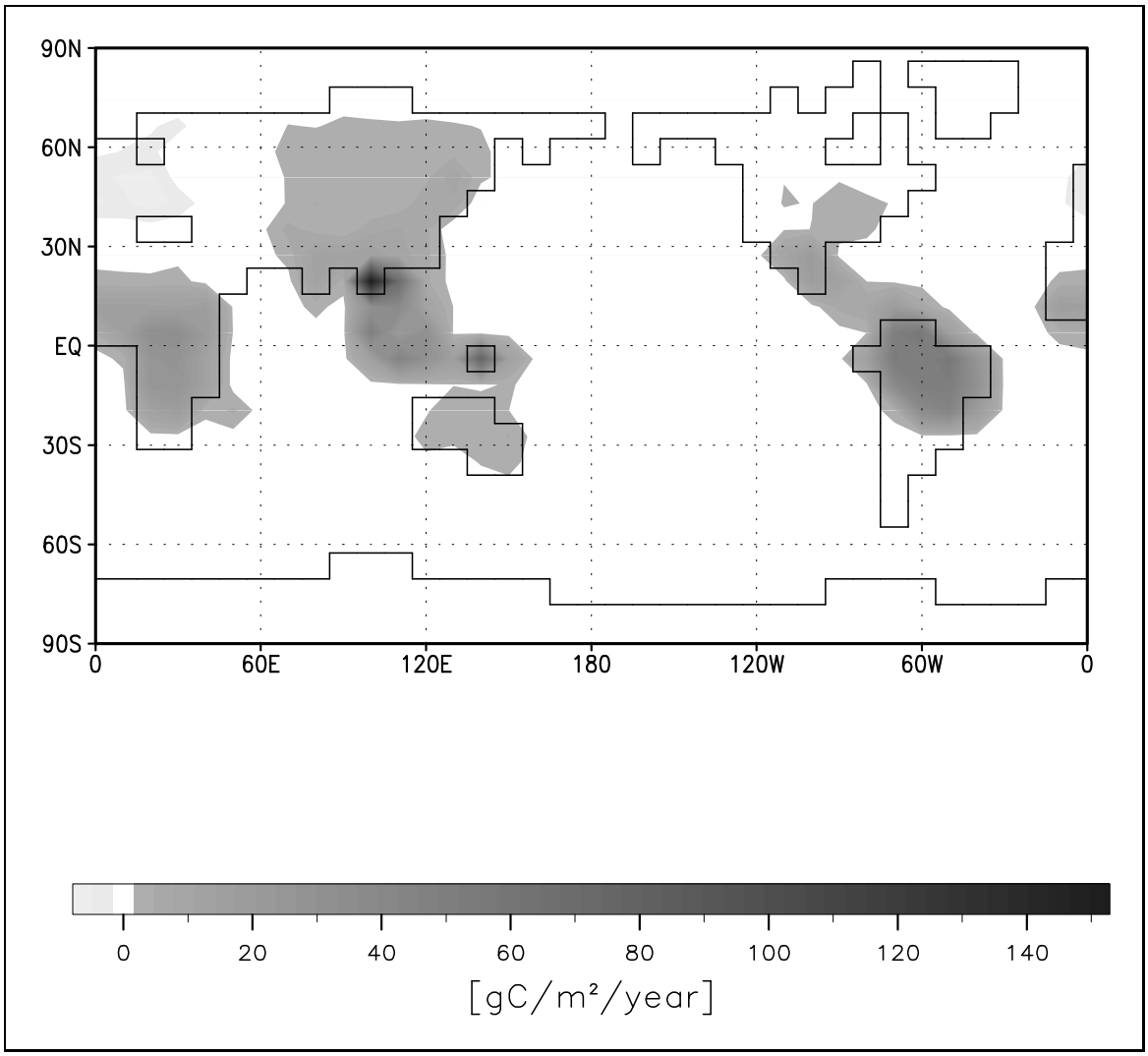

Figure 10: *Annual land use change flux.*

Compared to the biospheric and oceanic component the uncertainty is rather small, so that we exclude this component from the inversion by a procedure described in Sect. (5.3).

The a priori estimate for the sum of the flux contributions from terrestrial biosphere and ocean is displayed in Fig. (12). The annual mean is shown in the middle panel of Fig. (13).

Compared to the uncertainties in the concentrations, it is much more difficult to quantify the uncertainties in the fluxes. Yet these uncertainties are crucial parameters for the inversion: according to Eq. (A.4) the a posteriori estimate for $f^{'}$ minimizes the cost function

$$J(\tilde{f}) = {}^1\!/_2[\sum_{i=1}^{n_f}(\frac{f-\tilde{f}}{\sigma_f})_i^2 + \sum_{i=1}^{n_c}(\frac{c_{obs}-T\tilde{f}}{\sigma_c})_i^2] \quad . \tag{17}$$

A term with a large uncertainty has merely a small impact on the result of the inversion. Hence, by assigning large uncertainties to the fluxes we can perform a weighting in favor of the concentrations. In the following we describe our standard choice, which is intended to emphasize the weight on the

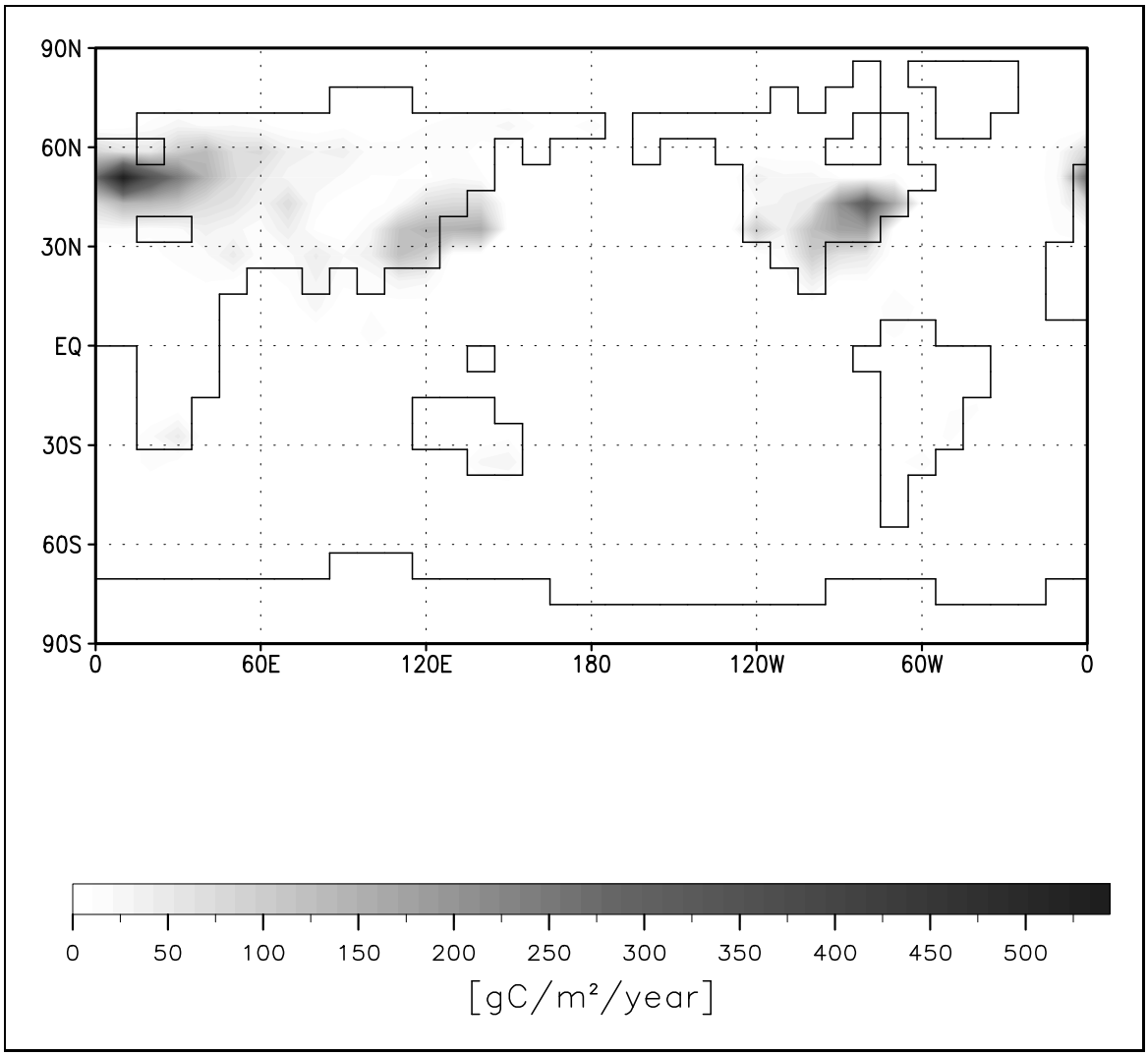

Figure 11: *Annual fossil fuel flux.*

atmospheric observations. Among the individual flux components, the recipe gives a smaller weight to the a priori values of those components we consider more uncertain. By and large we consider large fluxes more uncertain than small ones, yielding heigher weights for the small fluxes, which affects in particular oceanic fluxes.

In every grid cell with a land fraction of more than 1%, the terrestrial flux is considered to be the sum of NPP (see Fig. (14)), soil respiration, and land use change contributions. Each month the uncertainty for this sum of fluxes is determined by assuming independent uncertainties of 50% for the NPP and soil respiration components and an uncertainty of 100% for the land use change component. Although computationally convenient, the assumption of independent uncertainties for NPP and soil respiration neglects a small negative correlation induced by the SDBM constraint of locally balanced annual mean flux. If a grid cell contains vegetation, occasionally a small uncertainty might result from erroneous timing of the modeled fluxes. To avoid a high weight on these erroneous flux values by too low uncertainties we assume a minimum uncertainty of 0.12 kg/m^2/year for grid

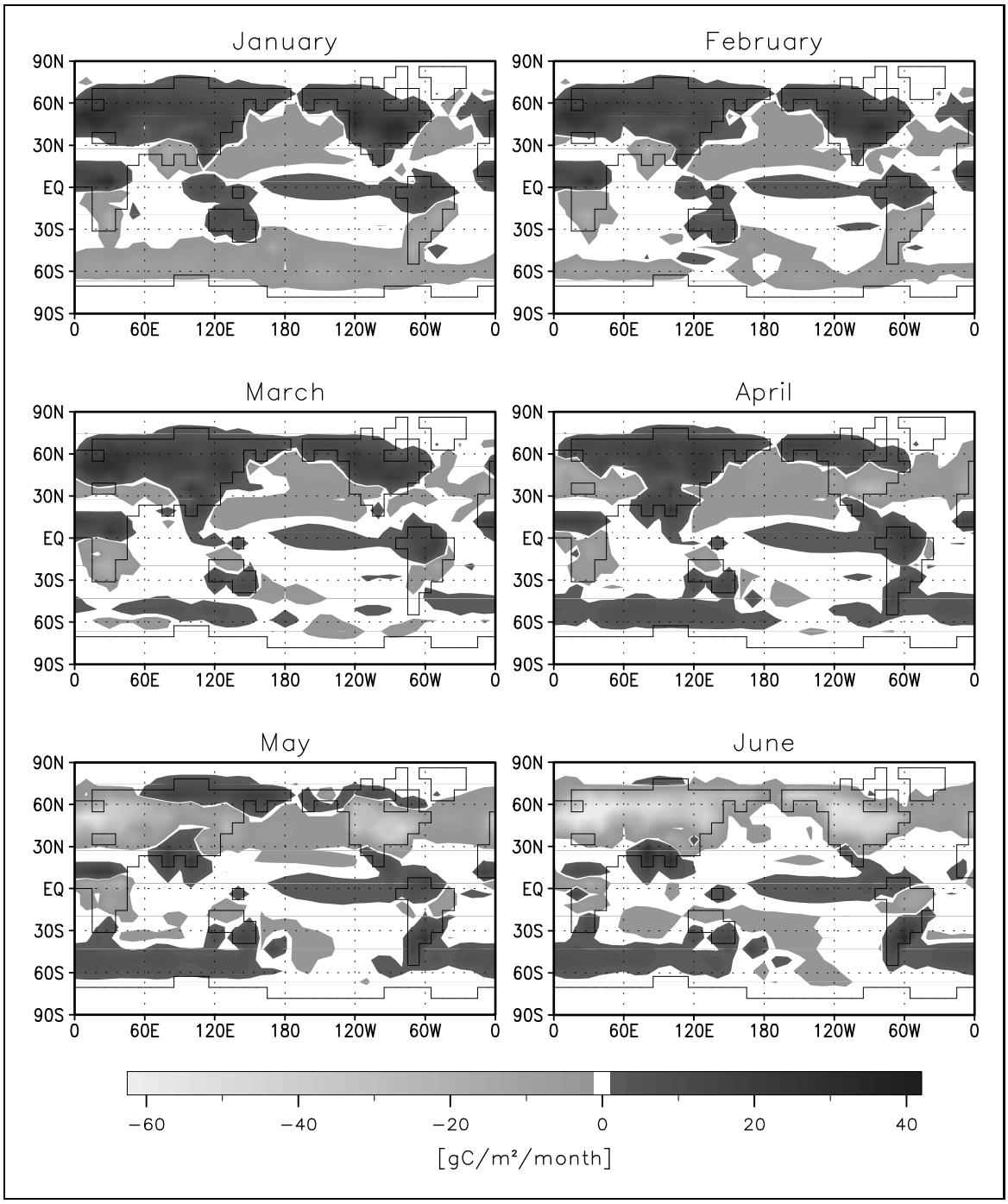

Figure 12: *A priori estimate of the sum of the flux contributions from terrestrial biosphere and ocean.*

cells with an annual mean NPP of more than 0.01 kg/m^2/year, which excludes deserts and ice covered regions. Finally, since our inversion procedure cannot handle zero uncertainties, they are replaced by the very low value of 10^{-12} kg/m^2/year.

The uncertainty for oceanic flux contributions is defined as follows. To every grid cell with an

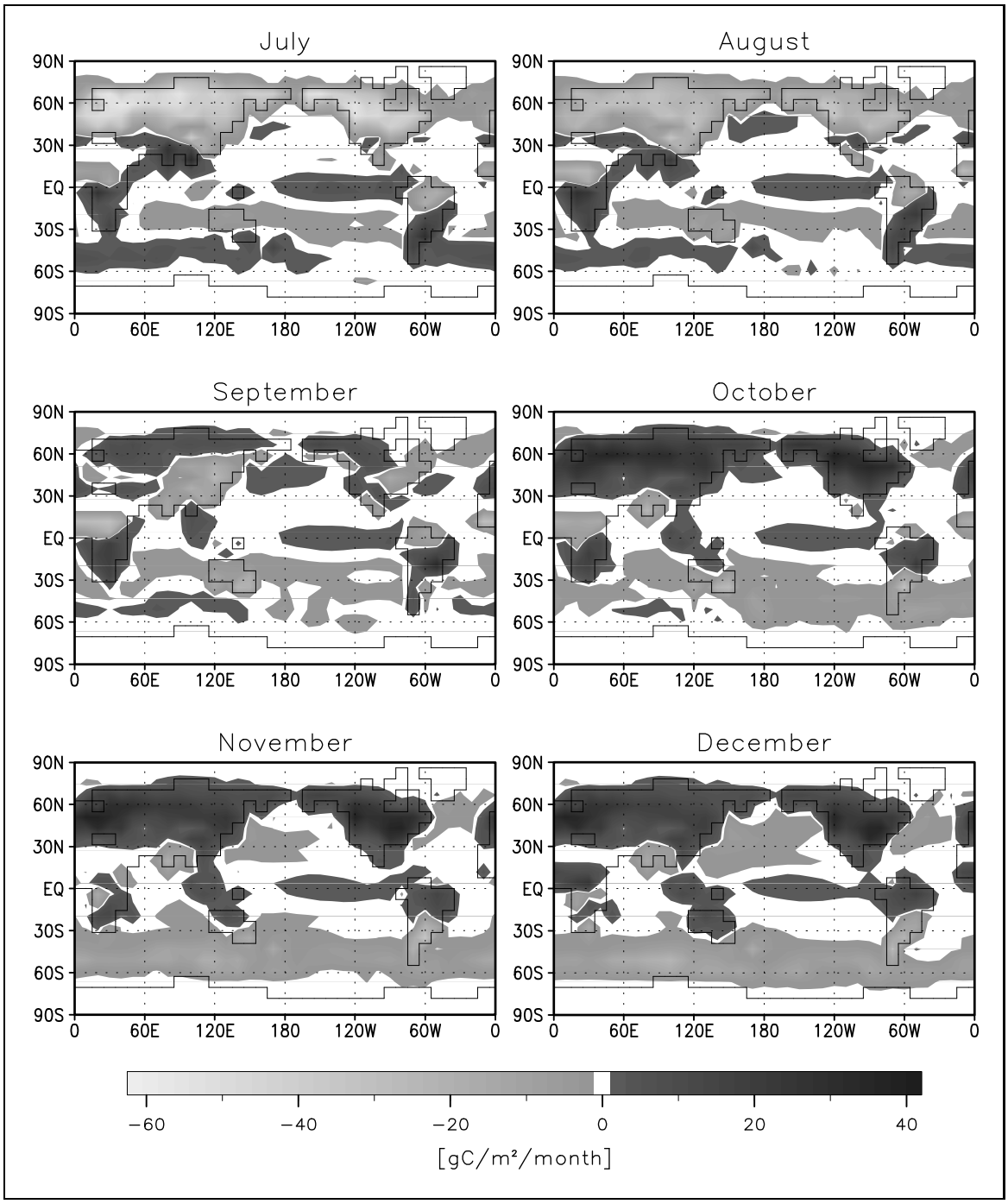

ocean fraction of more than 1% and with nonzero annual mean fluxes, we also assign the terrestrial minimum uncertainty of 0.12 kg/m^2/year. In the ocean, zero uncertainties are also replaced by the very low value of 10^{-12} kg/m^2/year. According to this recipe every grid cell has a terrestrial, or a ocean uncertainty, or both. In grid cells that have both, in proportion to the land fraction a mean uncertainty is assigned. The resulting uncertainties are displayed in Fig. (15).

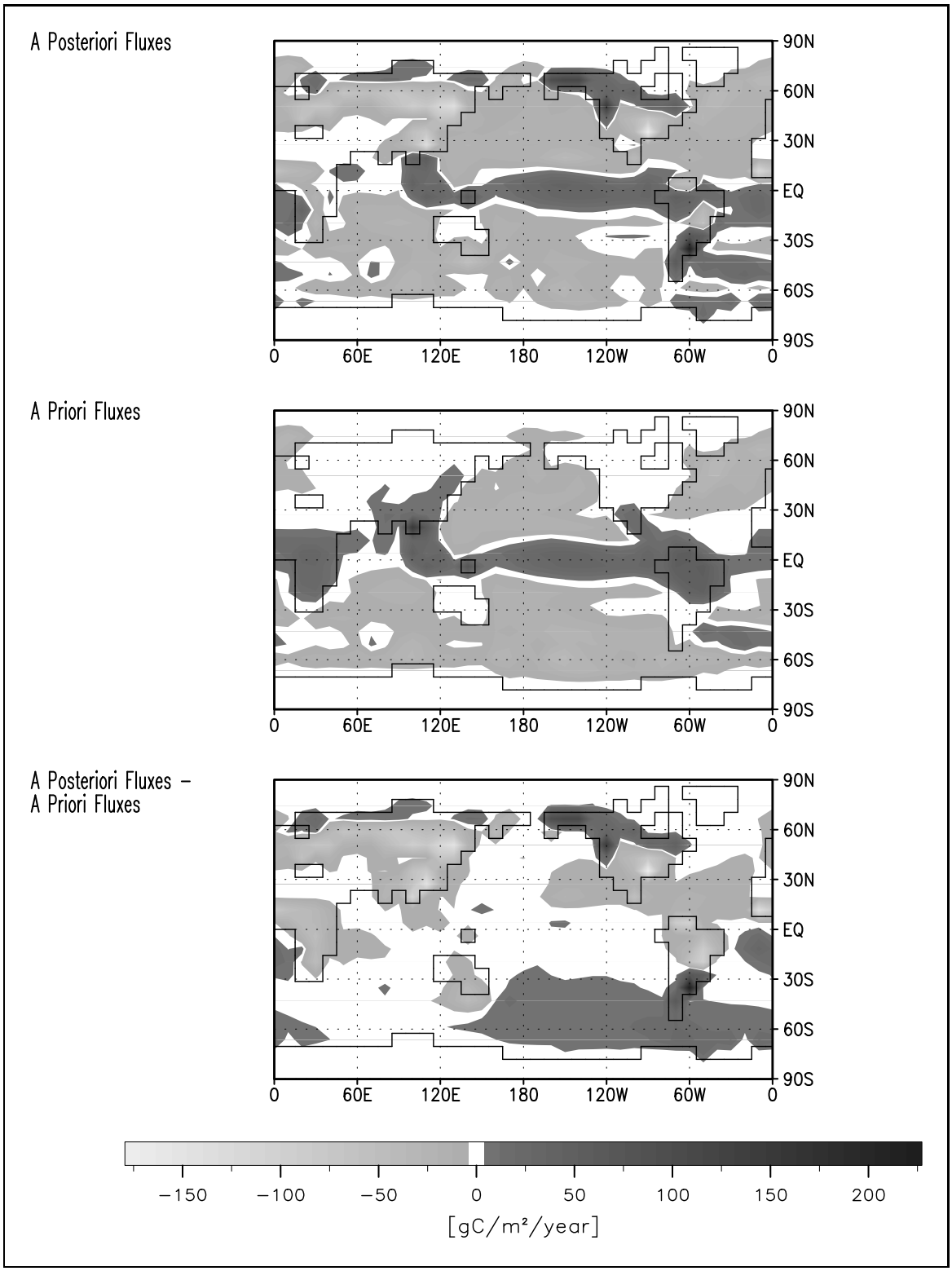

Figure 13: *Annual mean of the sum of the flux contributions from terrestrial biosphere and ocean; a posteriori (top), a priori (middle), and their difference (bottom); in the difference plot, positive values quantify an enhanced source or a reduced sink.*

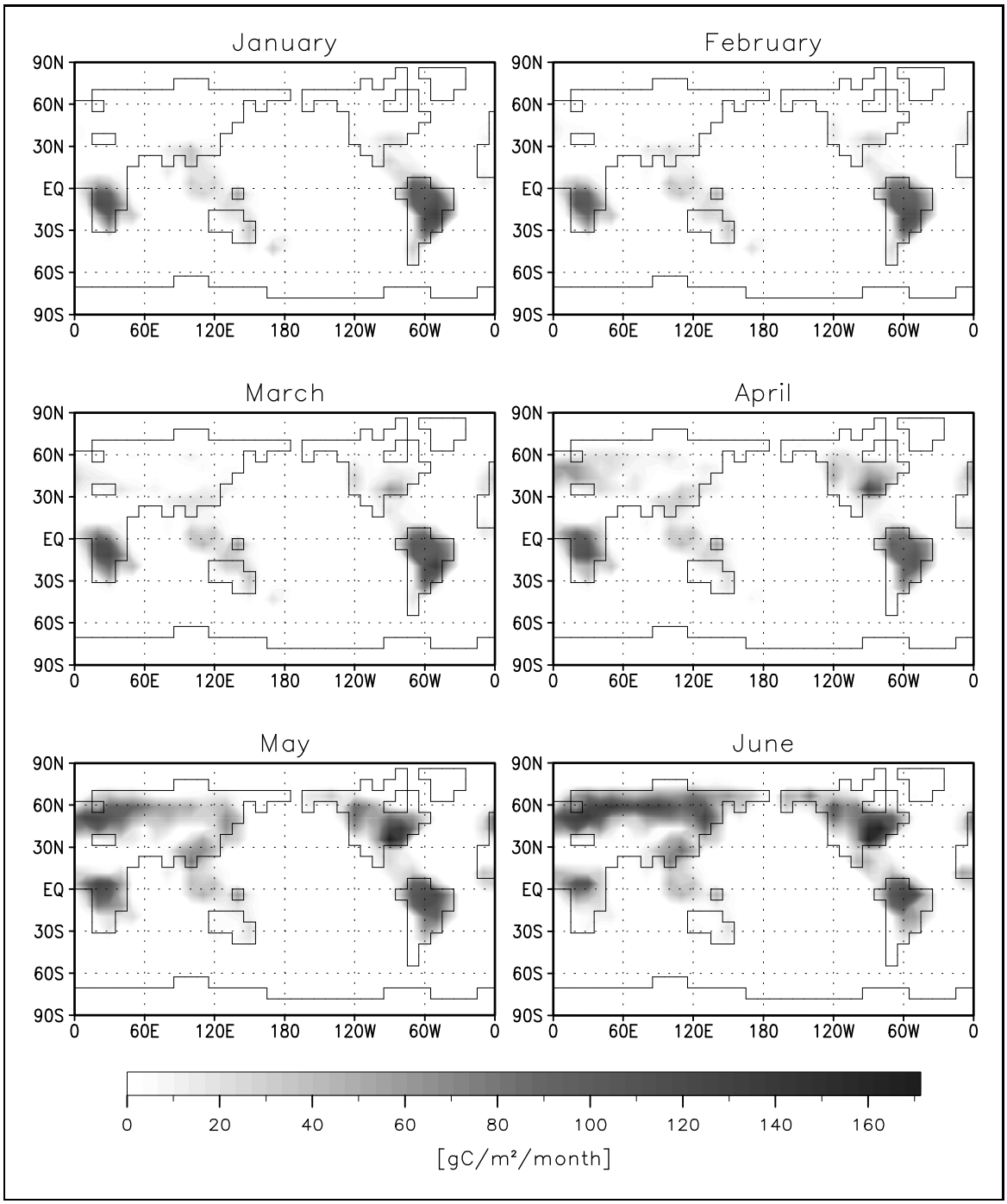

Figure 14: *Net primary productivity (NPP) computed by the SDBM.*

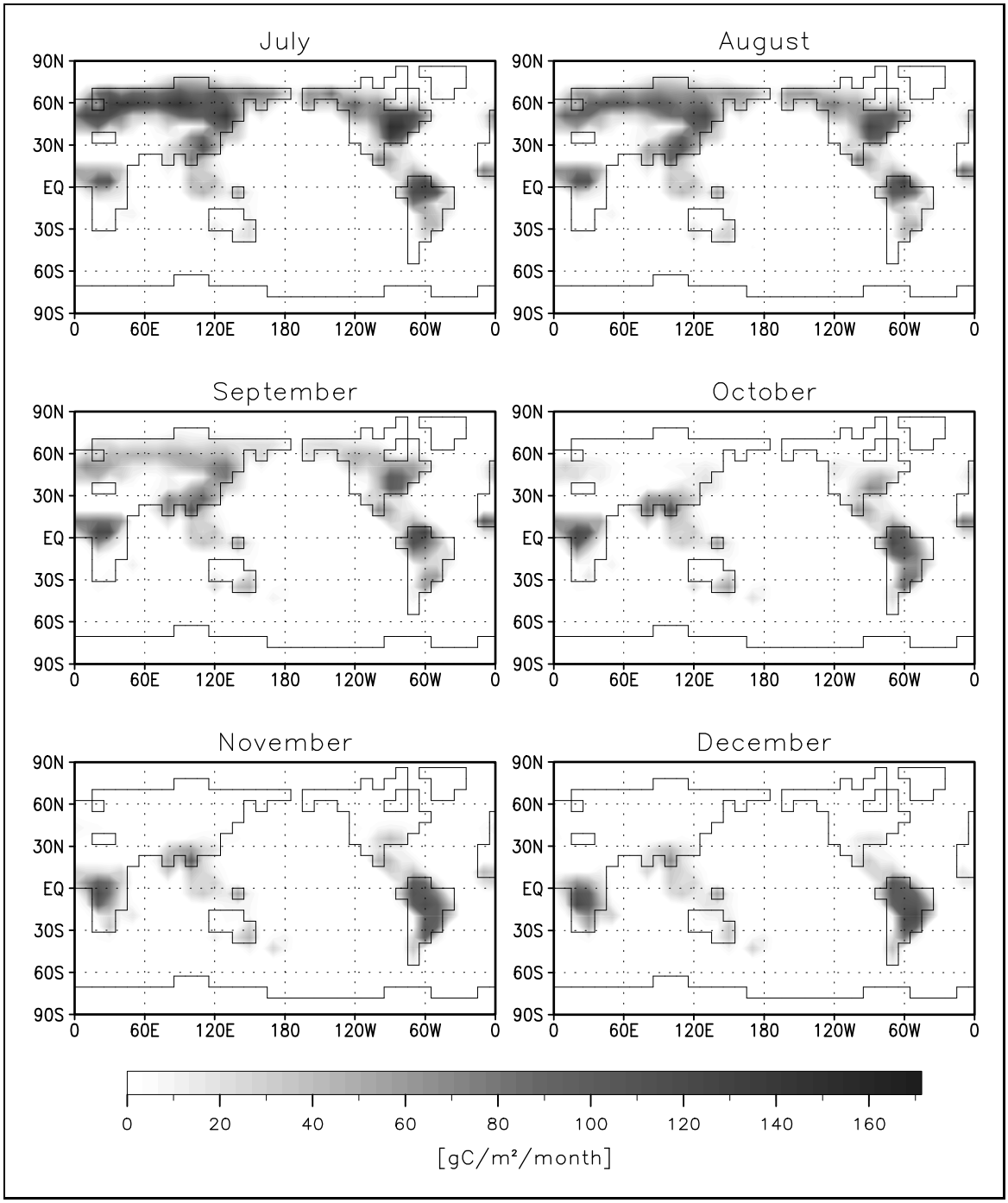
July
August
September
October
November
December
90N
60N
30N
EQ
30S
60S
90S
0
60E
120E
180
120W
60W
0
0
20
40
60
80
100
120
140
160
[gC/m²/month]

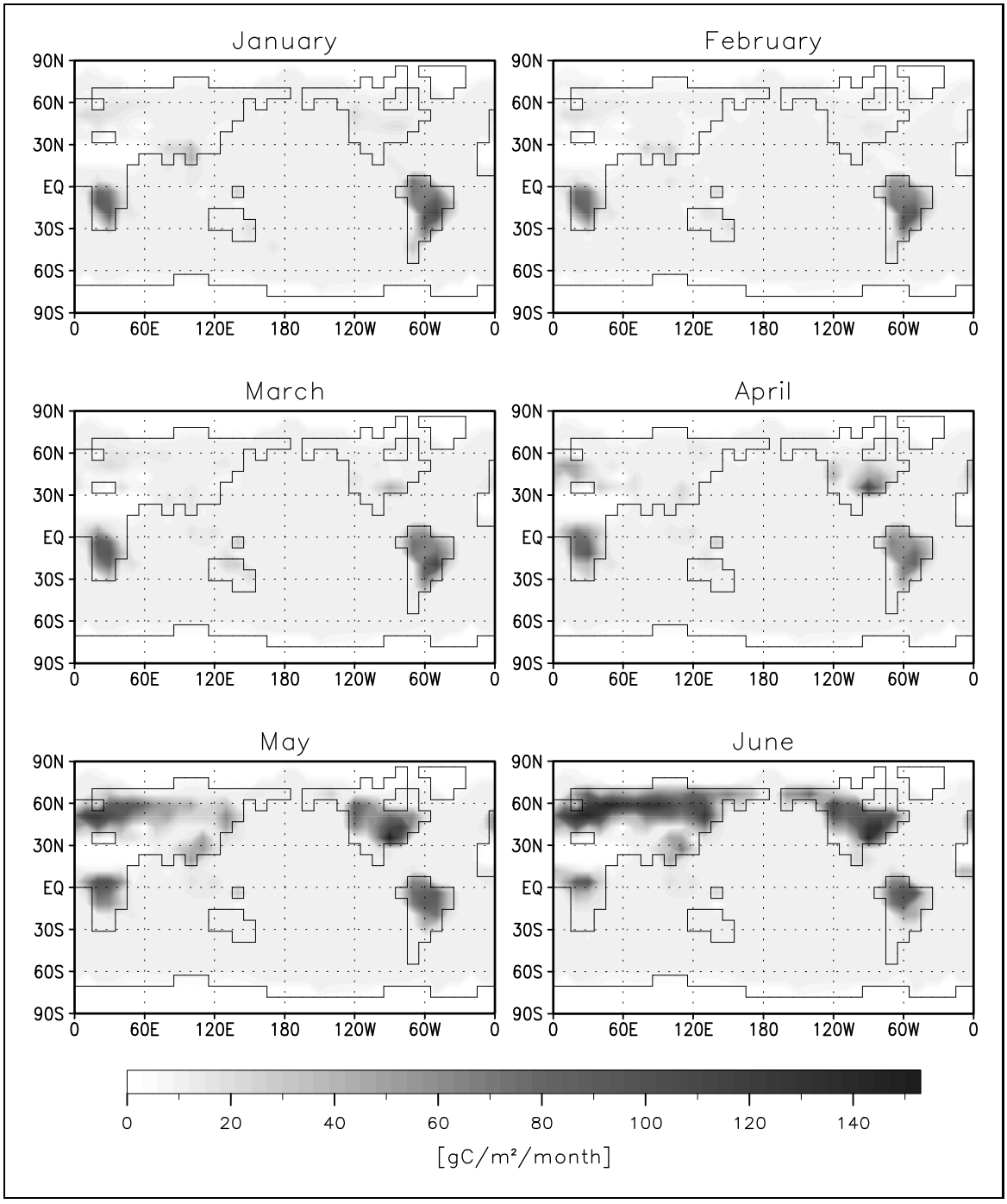

Figure 15: *A priori uncertainties of the sum of the flux contributions from terrestrial biosphere and ocean.*

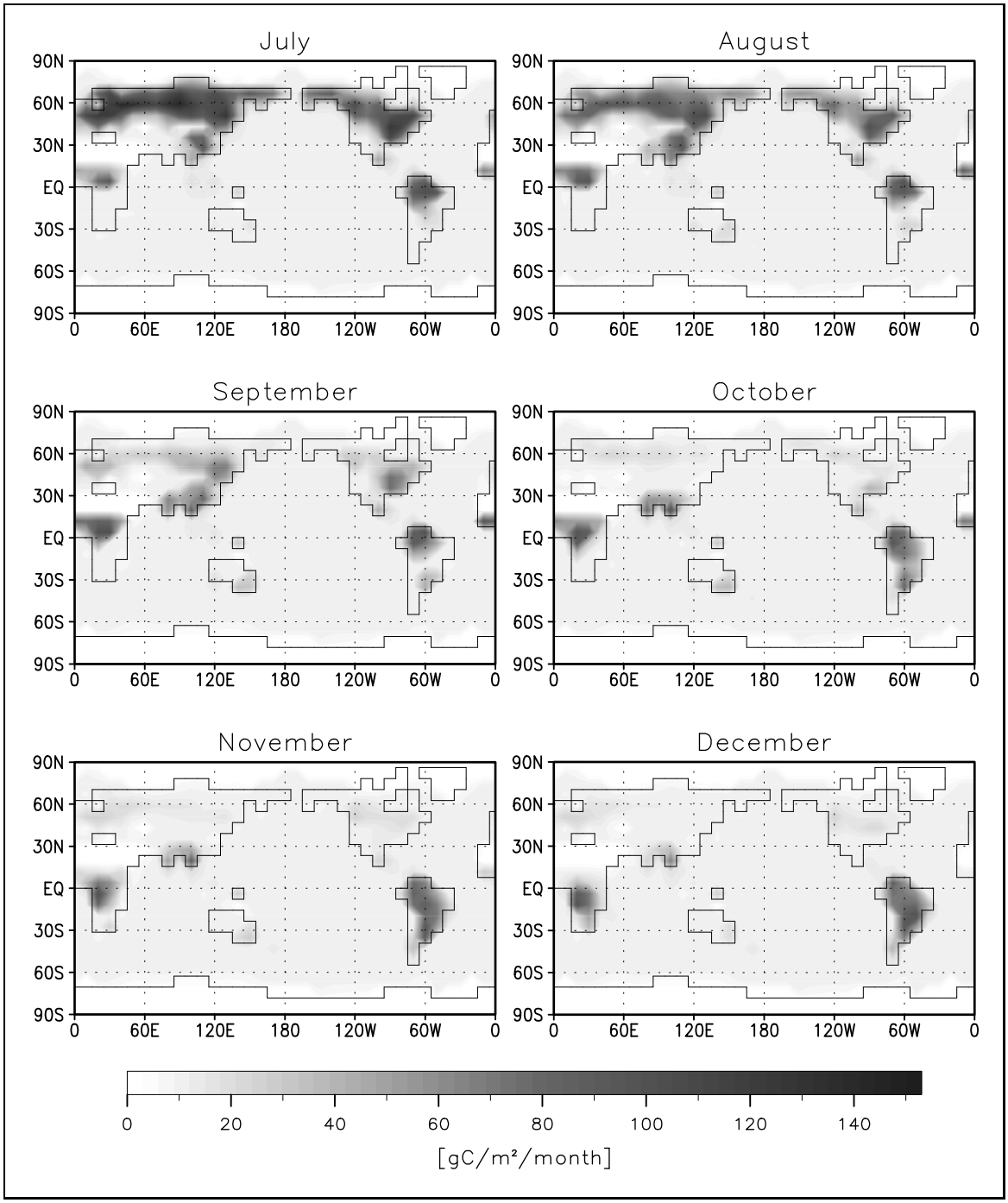
July
August
September
October
November
December
90N
60N
30N
EQ
30S
60S
90S
0
60E
120E
180
120W
60W
0
0
20
40
60
80
100
120
140
[gC/m²/month]

5.3 A Priori Concentrations

Globalview - CO_2 is a database of high quality atmospheric measurements coordinated by the NOAA/CMDL. The observational net comprises more than 60 sites, for which smoothed weekly data together with an estimate of their uncertainties have been prepared [*Globalview–CO2*, 1996]. In order not to be affected by problems of intercalibration between different networks, we have restricted the data to those measured in the NOAA laboratory. As discussed in Sect. (2), our model is appropriate to simulate the mean quasi-stationary seasonal cycle for a target period of a few years. In their study *Tans et al.* [1990] interpreted the observations from 1981 to 1987. We choose a similar target period from January 1981 to January 1987 excluding the El Niño year 1987. For this target period data from the 25 NOAA sites displayed in Fig. (2) were available. Unlike *Tans et al.* [1990] we have not excluded data from any particular site of the network like the mountain stations MLO and NWR. We have not used the version of the data set in which temporal gaps in the records have been closed by statistical procedures.

For comparison with our model, we extract from the observations the quasi-stationary seasonal cycle: At every station S and every month i in the target period, the mean concentration $c_{S,i}$ together with its uncertainty are computed. To quantify a periodic and a trend component, we employ a statistical model similar to (Eq. (1)):

$$c_{S,i} = c_{p,S,i} + b \cdot t_i + N_{S,i} = S_{S,i} + b \cdot t_i + \tilde{a}_S + N_{S,i} \quad . \tag{18}$$

Again, the periodic component c_p is decomposed into a periodic function S_S with zero mean and an offset $\tilde{a}_S$. For the observations, however, the offset in turn can be considered as the sum of two terms: The global mean concentration $\bar{c}_0$ at the beginning of the target period, and the spatial gradient a_S. The second term is the contribution of a global linear trend, where t_i is the length of the time interval from the beginning of the target period to the middle of the $i-$th month. The noise term $N_{S,i}$ can be attributed to deficiencies in the transport model as well as interannual variations in the fluxes and the transport, since these are not resolved by our model setup. The quantities c_p and b are estimated by a least squares fit together with their uncertainties.

To compare modeled (Eq. (7)) and observed quasi-stationary seasonal cycles, to the modeled periodic component the unknown global mean concentration $\bar{c}_0$ at the beginning of the target period has to be added:

$$b = \alpha \cdot \bar{f} \tag{19}$$

$$c_p = \bar{c}_0 + Tf - t \cdot \alpha \cdot \bar{f} \quad . \tag{20}$$

Including the $\bar{c}_0$ term in the matrix M of Eq. (9) and extending f by one "pseudo flux" component for $\bar{c}_0$, the unknowns are related to the observations by

$$c_{cgt} = Mf \quad . \tag{21}$$

As mentioned in Sect. (5.2), in the inversion we want to consider the fossil fuel component in the fluxes f_f as known, because its uncertainty is much smaller than the uncertainty of the oceanic and biospheric component. Due to linearity of Eq. (9), from the observations we can subtract the modeled quasi-stationary seasonal cycle component at the station locations resulting from the fossil

fuel source Mf_f. Eventually, we interpret f in Eq. (21) as the sum of the oceanic and biospheric components and c_{obs} as the observed response of the concentration.

For the data covariance matrix C_c in Eqs. (A.2) and (A.3), we assume a diagonal structure, i.e. there are no correlations among uncertainties of different observations. The fit to the observations yields estimates of the uncertainties of c_p and b. Another uncertainty, however, results from our model setup not taking account of the interannual variations of the transport. This uncertainty is estimated by computing 12 mean residue, one for each month. Since the residue are due to the interannual variation of both fluxes and transport, and our model only neglects the variation of the transport, this estimate can be considered as an upper limit of the resulting error. We compose the variances of c_p as the sum of the variances from the fit and the respective variance of the residue. The first contribution can be interpreted as a mixture of model error and observational error, while the second quantifies a model error. For the result of the inversion, however, this distinction is not important, since model error and observational error enter Eq. (A.2) only by their sum. The fossil fuel component in the fluxes is uncertain as well. The IPCC [*Houghton et al.*, 1995b] estimates a 90% confidence interval of $\pm$ 10% from the global annual mean flux. For convenience, we do not assume an uncertainty in the pattern of the emissions. Thus, the resulting variances in the simulated fossil fuel component in the quasi-stationary seasonal cycle can be easily computed and added to the estimates derived above.

In our inversion, we consider the global mean concentration $\bar{c}_0$ at the beginning of the target period as unknown. In order to allow for a high flexibility, we assume the extremely high uncertainty of $\pm$ 1000 ppmv. The prior estimate is derived from the fit to the observations (see Eq. (1)) by computing the mean offset $\tilde{a}$ for all stations. The trend b is 1.41 ppmv/year. The uncertainty from the fit is negligibly low, so that as prior uncertainty we assume the contribution from the uncertainty of the fossil fuel emissions which is 0.16 ppmv/year.

Fig. (16) shows the observed and modeled quasi-stationary seasonal cycles for 1981. The observations and their uncertainties have been composed of the fit as described above. Two versions of the modeled quasi-stationary seasonal cycle are displayed: The first results from the prior estimate of the fluxes, which have been described in Sect. (5.2). The second results from the posterior estimate of the fluxes determined by the inversion. They will be discussed in Sect. (5.5).

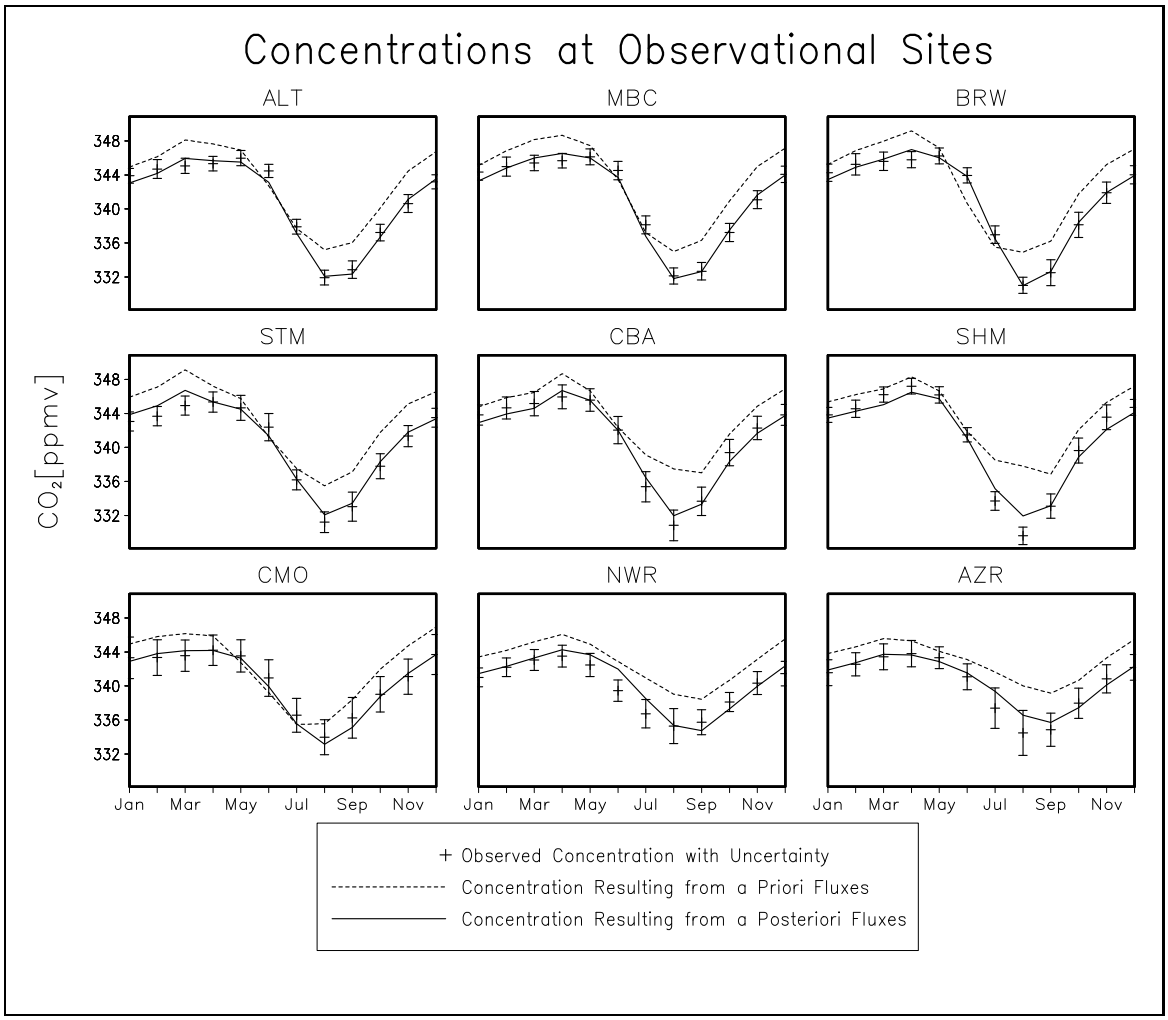

Figure 16: *Observed concentration with mean quasi-stationary seasonal cycle for the first year of the target period, 1981. Error bars reflect observational uncertainties as well as uncertainties due to interannual variations. Modeled concentration resulting from a priori and a posteriori estimates of fluxes; see Fig. (2) or Table (2) for station locations.*

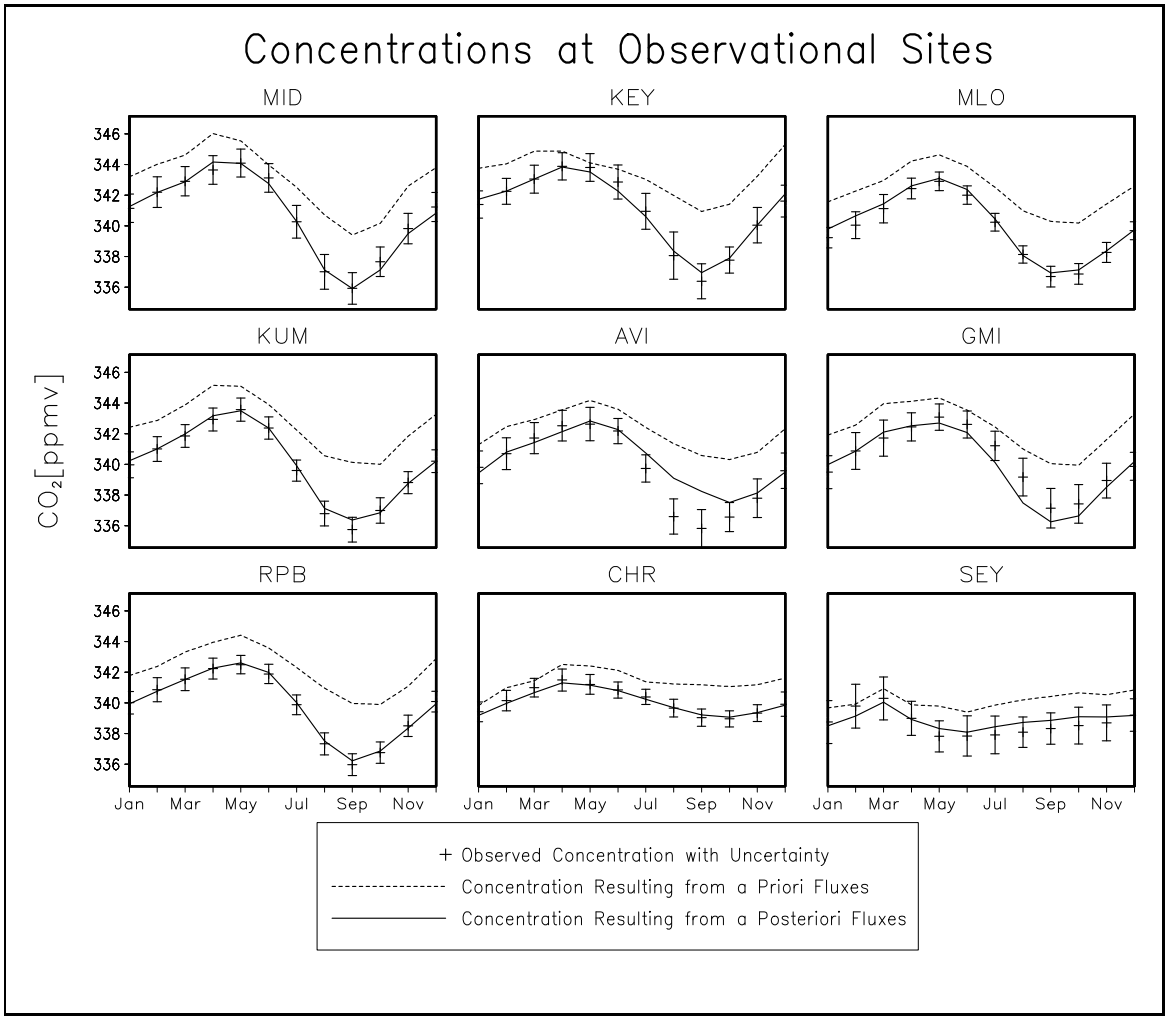
Concentrations at Observational Sites
MID
KEY
MLO
KUM
AVI
GMI
RPB
CHR
SEY
CO2[ppmv]
346
344
342
340
338
336
Jan
Mar
May
Jul
Sep
Nov
+ Observed Concentration with Uncertainty
Concentration Resulting from a Priori Fluxes
Concentration Resulting from a Posteriori Fluxes

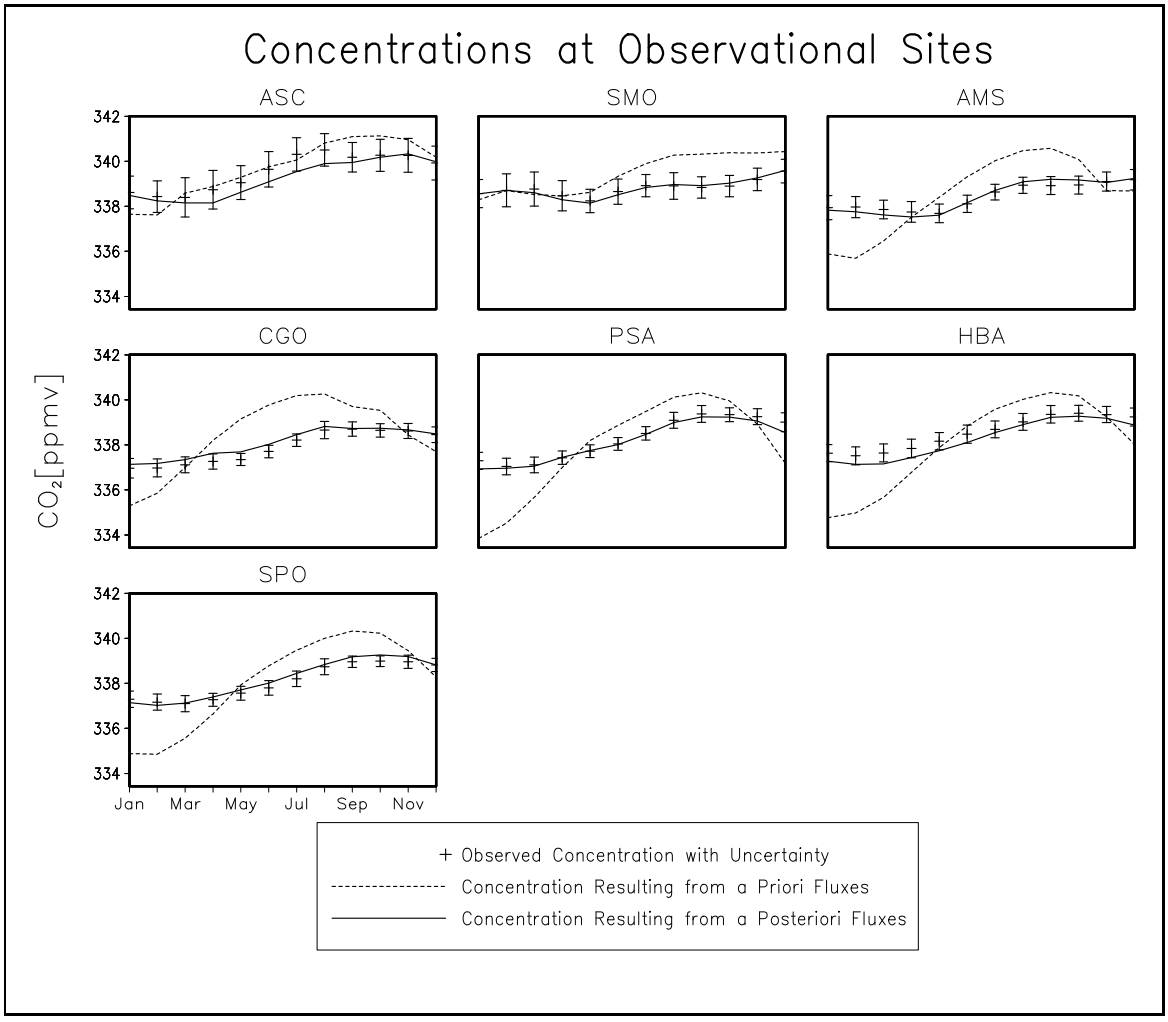
Concentrations at Observational Sites
ASC
SMO
AMS
CGO
PSA
HBA
SPO
342
340
338
336
334
CO2[ppmv]
Jan
Mar
May
Jul
Sep
Nov
+ Observed Concentration with Uncertainty
Concentration Resulting from a Priori Fluxes
Concentration Resulting from a Posteriori Fluxes

5.4 Singular Value Decomposition

The information on the atmospheric transport is combined with atmospheric observations and the a priori information on the fluxes according to Eq. (A.3). Technically, the basis of our inversion consists of a Singular Value Decomposition (SVD) of the model matrix M in Eq. (21). Since the SVD is derived e.g. in *Menke* [1989] and well described e.g. in *Press et al.* [1986], we only give a brief summary. The aim of this subsection is to show how the SVD is applied to our problem.

In the spaces of fluxes and concentrations, by an SVD two sets of n_c basis vectors are derived, with respect to which the matrix M is diagonal: the right hand singular vectors and the left hand singular vectors. The diagonal elements are called singular values. The left hand singular vectors span the complete space of concentrations, while the right hand singular vectors only span a subspace of the space of fluxes. Arranging the associated singular vectors column by column in two matrices, U for the left hand singular vectors and V for the right hand singular vectors, and the singular values on the diagonal of a third matrix D, so that the associated singular vectors and values are in the same position within their respective matrices, our matrix M can be expressed as

$$M = UDV^T \quad , \tag{22}$$

where V^T is the transposed of V.

Requiring orthonormality of the singular vectors and non negativeness of the singular values defines the singular values uniquely. U, D, and V are almost uniquely defined:

- Permutations simultaneously changing the order in all three matrices are possible.
- The singular values do not necessarily differ from each other (The identity matrix represents a pathological example). Simultaneous rotations of right hand and left hand singular vectors within the subspaces corresponding to the same singular value are possible, because these rotations do not disturb the orthonormality. For one-dimensional subspaces, i.e. for singular values appearing only once in D, such a rotation degenerates to a simultaneous flip of the signs of both, the associated left hand and right hand singular vectors.

Through the orthonormality condition, the SVD depends on the units in the spaces of fluxes and concentrations. As units in both spaces we choose multiples of the prior uncertainties, i.e. the prior covariance matrices are represented by the respective identity matrices, both of which, for convenience, we denote by 1. For the only units being intrinsic to the problem are the prior uncertainties; we will refer to them as natural units. In these units, a unit change of a flux component has much higher impact on the simulated concentrations, if this flux component has a high prior uncertainty. Consequently, the right hand singular vectors associated to the highest singular values tend to be dominated by flux components with high uncertainty. Apart from this, flux components that, due to atmospheric transport, have a high impact on the concentrations at one or several stations project well on the right hand singular vectors corresponding to the highest singular values. Those flux components are well observable by the network.

The SVD of M is carried out by a library routine from NAGLIB [*NAGLIB*, 1987]. Fig. (17) shows the spectrum of singular values of M in descending order. Except for the first singular value, which is by three orders of magnitude higher than the second one, the spectrum is concentrated on

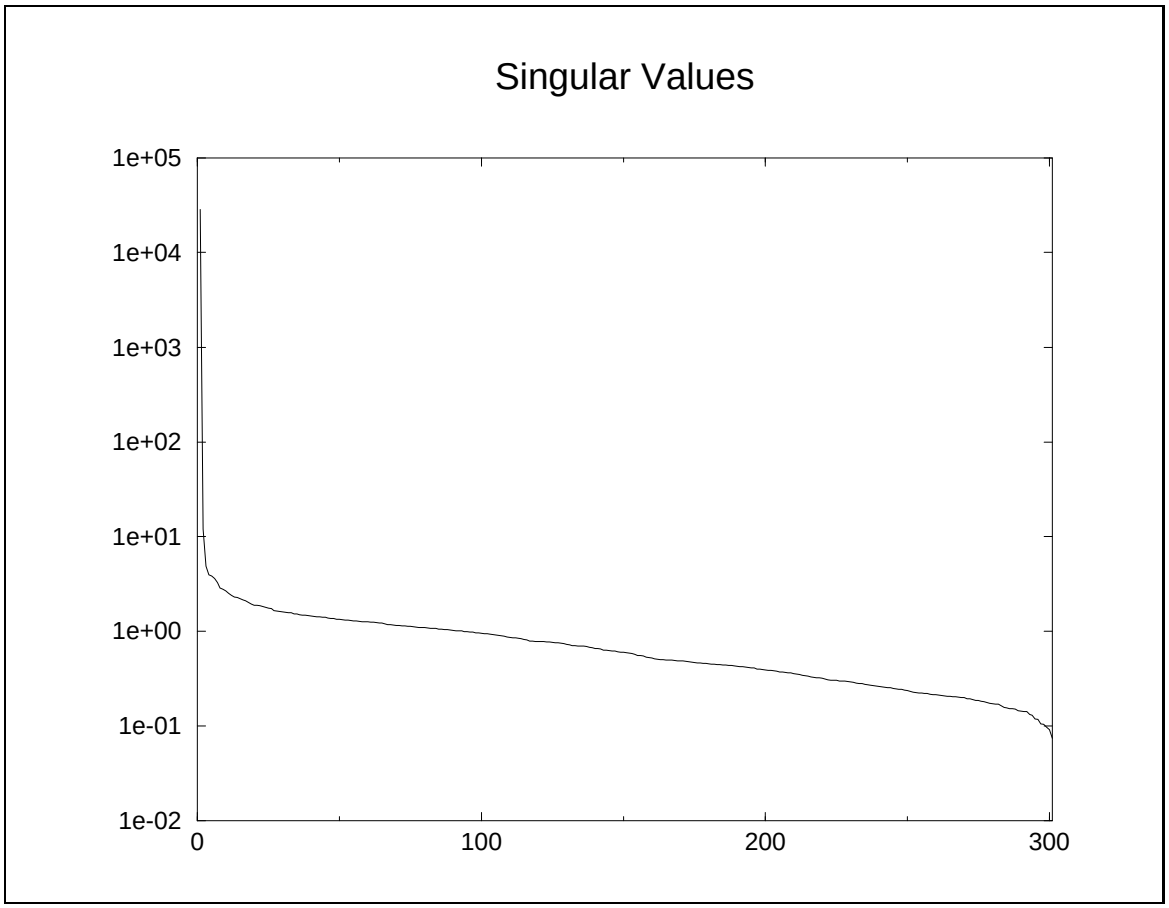

Figure 17: *Spectrum of Singular Values.*

a relatively small interval on the positive axis: The difference between the second largest and the smallest singular values is less than three orders of magnitude. In particular, none of the singular values is zero, because the accuracy of our routine is higher than these 5–6 orders of magnitude. Hence, the following three equivalent statements hold: (i) Our matrix M has full rank, i.e the rows are linearly independent. (ii) The space spanned by the right hand singular vectors is perpendicular to the null space of M (denoted by $N(M)$) being defined as the subspace of the space of fluxes formed by all f with $Mf = 0$. (iii) The range of M is the entire space of concentrations. Using the terminology of *Menke* [1989], our inverse problem is not overdetermined, since for any vector of observations at the stations, we can find a flux vector, that satisfies Eq. (9), i.e that yields a consistent vector of simulated concentrations. In other words, the observations cannot contradict each other. But, of course, the problem is underdetermined: Together with one flux field satisfying Eq. (9) comes a whole $n_f - n_c$ dimensional subspace of flux vectors that satisfy Eq. (9) (All flux vectors satisfying Eq. (9) differ by a vector in $N(M)$).

In the SVD all quantities of interest are expressed most naturally and most conveniently in natural units. According to Eqs. (A.2) and (A.7), the posterior covariance matrix takes the form

$$C_f^{'} = C_f - R_m = 1 - R_m = 1 - V\frac{D^2}{1+D^2}V^T \quad , \tag{23}$$

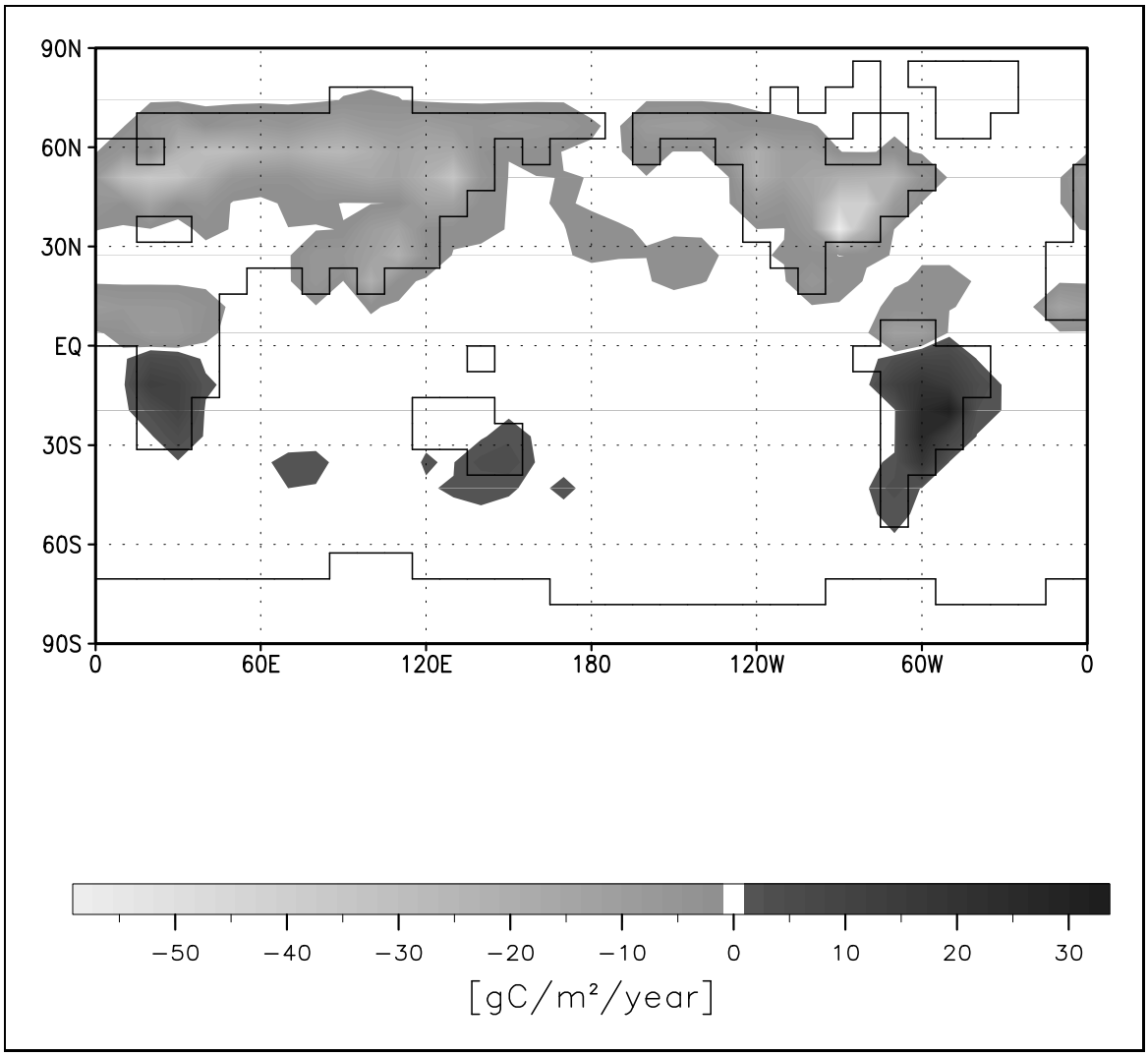

Figure 18: *Annual mean fluxes computed from the second right hand singular vector.*

where R_m is our notation for the model resolution matrix. Thereby we exploit that $VV^T f = 0$ for all f in $N(M)$. In the directions of the right hand singular vectors corresponding to the highest singular values, the uncertainty of the fluxes is most efficiently reduced. As explained above, those singular vectors are dominated by flux components with high uncertainty. This is consistent within the Bayesian framework, because it is easier to improve the degree of knowledge about those components that a priori are most uncertain. In $N(M)$, the uncertainty is not reduced at all. Of course, it is interesting to see which directions in the space of fluxes are constrained by the observations and how well they are constrained. The first singular value is about 28400. The corresponding right hand singular vector is dominated by a component of 1000 ppmv for the correction of the global mean concentration at the beginning of the target period, which we introduced as additional unknown in Sect. (5.2); all flux components are close to zero with a global annual mean flux of $-1.3 \cdot 10^{-4}$ GtC. The corresponding left hand singular vector consists of a uniform concentration of about $3.52 \cdot 10^{-2}$ ppmv; the trend component is extremely small. These

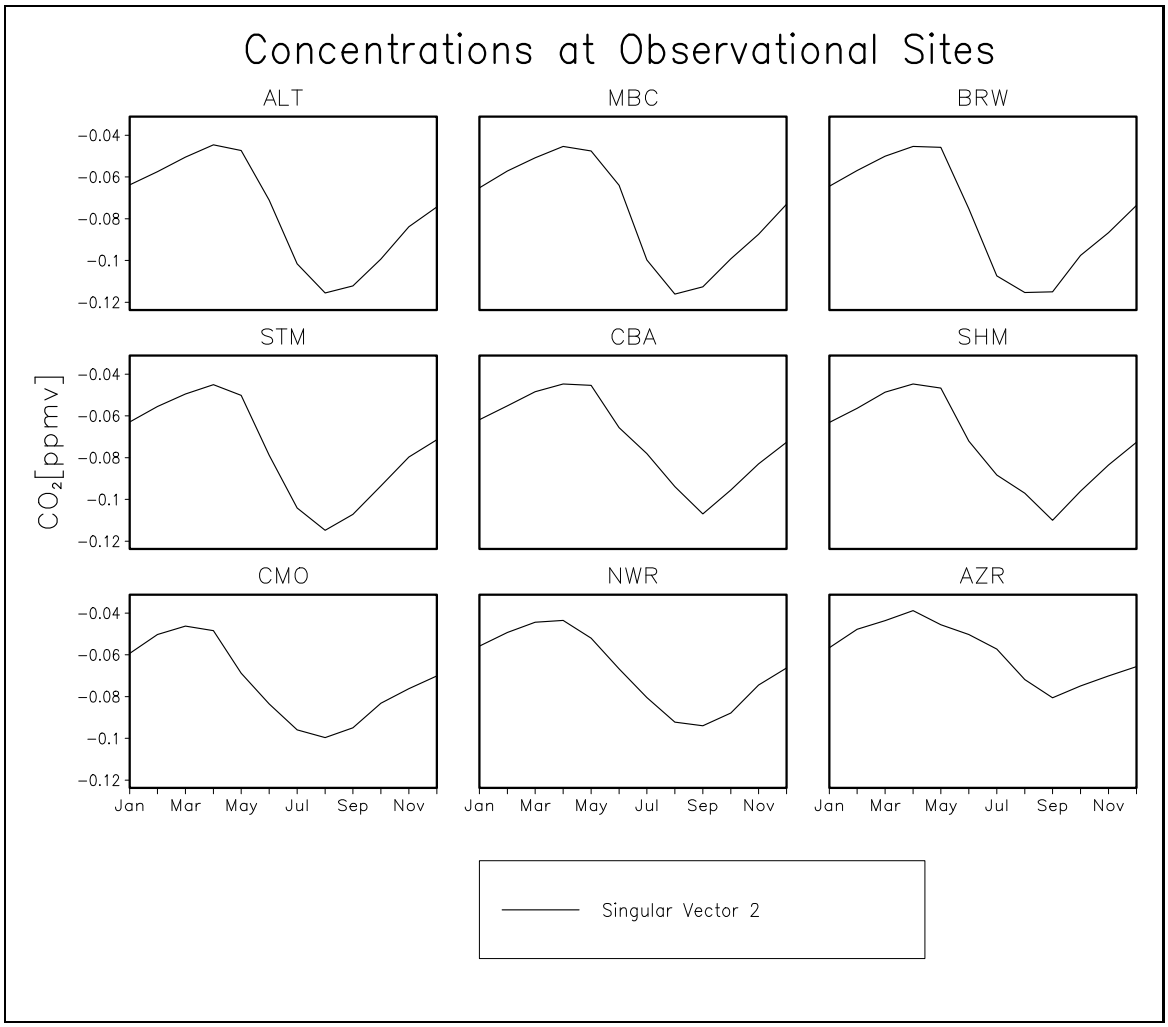

Figure 19: *Concentrations at the station locations contained in the second left hand singular vector.*

numbers are consistent: Multiplying M by this right hand singular vector according to Eq. (22) yields $3.52 \cdot 10^{-2}$ ppmv $\times$ 28400 $\approx$ 1000 ppmv, which corresponds to the 1000 ppmv correction of the initial concentration component. According to Eq. (23), the uncertainty in the direction of the first right hand singular vector is about $\frac{1}{1+28400^2} \approx 10^{-9}$ natural units. The second singular value is 12. The component of the global mean concentration is −0.2 ppmv; the annual mean flux (see Fig. (18)) is positive in the southern hemisphere and negative in the northern hemisphere with a global mean of −0.6 GtC. The concentration (see Fig. (19)) is positive at the southern hemisphere stations and negative at the northern hemisphere stations; the trend component is only −0.02 ppmv/year. This singular value is mainly associated to the north-south gradient of the concentration. Its posterior uncertainty is of order 10^{-2} natural units. The next few singular values are primarily associated with the seasonal cycles in the fluxes and the concentrations. The remaining singular values range from 4.9 to 0.074, so that their posterior uncertainties range from 0.040 to 0.99 natural units. A detailed discussion of all singular values and vectors is far beyond the scope of this thesis.

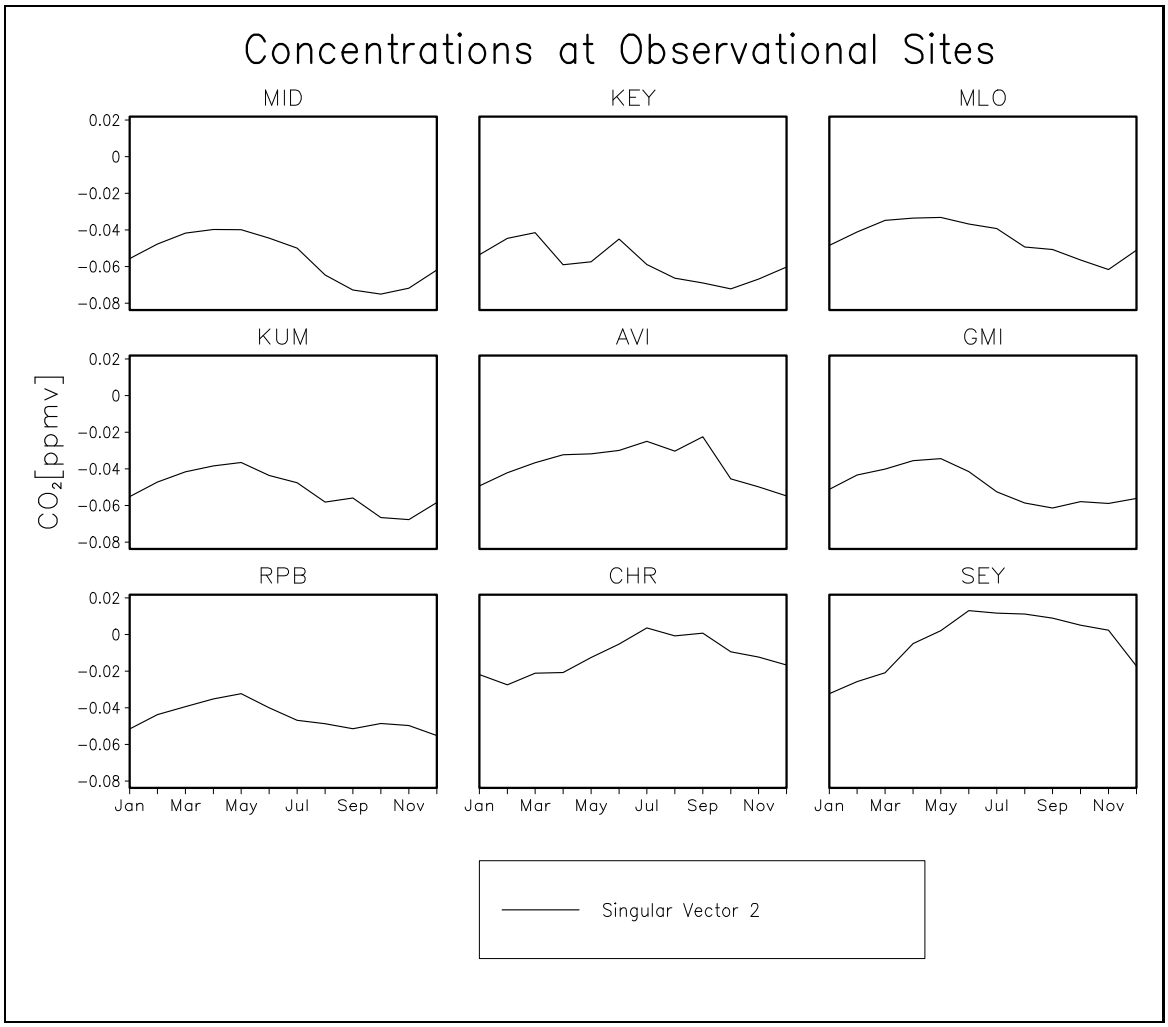

According to Eq. (A.3), the inverse is

$$M^{-1} = V \frac{D}{1+D^2} U^T \quad : \tag{24}$$

A misfit between observed and modeled concentrations yields a correction in the subspace of fluxes that is perpendicular to $N(M)$. The atmospheric data do not add any information to $N(M)$. A misfit in the direction of a left hand singular vector that is associated to a low (high) singular value yields a large (small) correction of the fluxes in the direction of the associated right hand singular vector. For the largest, the second largest, and the smallest singular value, these amplification factors $D/(1+D^2)$ take the values $3.52 \cdot 10^{-5}$, $9.01 \cdot 10^{-2}$, and $7.39 \cdot 10^{-2}$, respectively.

Without the stabilizing effect of the a priori information, being reflected by the 1 in the denominator of Eq. (24), the amplification factor would be the pure reciprocal of the singular value. Systematic errors projecting well on the left hand singular vectors associated to small singular values would be subject to tremendous amplifications. In this situation, the spectrum of singular values usually is truncated to get rid of these "nuisance" directions at the cost of reducing the subspace of the space of fluxes that can influence the concentrations [*Menke*, 1989; *Enting*, 1993; *Brown*, 1995].

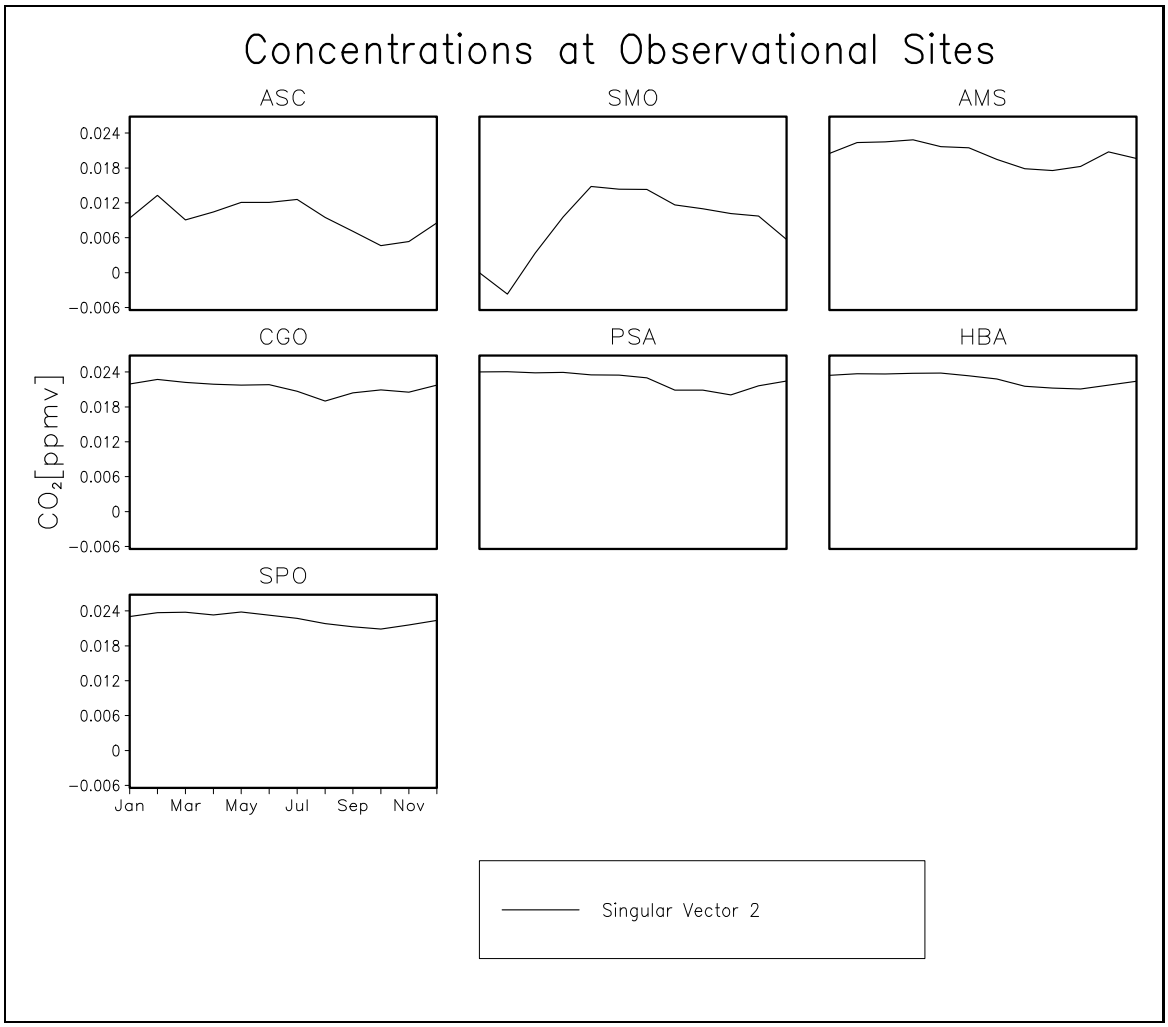

In the direction of a particular right hand singular vector, the reduction of variance and the adjustment of the fluxes by the inversion are coupled through the corresponding diagonal factors in the SVD. The adjustment, however, also depends on the misfit in the direction of the corresponding left hand singular vector. If this misfit is small, the variance is reduced without any adjustment.

5.5 A Posteriori Fluxes

The a posteriori probability distribution in the space of fluxes is Gaussian (see Sect. (A)) and thus can be represented by its mean and its covariance matrix. The dimensions of our problem make a discussion of the full covariance matrix difficult, similar to the discussion of all singular vectors in Sect. (5.4), which is another representation of the a posteriori probability distribution.

Single components of the flux vector, spatial or temporal means, however, are easier to discuss. Since they are derived from the flux vector by linear projections, their one-dimensional probability distributions are Gaussian as well. The centers of these distributions are our best estimates of the respective quantities; we will refer to these centers as posterior values. The variances of these distributions quantify the uncertainties of the respective estimates. The square roots of the variances are the standard deviations; we will refer to them as posterior uncertainties. One must keep in mind that a loss of information is the cost of this compression by projections.

Fig. (20) shows the a posteriori sum of the terrestrial and oceanic flux components. The predominant feature is the seasonality of the land components: On the northern hemisphere, beginning in May at the mid latitudes and in June at the high latitudes, the terrestrial biosphere acts as a sink. From September in the high latitudes and October in the mid latitudes, in contrast, CO_2 is released by the biosphere. The fluxes over India exhibit a different seasonality: They are positive from April to August and negative from September to February. In the Tropics there is release in winter and uptake in summer and autumn: Between the northern and the southern hemisphere the phases are shifted by 6 months. In the South American mid latitudes the phase of the fluxes is opposite to the one in the northern mid latitudes. Australia has a peculiar seasonality: Its phase is similar to the northern hemispheric phase. Over the ocean the seasonality is less pronounced. In the Southern Ocean there is uptake from November to February and a slight release from April to July. From December to May the North Atlantic is a slight sink.

In the annual mean (Fig. (13)) there is a substantial terrestrial sink in the northern mid latitudes contrasted by a small source in the northern high latitudes. The African tropics are a sink, while the South American tropics exhibit a spatially alternating source-sink pattern. Australia is a small sink. The ocean takes up CO_2 in most regions. the Equatorial Pacific, however, is a strong source, and the South Atlantic and the Southern Ocean at high latitudes are a smaller source. In addition, localized sources are induced in the neighborhood of some of the stations (Cape Meares in Oregon, Point Barrow in Alaska), and localized sinks are induced around Cape Grim in Tasmania and Hawaii. Fig. (22) shows the zonal means; the global annual mean sink is 2.3 ± 0.3 GtC.

To understand the behavior of the inversion procedure in detail, it is convenient to consider the cost function introduced in Eq. (17). The optimal flux field minimizes the sum of two contributions: the deviation of the posterior fluxes from the prior fluxes and the misfit between modeled and observed concentrations. Thereby the prior uncertainties are weighting factors. Fig. (16) shows the observed quasi-stationary seasonal cycle as well as the simulations with the prior and the posterior fluxes. In Fig. (21), the difference of the posterior and prior fluxes is displayed. A priori, the global annual mean flux is 0.0 ± 1.5 GtC. To match the global trend, however, a net sink of 2.3 GtC is needed. To achieve this, the inversion procedure tends to reduce those flux components with relatively high uncertainty, because the corresponding deviation of the prior estimate has a small weight in the cost function. According to the spatial distribution of the prior uncertainties (see

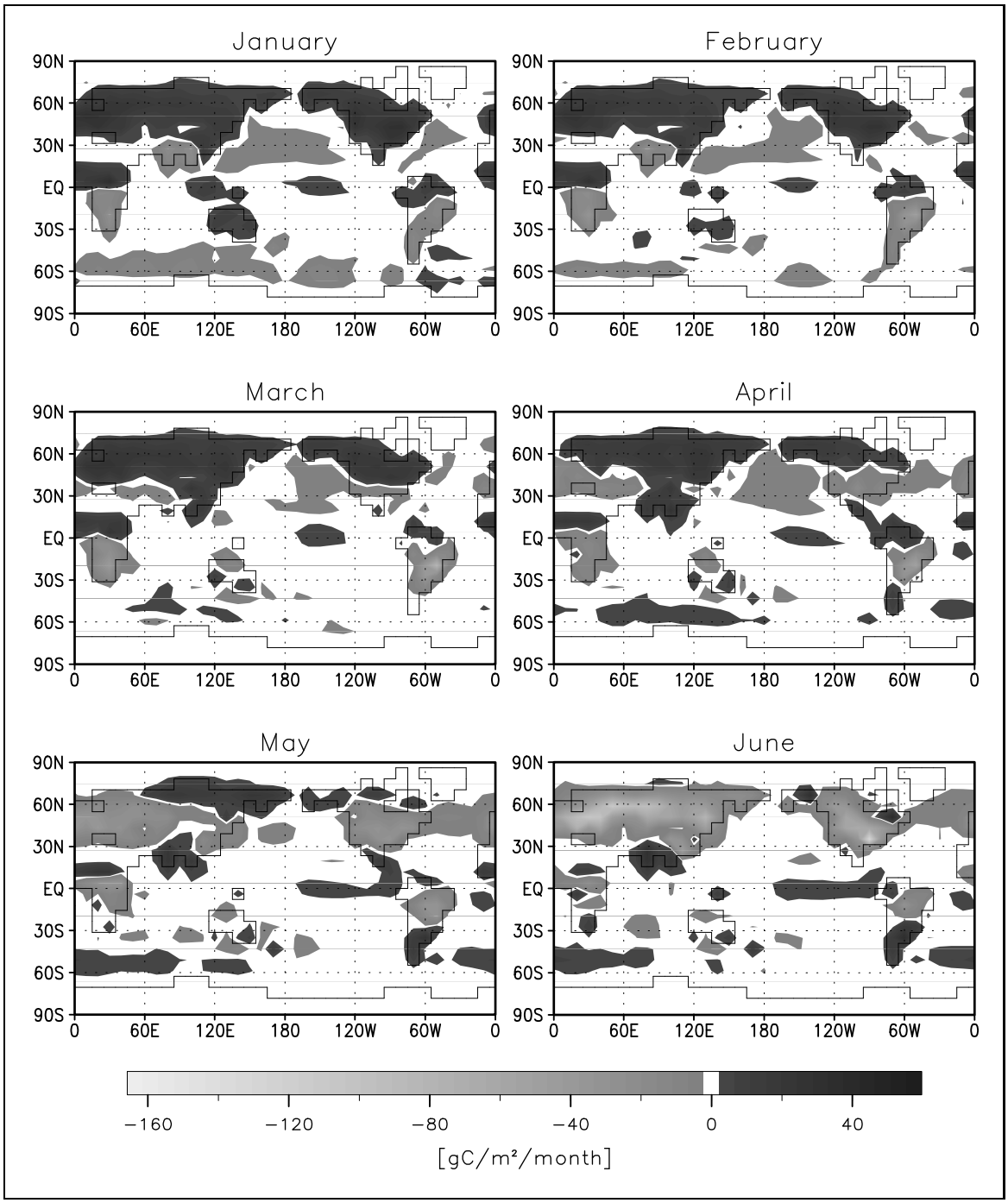

Figure 20: *A posteriori sum of the terrestrial and oceanic flux components.*

Fig. (12)), this criterion favors primarily terrestrial locations for adjustments. At which locations the fluxes are actually adjusted is determined by the spatio temporal variations in the observed concentrations.

In January 1981, the beginning of the target period, the inversion yields a global mean concentration of 338.9 ± 0.1 ppmv, which is by 0.4 ppmv smaller than the prior value. This difference can

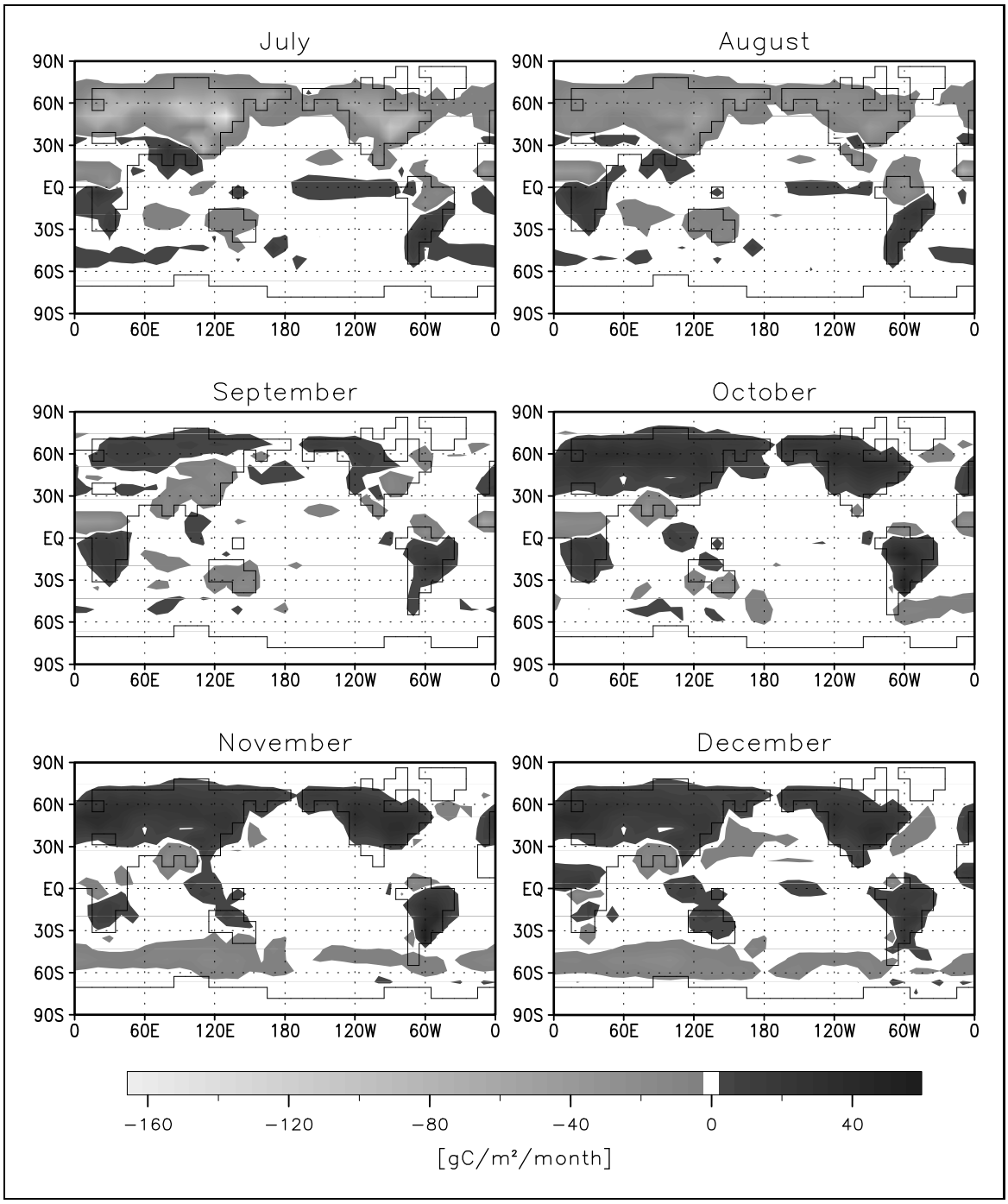

be clearly attributed to the higher weight of the northern hemisphere in the computation of the prior initial global mean concentration, which is caused by inhomogeneity of the network. Due to an extremely high uncertainty of 1000 ppmv, the inversion procedure was essentially free to choose the initial concentration to match the observations. Even after subtracting this small offset from the concentrations resulting from the prior fluxes displayed in Fig. (16), in the northern hemisphere these concentrations are too high. In contrast, at the southernmost stations these concentrations are slightly too low. To flatten this north-south gradient, the inversion procedure enhances the

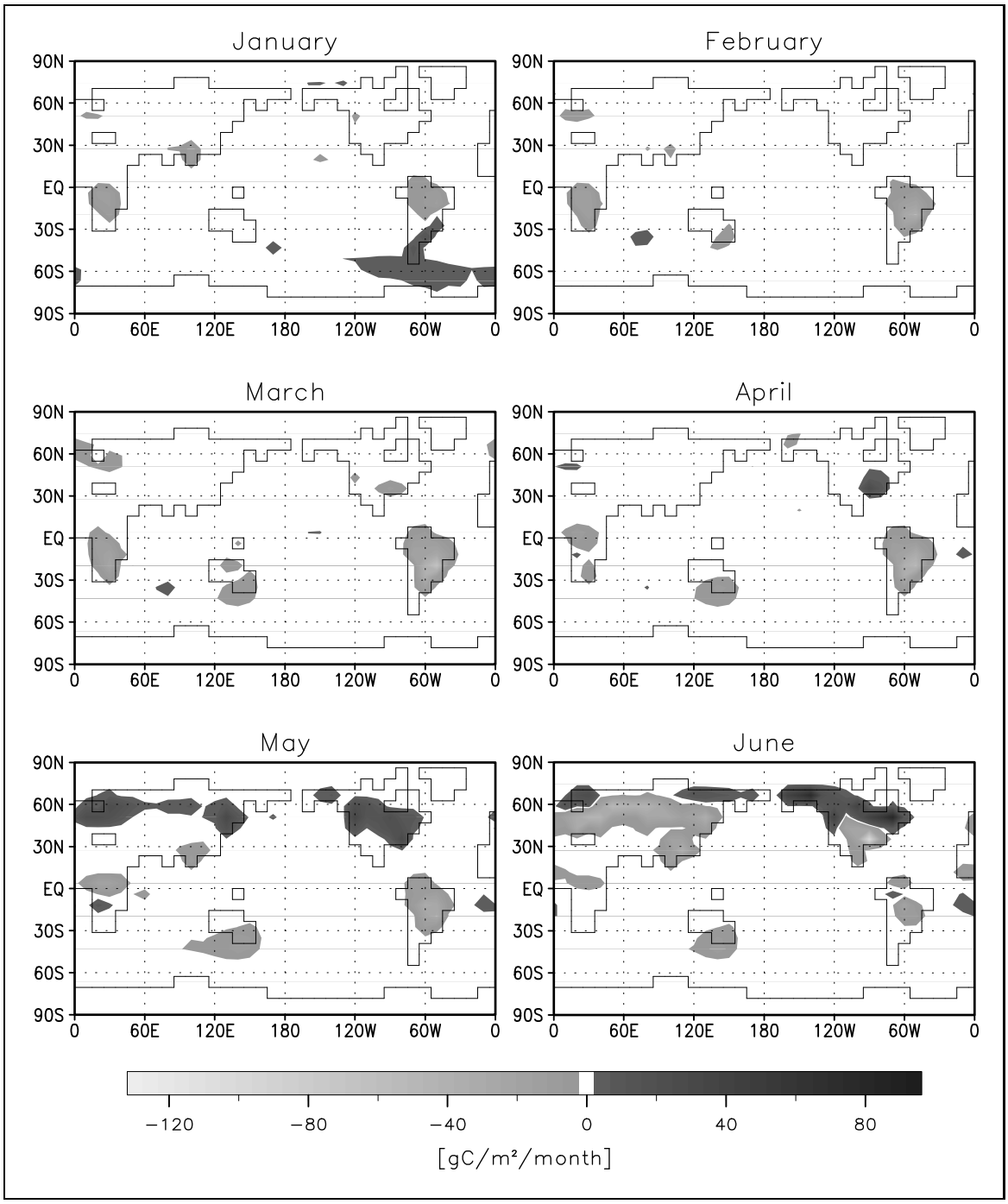

Figure 21: *Seasonal cycle of the difference of the a posteriori and a priori flux estimates; positive values quantify an enhanced source or a reduced sink.*

net sink in the north and reduces the net sink in the south, which is obvious from a comparison of the posterior and prior zonal mean fluxes that are depicted in Fig. (22). Thereby the largest adjustments (see Fig. (13)) are performed in terrestrial regions with high NPP, soil respiration, or land use change fluxes, because of the corresponding high a priori uncertainty as explained above.

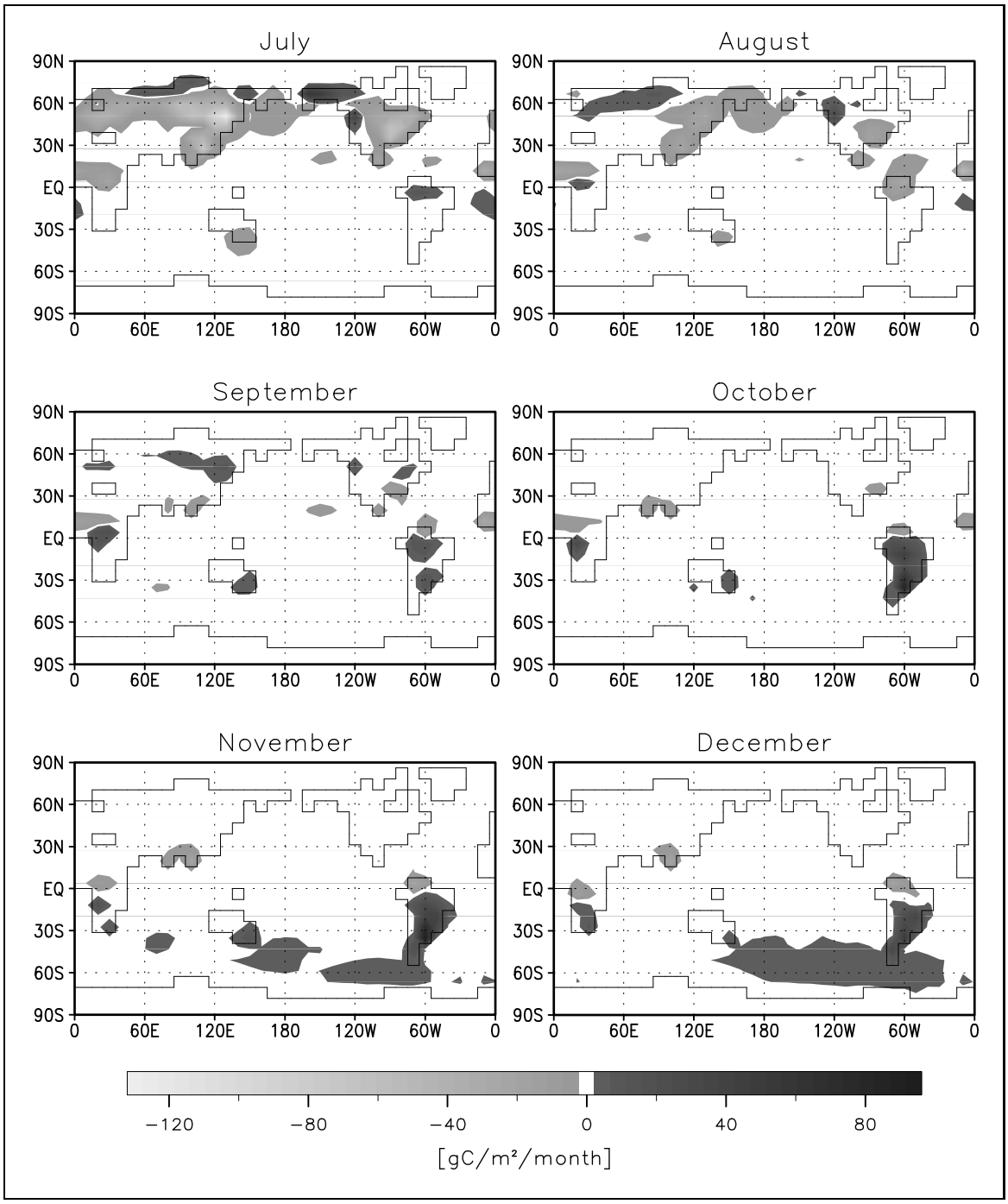

A fraction of this adjustment also can be attributed to an enhanced uptake by the northern oceans, which will be discussed in Sect. (5.7).

Besides these global scale features, at a couple of stations in the phase and the amplitude of the seasonal cycle, there are mismatches between observed concentrations and those concentrations simulated with the prior fluxes. To improve the match, it is optimal, in terms of the cost function (Eq. (17)), to correct the fluxes locally at the grid cells and months in which the impact of the

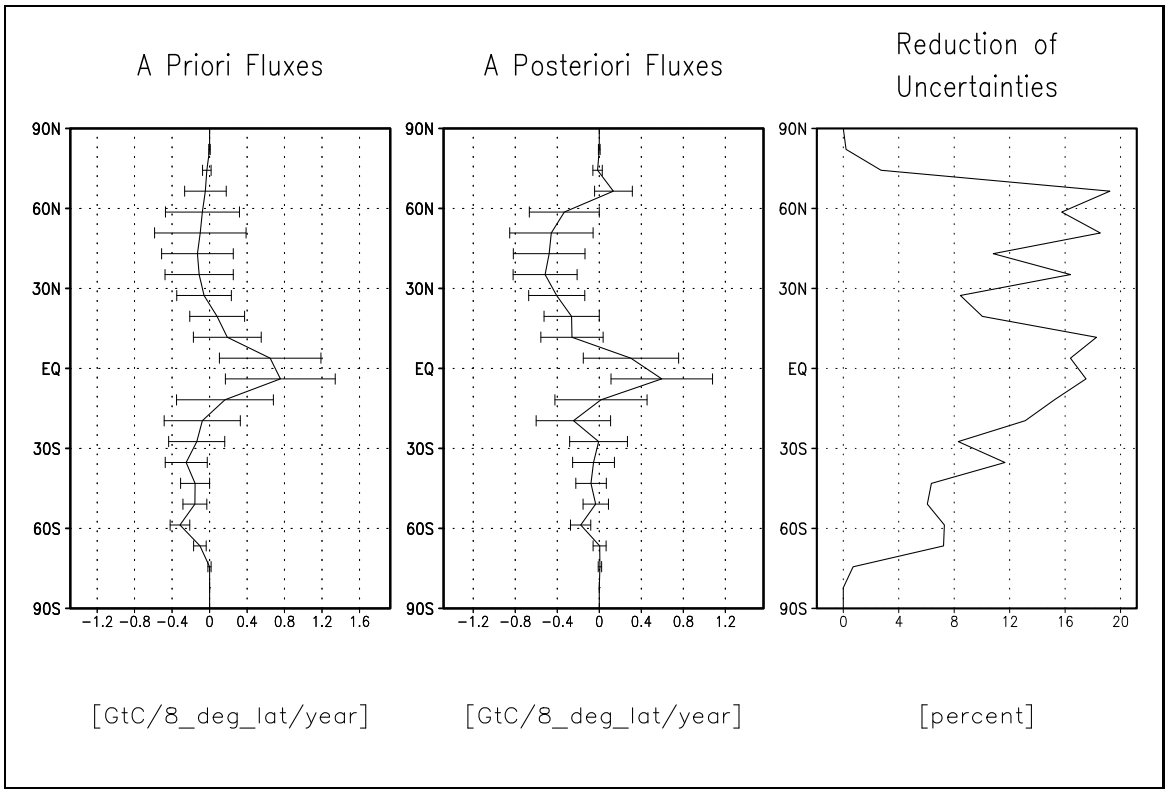

Figure 22: *A priori and a posteriori uncertainties for the zonal and annual mean of the sum of the biospheric and oceanic flux components and the difference of their quotient from 1 in %. Values close to 100 quantify small posterior uncertainty.*

correction on the mismatching concentration is strongest. For a few stations and months, the impact has been depicted in Sect. (4). For example, at point Barrow in Alaska (BRW) for the prior estimate of the fluxes the resulting summer draw down in the concentration is early by about one month compared to observations. This yields strong mismatches in June and July, for which the inversion compensates by a correction of the fluxes. According to Fig. (5), for the June mean concentration, a June flux correction in the few grid cells around BRW and slightly east of BRW has the largest impact. The northern grid cells are oceanic and have a smaller prior uncertainty, while the southern grid cells are terrestrial and have a much higher uncertainty. The difference in the uncertainties are so large, that adjusting primarily the southern grid cells is optimal. For equal uncertainties, however, equally distributed adjustments in all grid cells with high impact would yield a smaller sum of squared adjustments than unequally distributed adjustments and thus would be optimal: A least squares fit in general tends to smooth. For the July mean the situation is similar. Possible reasons for the mismatch of concentrations are inaccuracies in the prior estimates of the fluxes, in our model, or in the observations. In their publication, *Knorr and Heimann* [1995] name a number of possible reasons for an overestimation of the length of the summer draw down in their model. Furthermore, the satellite data used by the SDBM are less accurate in the high latitudes.

Concerning the model of the atmospheric transport, *Rehfeld* [1994] has performed a number of simulations for radioactive tracers with a 19 layer version of TM2. He found some disagreements

between modeled and observed concentrations in the polar regions, which he traces back to deficiencies in the meteorological data or reduced numerical stability at very high latitudes due to smaller size of the grid cells.

Another possible reason for local mismatches is associated with the baseline selection procedure. This problem has been addressed by *Ramonet and Monfray* [1996], e.g. for the station at Cape Grim in Tasmania (CGO). To take samples being representative for large scale air masses at the station observational data are rejected, whenever they are likely to be influenced by fluxes from southern Australia. Baseline conditions are defined according to criteria such as the weather regime or wind direction and speed at the station. *Ramonet and Monfray* successfully reduced the misfit by mimicking the baseline selection procedure in a high resolution version (2.5^o by 2.5^o in the horizontal) of TM2. The modeled concentration became lower from March to August and higher from September to November. As depicted in Fig. (21) around the south of Australia, our inversion procedure reduces the fluxes from February until August, while the fluxes are increased from September to November. Since in our model we did not mimic the selection procedure, at least a part of the correction of the fluxes compensates for this deficiency of our model. For Cape Meares in Oregon, they reported the same phenomenon. Unfortunately, they did not study the records of BRW.

Another problem of our model is the poor resolution of the planetary boundary layer: In the lowest model layer, which is about 300-400 meters thick, the concentration has a linear vertical profile. In reality, however, for a tracer emitted at the surface, the vertical profile is different: It is well mixed only within the boundary layer, whose height exhibits a diurnal and a seasonal cycle. Hence, the volume that is available for rapid mixing of the tracer is overestimated in the model, and since especially the photosynthetic activity of the biosphere shows a diurnal and a seasonal cycle, too, there are correlations that might be underestimated by TM2. In the diurnal and annual means of the CO_2 concentration due to these correlations nonzero contributions even for zero net mean fluxes can occur [*Pearman and Hyson*, 1980; *Heimann and Keeling*, 1989; *Denning*, 1995]. A better resolution of the planetary boundary layer by the transport model would not only improve the simulation of these contributions, it also would allow to make the representation of the sampling process at the station locations more accurate, because the samples are usually taken at a particular time of the day.

According to Eq. (A.8) the diagonal of the model resolution can be expressed by subtracting the quotient of the variances of the respective components from 1. This reduction of uncertainty quantifies how the additional information from the atmospheric data has improved our knowledge of the fluxes. In general, the reduction of uncertainty by the atmospheric data is very small, reflecting the fact that, on this small scale, a sparse network does not provide much information. For a particular flux component, the reduction of uncertainty is high, whenever this component projects well on one of the dominant right hand singular vectors. As discussed in Sect. (5.4), this gain of information is high for flux components having a high prior uncertainty or flux components being well observable by the network. Both criteria are reflected in the maps.

For temporal and spatial means, the reduction of uncertainty, i.e. the difference between 1 and the quotient of uncertainties, is a more natural quantity than means of the diagonal of the model resolution matrix. Fig. (24) shows the prior and posterior uncertainties for the annual mean as well as their quotient subtracted from 1, while Fig. (22) shows the same quantities for the zonal means.

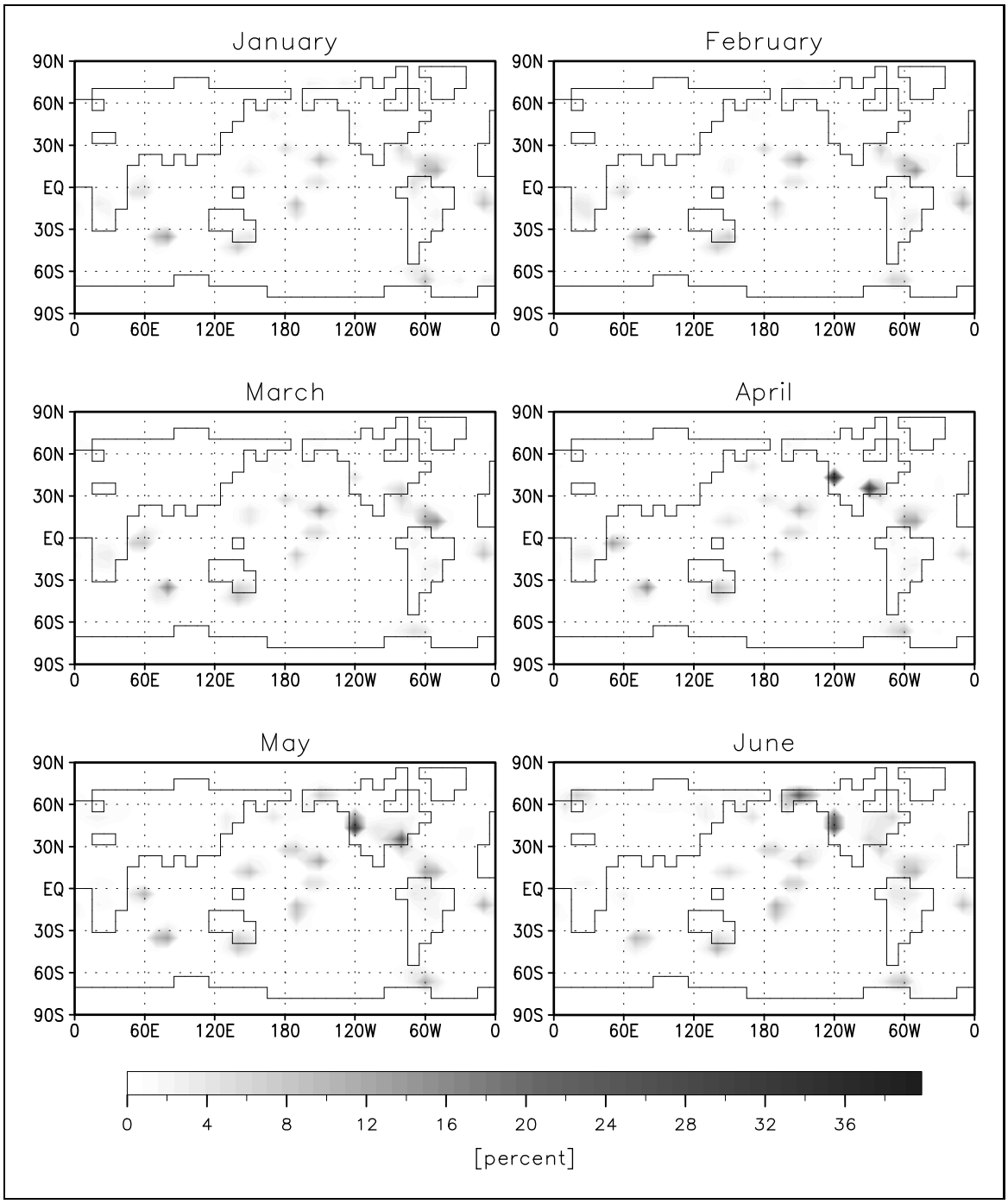

Figure 23: *Quotient of priori and a posteriori uncertainties for the sum of the biospheric and oceanic flux components subtracted from 1 in %. Values close to 100 quantify small posterior uncertainty.*

Also for these means the reduction of uncertainty is strongest in well observable areas and areas with high prior uncertainty.

Comparing the reductions of uncertainty for single flux components, annual means, and zonal

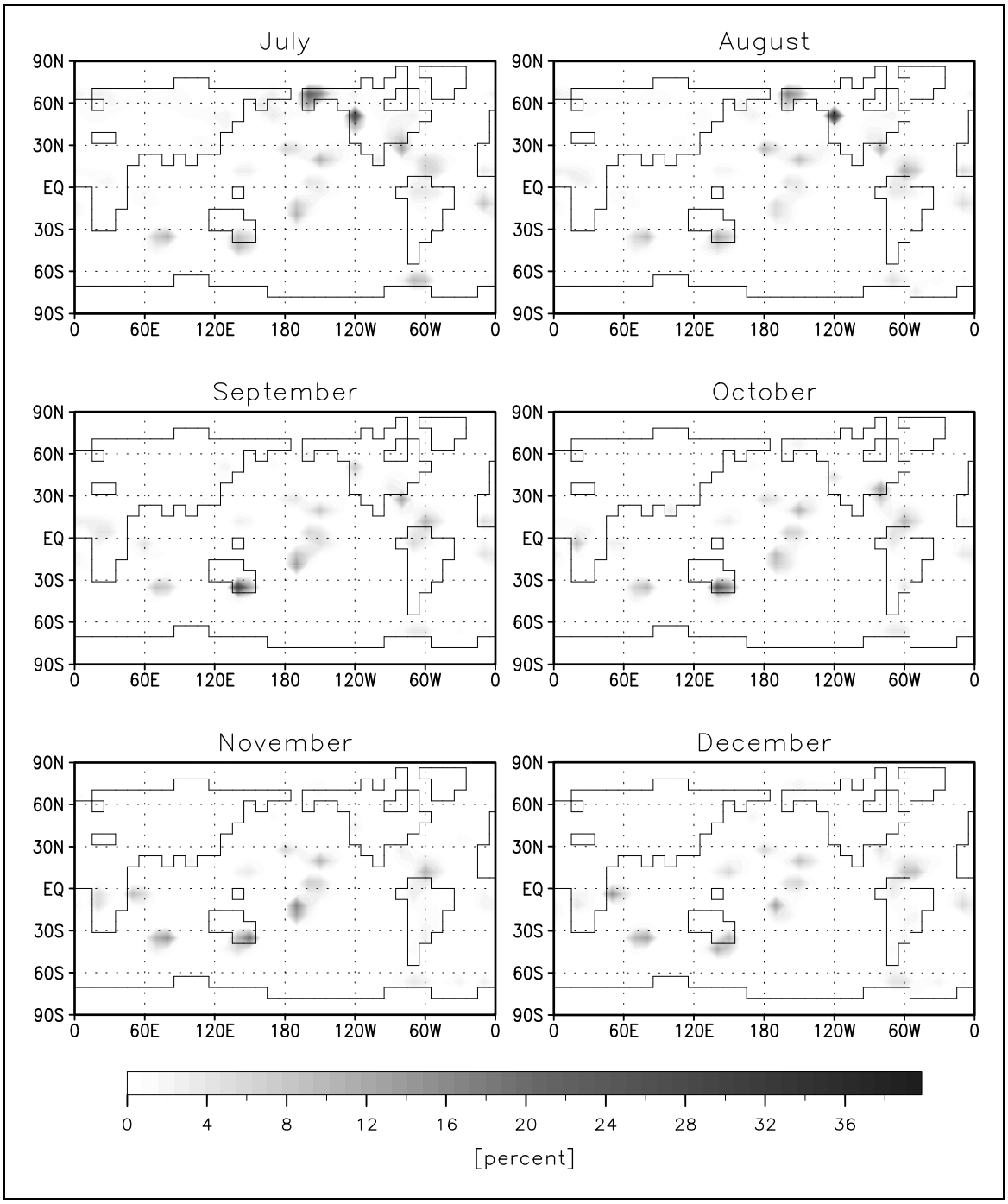

and annual means, two points are worth noting: First, the average reduction of uncertainty increases significantly with increasing degree of accumulation of components: By the inversion we learn more on larger scales than on smaller scales. Second, although we have high prior uncertainties, even for the 24 zonal and annual mean fluxes, the reduction of uncertainty remains lower than 15 %. In contrast, an alternative approach to the inverse problem, e.g. with 24 prescribed zonal and annual mean patterns and the same prior uncertainties, certainly would result in a much better reduction of uncertainty. This lower posterior uncertainty, however, is to a certain degree artificial, because

the additional information simply is due to coupling the fluxes from many grid cells to flux patterns without allowing variations within the patterns. Simplification of the model by reducing its degrees of freedom would improve the reduction of variance. At the same time, however, the simulation of the concentrations at the stations would become less realistic. An alternative way to reduce the inverse problem's degrees of freedom without simplifying the model is to assume correlated prior uncertainties for the fluxes.

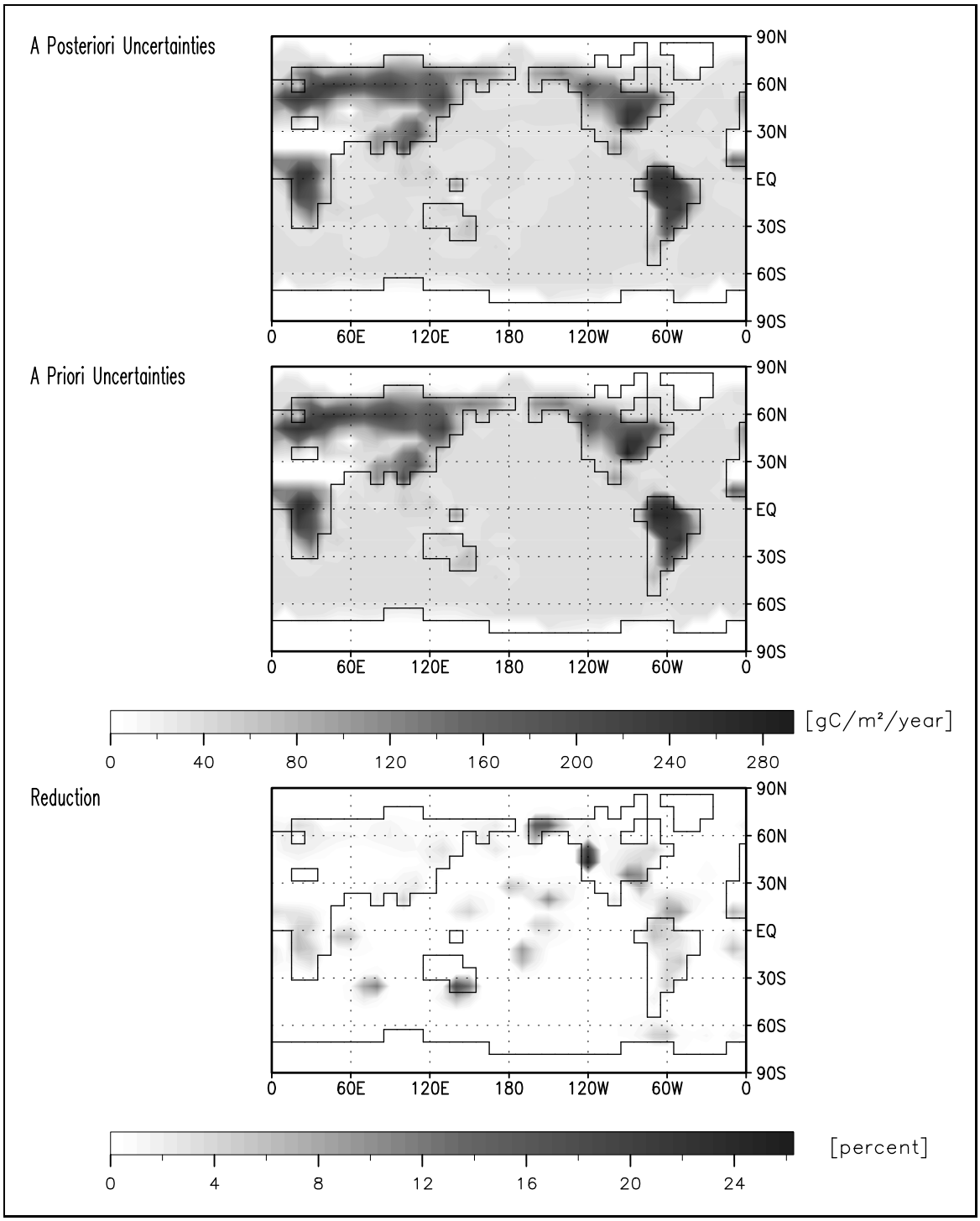

Figure 24: *A priori and a posteriori uncertainties for the annual mean of the sum of the biospheric and oceanic flux components and the difference of their quotient from 1 in %. Values close to 100 quantify small posterior uncertainty.*

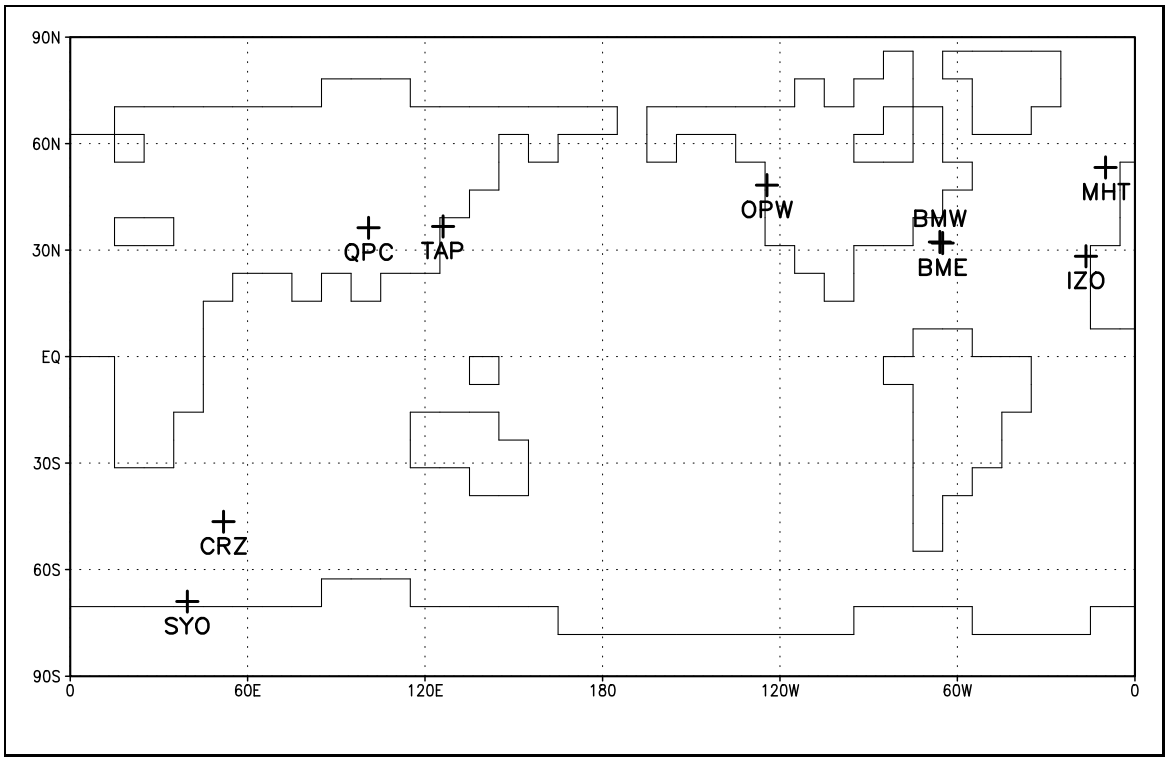

Figure 25: *Monitoring stations whose observational data we use to test our a posteriori fluxes.*

5.6 Simulated Concentrations

In this subsection we compare the posterior concentrations, i.e. the concentrations resulting from the posterior fluxes, to observations from two sets of stations: those whose data are used and those whose data are not used in our inversion.

For all stations whose data are included in the inversion, Fig. (16) shows the observations as well as the sets of simulated concentrations resulting from the prior and posterior fluxes. The contributions from the initial concentration, the global trend, and the seasonal cycle are used to compose the concentrations of 1981, the first year of our target period. In general, the posterior fluxes yield concentrations being consistent with the observations. On one hand this can be interpreted as a consequence of the underdeterminancy of the inverse problem and the small weight of the prior flux estimates. On the other hand the good fit indicates that there are no serious contradictions within and between both, the observations and the a priori information on the fluxes. In detail, most of the remaining mismatch is due to a too weak simulated summer draw down at a number of sites on the northern hemisphere.

In Fig. (25) we display a number of stations, whose observations we did not use for the inversion procedure. SYO does not belong to the NOAA/CMDL stations, and the other stations did not make observations during the full target period. Yet, employing a statistical model, *Masarie and Tans* [1995] managed to extend these records into our target period. Using data from other stations and other time periods their data extension procedure constructed pseudo data. Clearly, these pseudo data are not independent from the data we already use, so that we could not include them in our

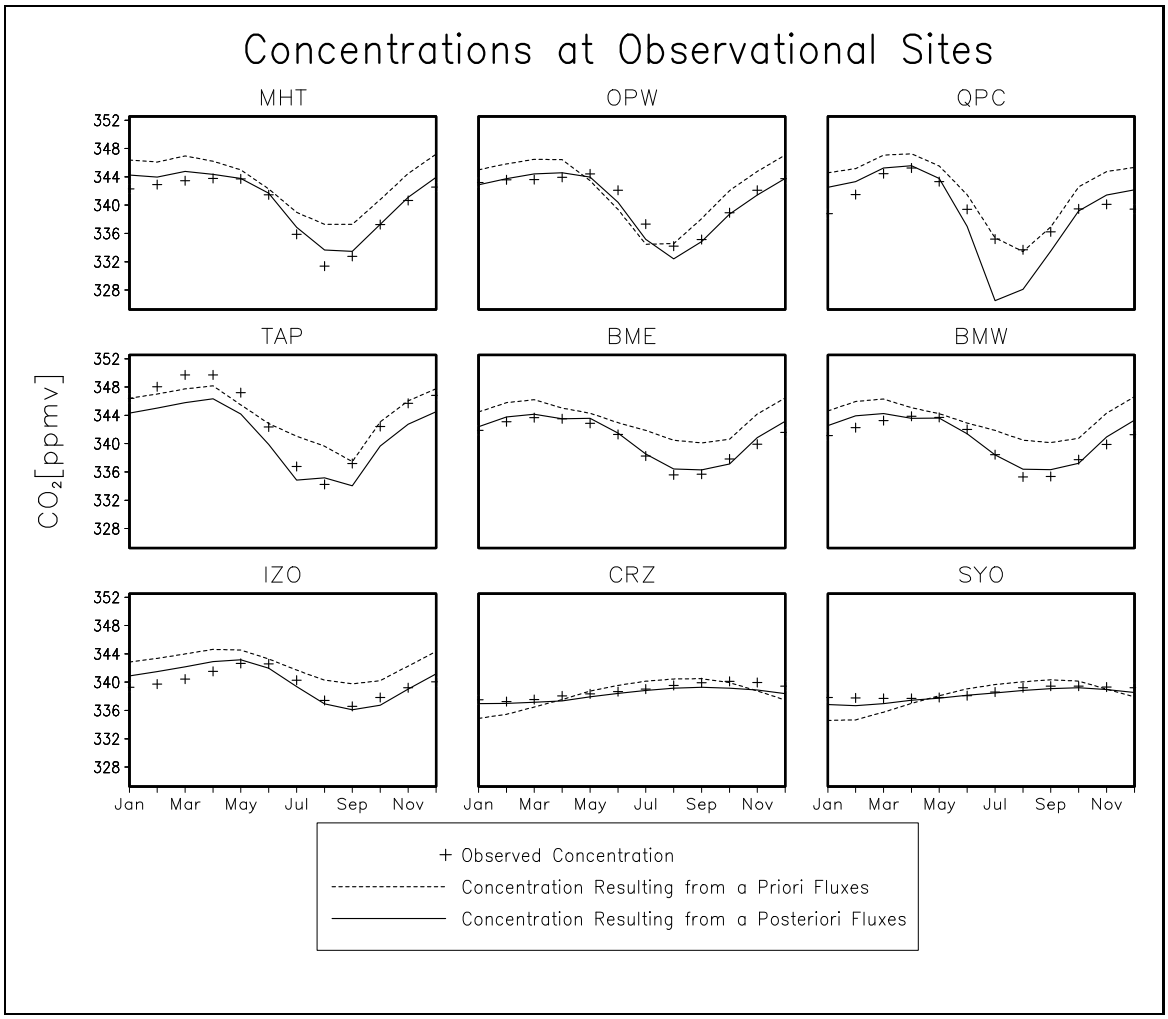

Figure 26: *Observed concentration with mean quasi-stationary seasonal cycle composed to represent the first year of the target period, 1981. SYO does not belong to the NOAA/CMDL stations; data at the remaining stations have been extended to target period. These data are not included in our inversion. Modeled concentration resulting from a priori and a posteriori fluxes. Fig. (25) shows station locations.*

inversion. Therefore and due to the considerable amount of new information that nevertheless is contained, these data provide an opportunity to test our posterior flux fields.

Fig. (26) shows the observed and modeled quasi-stationary seasonal cycle for 1981. The observations are composed as described in Sect. (5.3) and above. The agreement is improved by the inversion at all sites except for the stations QPC and TAP. These stations are mainly influenced by the south-eastern part of the Asian continent, which is not well observed by our network (see Fig. (2) and Fig. (24)), but which has a high prior uncertainty. The inversion yields a flux field that over all is consistent with these additional observations although the weight on the observations is high.

Table 3: *Uptake/release of some oceanic regions and the global sum in GtC/year for 1981–1986; prior and posterior values, scaling factor, values derived from observed air–sea partial pressure differences by Tans et al. [1990].*

	Location	Prior	Posterior	Scaling	Tans et al.
Atlantic subarctic	50°N–90°N; 90°W–20°W	−0.17 ± 0.04	−0.18 ± 0.03	1.75	−0.23
Atlantic gyre	15°N–50°N; 90°W–20°W	−0.17 ± 0.11	−0.33 ± 0.10	1.42	−0.30
North Pacific	15°N–90°N;110°E–90°W	−0.55 ± 0.17	−0.72 ± 0.16	1.21	−0.06
Equatorial	15°S–15°N;180°W–180°E	0.55 ± 0.28	0.55 ± 0.25	1.05	1.62
Southern gyres	50°S–15°S;180°W–180°E	−0.84 ± 0.26	−0.62 ± 0.23	1.19	−2.39
Antarctic	90°S–50°S;180°W–180°E	−0.51 ± 0.14	−0.20 ± 0.12	1.03	−0.20
Sum		−1.69 ± 0.46	−1.50 ± 0.41		−1.6
Total ocean		−1.70 ± 0.45	−1.40 ± 0.40	1.26	

5.7 Oceanic and Terrestrial Fluxes

For every grid cell and every month, as discussed in Sect. (5.5), we can compute a posterior flux field and a posterior uncertainty. To infer information about the processes that control these fluxes, rather than a division into grid cells a division into regions associated to these processes is needed. For example, we would like to separate the oceanic and terrestrial contributions to the fluxes. In this subsection, first, we give a recipe to perform the necessary bookkeeping for accumulation of flux components. Then this recipe is then applied to infer the fluxes for a partitioning of the ocean into the regions used in the study of *Tans et al.* [1990], which allows to compare results. Furthermore we present the net fluxes for some countries and continents.

For grid cells crossed by a coastline, in general, there is no way to distinguish between land and ocean contributions. Splitting the flux in proportion to the grid cell's land fraction provides at least a crude recipe. In many of these grid cells, however, a small oceanic flux is dominated by a much larger terrestrial flux. Hence, this crude recipe is likely to yield an unrealistic estimate of the oceanic contribution, while the error for the land contribution in general is much lower. Hence, to estimate regional oceanic fluxes, we slightly modify our recipe. As described in Sect. (5.2) a quasi zero terrestrial uncertainty of 10^{-12} kg/m^2/year has been assigned to flux components with negligible terrestrial contribution to the flux. Except those flux components with quasi zero terrestrial uncertainty, all grid cells with a land fraction of more than 1% are regarded as land grid cells and their flux contribution is neglected in the computation of the regional mean. By this procedure we clearly miss a fraction of the oceanic fluxes, which we try to correct in a second step: Comparison of the posterior and prior flux fields (Figs. (20), (12), and (13)) indicates only small differences. To account for the missing fraction of the oceanic flux, we simply scale the posterior regional mean in the same proportion as the prior mean has to be scaled to recover its accurate mean.

According to this scaling recipe, we compute the annual mean fluxes for a partitioning of the ocean into six regions defined by *Tans et al.* [1990]. For all regions the prior and posterior values as well as the scaling factor are listed in Table (3). The last column contains estimates derived by *Tans et al.* on the basis of observed air–sea differences in the partial pressure of CO_2. The last but one line contains the sum, whose uncertainties are derived from the uncertainties of the regional

estimates neglecting correlations. The numbers in the last line result from scaling the entire ocean with a single factor derived for the entire ocean. The sum of the posterior regional uptakes is by 0.1 GtC higher as the posterior uptake computed by scaling the entire ocean, which is caused by the lower regional scaling factor of the equatorial source as compared to the global scaling factor. The low reduction of uncertainty of about 10% indicates that even on global scale our data are insufficient to distinguish between oceanic and biospheric fluxes.

By means of our inversion we have constructed a global flux field that achieves a high degree of consistency with the atmospheric data. Its ocean uptake is about 1.5 GtC. In contrast, in their study *Tans et al.* concluded an ocean uptake of less than 1 GtC after comparing the atmospheric response to several flux scenarios. The oceanic flux fields of *Tans et al.* are based on observations of the air–sea differences in the partial pressure of CO_2 during two periods: from January to April and from July to October. After closing spatial and temporal gaps by interpolation, employing an empirically derived expression for the monthly gas exchange coefficient *Tans et al.* transformed partial pressure differences into the regional CO_2 fluxes in Table (3). Yet combining these ocean flux fields with reasonable land flux fields their simulated atmospheric response showed a significantly steeper north-south gradient in the atmospheric concentrations as observed, until they also varied the fluxes in the equatorial and southern oceans.

A difference to our study consists in the transport models: *Tans et al.* used the GISS model instead of TM2. Without performing our inversion with the GISS model, it is not possible to quantify the resulting a posteriori fluxes. Results of a transport model intercomparison [*Rayner and Law*, 1995; *Law et al.*, 1996] suggest that TM2 would yield an even steeper north-south gradient for the scenarios of *Tans et al.*, which even would have amplified the difference to our study.

Taylor et al. [1991] discussed the effect of missing the spring phytoplankton bloom due to the temporal gaps in the partial pressure measurements used by *Tans et al.*. Their conclusion is that due to the resulting underestimation of the partial pressure difference in the temporal gaps *Tans et al.* miss a significant fraction of the CO_2 fluxes. A further source of uncertainty consists in the gas exchange coefficient. *Tans et al.* point out that their values are about 100% higher than the values of *Liss and Merlivat* [1986]. Our prior estimate is based on a model of the ocean carbon cycle, in which a plankton model is embedded and, thus, is consistent with oceanic circulation and the dynamics of phytoplankton population. Using a gas exchange coefficient derived from the *Liss and Merlivat* [1986] formulation [*Heimann and Monfray*, 1989], the model simulates the fluxes together with a partial pressure difference that is in the range of observations [*Kurz*, 1993]. Applying the interpolation procedure of *Tans et al.*, in her model *Kurz* misses 0.53 GtC of its global ocean uptake. Adjusting slightly this prior ocean flux field our objective search algorithm succeeded in finding a flux scenario that is consistent with both, the atmospheric observations and the partial pressure differences and has an oceanic sink of 1.5 GtC.

The model of the ocean carbon cycle does not simulate any significant north south transport of carbon by the thermohaline circulation [*Weber*, 1996]. By enhancing the oceanic sink in the northern hemisphere and reducing the oceanic sink in the southern hemisphere (see Table (3)), the inversion suggests such a transport, confirming the conclusions of *Keeling et al.* [1989b]. The magnitude of our global oceanic sink, however, is smaller than the 2.3 GtC they inferred for 1984. Furthermore the location of our Atlantic sink is farther south than expected. Probably our oceanic sink would be slightly enhanced by increasing the assumed uncertainties for the oceanic a priori

Table 4: *Net land uptake and release of some countries and continents and in the global mean in GtC/year for 1981–1986.*

Country/Continent	Prior	Posterior	Fossil fuel
USA	0.01 ± 0.37	−0.16 ± 0.27	1.09
Australia	0.01 ± 0.11	−0.02 ± 0.10	0.06
China	0.07 ± 0.29	−0.38 ± 0.25	0.58
Europa	−0.02 ± 0.22	−0.08 ± 0.20	1.13
USSR	0.03 ± 0.47	−0.54 ± 0.32	0.99
India	0.02 ± 0.13	−0.02 ± 0.12	0.12
Total land	1.18 ± 1.33	−1.04 ± 0.53	5.27

fluxes as discussed in Sect. (5.2).

Assuming a global yearly fossil fuel emission of 5.3 GtC, the inversion reveals an oceanic sink of 1.5 GtC and a total sink of 2.3 GtC, so that the terrestrial biosphere has to account for the residual of 0.8 GtC. For some countries and continents Table (4) opposes industrial emissions to prior and posterior magnitudes of the biospheric sink as computed according to the simple recipe described above. Although the recipe tends to overestimate the biospheric uptake by including a fraction of the oceanic sink, none of the countries or continents can compensate its emissions. Maybe Australia is an exception. Part of the Australian sink, however, can be attributed to the failure of our model to mimic the baseline selection as discussed in Sect. (5.5). The inaccuracy of the simple recipe is illustrated by the last line: The global prior yearly biospheric fluxes is underestimated by 0.5 GtC = 1.7 GtC – 1.2 GtC (a priori value is 1.7 GtC from land use change), and the global posterior yearly biospheric flux is underestimated by 0.2 GtC = – 0.8 GtC – (– 1.0 GtC) (a posteriori biospheric flux via the budget is –3.0 GtC + 5.3 GtC – 1.5 GtC = – 0.8 GtC).

5.8 Sensitivity Experiments

For all posterior flux estimates the Bayesian approach enables us to compute uncertainties quantifying our posterior state of information. These posterior uncertainties are inferred from the prior uncertainties of fluxes and observations using our knowledge about the transport. The reliability of these ingredients and our ability to formalize our information in mathematical expressions determine to which degree our posterior state of information reflects reality, and in particular whether the true values of our posterior estimates are likely to be in the range specified by their posterior uncertainties. Clearly, these posterior uncertainties only reflect the fraction of uncertainty resulting from factors that we managed to incorporate in our inversion procedure.

While some of these sources of uncertainty not incorporated in our inversion procedure, such as the deviations from the Gaussian assumption or linear transport, cannot be handled by the inversion procedure, others, such as errors in the transport model, can be explored by feeding our inversion procedure with a different set of numbers. To explore at least the latter type of uncertainty we perform three inversions, in each of which we vary a particular subset of the numbers we provide to the inversion procedure: the transport matrix, the observational network, or the a priori information.

Our transport matrix represents a TM2 setup driven by meteorological data from 1987. To explore the sensitivity of the posterior fluxes to the transport matrix, we performed an inversion, for which we replace our matrix by a matrix derived with meteorological data from 1986. Comparing the transports of the El Niño year 1987 to that of the "ordinary" year 1986 can be expected to illustrate range for possible changes in the posterior fluxes that can be achieved by changing the year of meteorological data. In the annual mean Fig. (27) reveals differences on continents north of 40^oN as well as in the El Niño influenced regions. Compared to the posterior uncertainties (Fig. (24)), however, these differences are slight. This indicates the success of our attempt to include the uncertainty caused by the interannual changes in transport, which is described in Sect. (5.3). On larger spatial scales, the differences remain low as well. For instance, the posterior uptake by the oceanic regions defined in Table (3) and by the countries or continents named in Table (4) change by less than 10%. The single exception is China, whose yearly biospheric uptake is reduced from 0.38 GtC to 0.30 GtC. Changes in the zonal mean are small, too (see Fig. (28)). The total ocean uptake remains 1.5 GtC.

For their study *Tans et al.* [1990] excluded the data from the stations CMO, NWR, MLO, and RPB (see Fig. (2)). To explore the sensitivity of our posterior fluxes to slight changes in the observational network we perform an inversion for their network. Comparing the annual means of the posterior fluxes, besides a strong local change around CMO, Fig. (29) reveals slight changes in North America, Asia, Africa, and even South America. Again, in all oceanic regions defined in Table (3) and in all countries or continents named in Table (4), the changes remain lower than 10%. Changes in the zonal mean are small, too (see Fig. (30)). With an unchanged total oceanic sink of 1.5 GtC, the fit of the observations is equally good.

Replacing the a priori information on the land fluxes by a more simple formulation, we explore the sensitivity of our posterior fluxes to changes in the a priori information. In contrast to our standard case, the a priori estimate for the land flux is formed simply by the fields from the SDBM, i.e. we do not account for land use change. The prior uncertainties are based on the net exchange

fluxes, rather than on the individual contributions of NPP and soil respiration as in our standard case: We use the absolute value of a flux component, whenever it is larger than 0.12 kg/m^2/year, which is about the value of a large oceanic flux. For most of the remaining flux components we assume an uncertainty equal to this value of 0.12 kg/m^2/year. For grid cells covered by deserts or ice, however, we do not want to assume large uncertainties. In order to exclude land grid cells without vegetation we employed the net primary productivity (NPP) computed by the SDBM (see Fig. (14)). If its annual value is less than 0.01 kg/m^2/year, in the respective grid cell for all months we assume an uncertainty of 10^{-12} kg/m^2/year. Components with such a small prior uncertainty are essentially treated as constant by the inversion procedure, i.e. the a priori value is hardly changed. For ocean grid cells permanently covered by ice we assume as well the extremely low uncertainty of 10^{-12} kg/m^2/year in every month. Our criterion for identifying these grid cells is an annual oceanic flux of less than $5 \cdot 10^{-4}$ kg/m^2/year. Fig. (31) shows the resulting uncertainties for the annual mean fluxes.

In a previous study [*Kaminski et al.*, in press] we performed the inversion including the a priori information described above and discussed the a posteriori fields in detail. For the annual mean Fig. (32) shows the difference between the a posteriori fluxes for modified a priori information and the a posteriori fluxes for our standard case. In contrast to the sensitivity experiments discussed above, Fig. (32) reveals large differences between both posterior flux fields: By changing the a priori information, i.e. the spatial distribution of the prior uncertainty and the missing land use change contribution, terrestrial sources and sinks are shifted, which is also reflected by changes in the zonal mean (see Fig. (33)). With a slightly reduced oceanic uptake of 1.3 GtC the fit of the observations is as good as in the standard case.

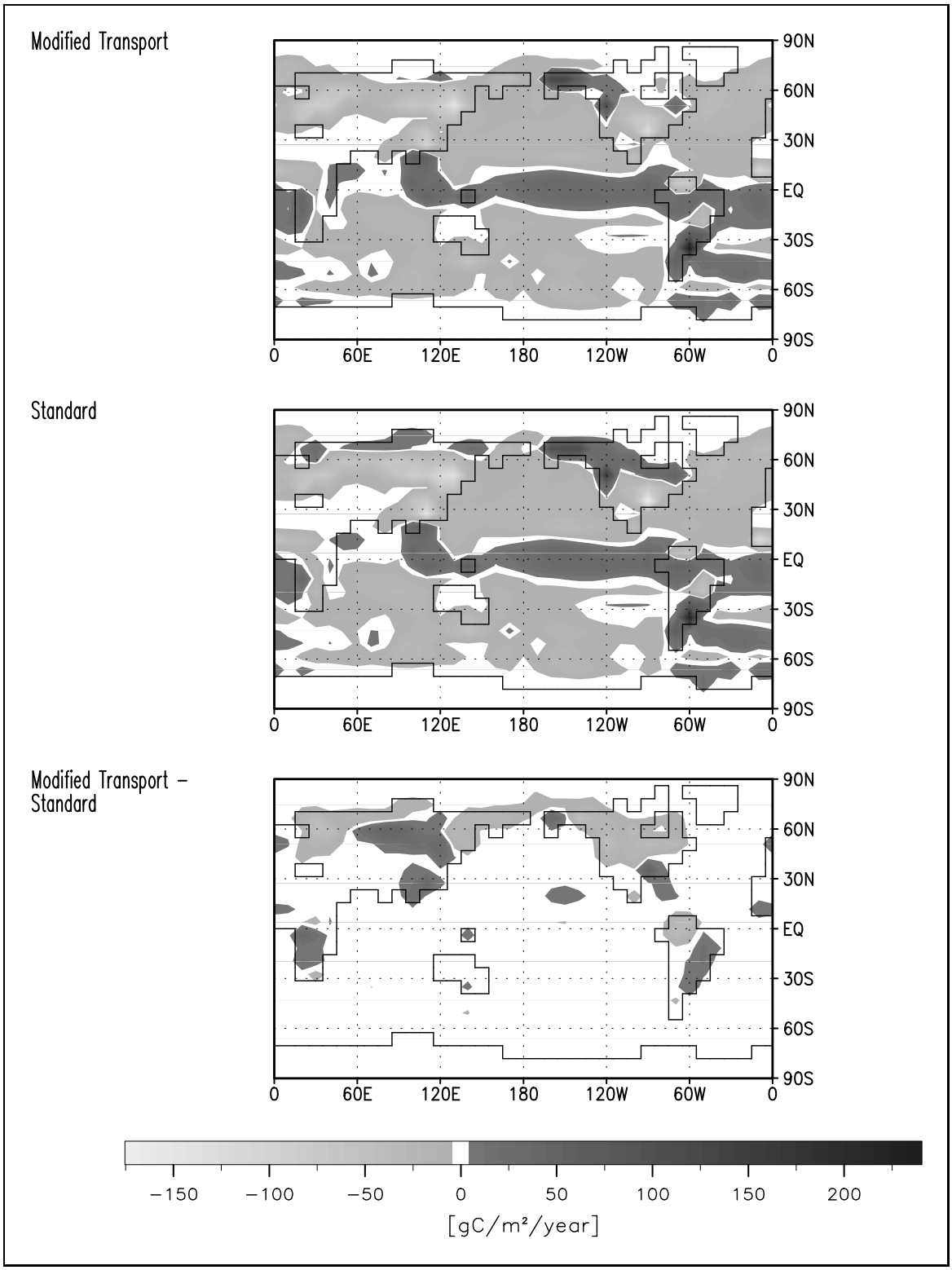

Figure 27: *A posteriori estimate of annual mean of the sum of the flux contributions from terrestrial biosphere and ocean; inversion of different transport matrix (top), standard inversion (middle), and their difference (bottom); in the difference plot, positive values quantify an enhanced source or a reduced sink due to the modification.*

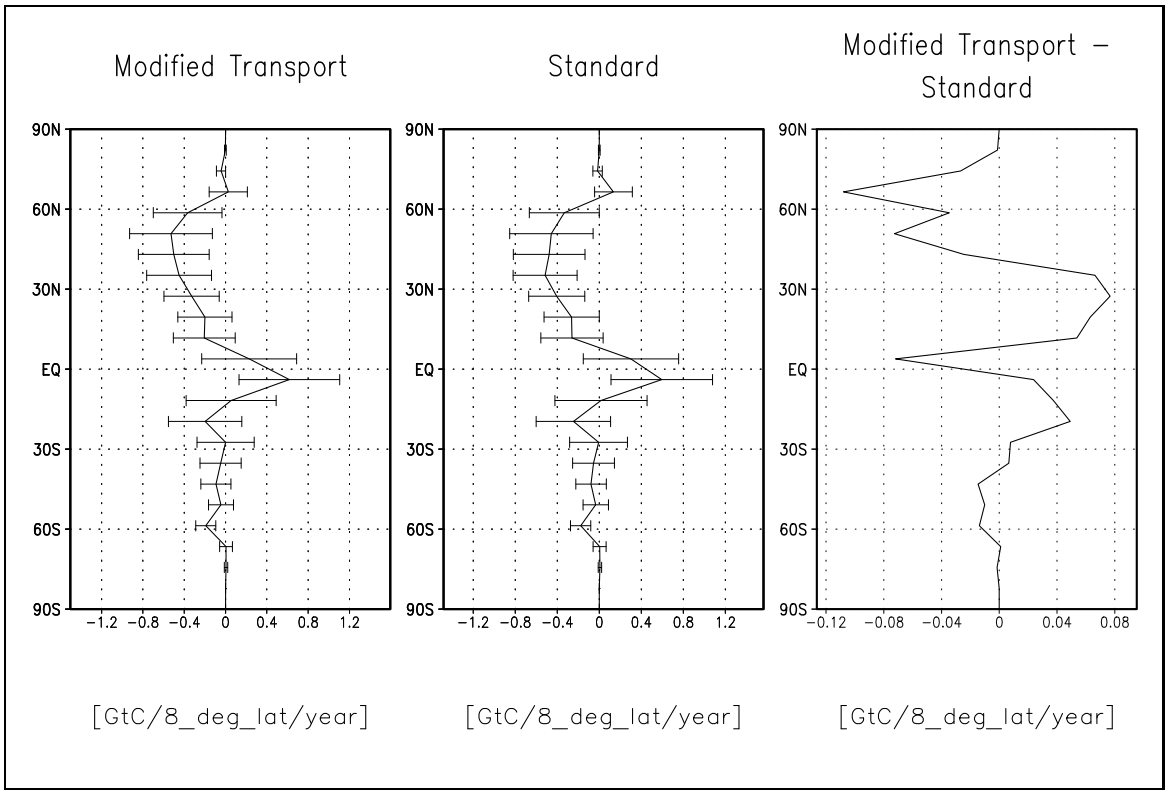

Figure 28: *A posteriori estimate of zonal and annual mean of the sum of the flux contributions from terrestrial biosphere and ocean; inversion of different transport matrix (left), standard inversion (middle), and their difference (right); in the difference plot, positive values quantify an enhanced source or a reduced sink due to the modification.*

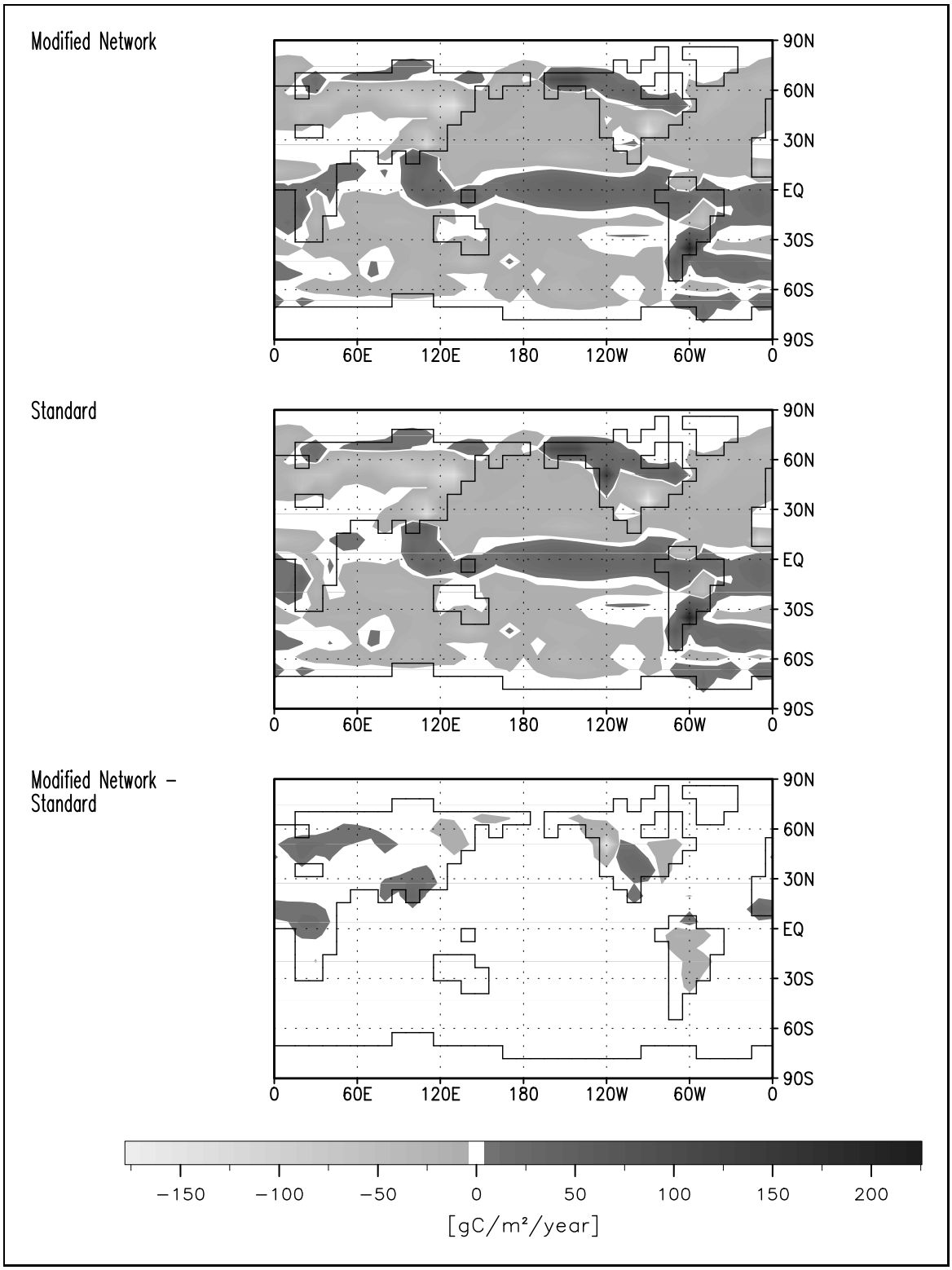

Figure 29: *A posteriori estimate of annual mean of the sum of the flux contributions from terrestrial biosphere and ocean; inversion with modified network (top), standard inversion (middle), and their difference (bottom); in the difference plot, positive values quantify an enhanced source or a reduced sink due to the modification.*

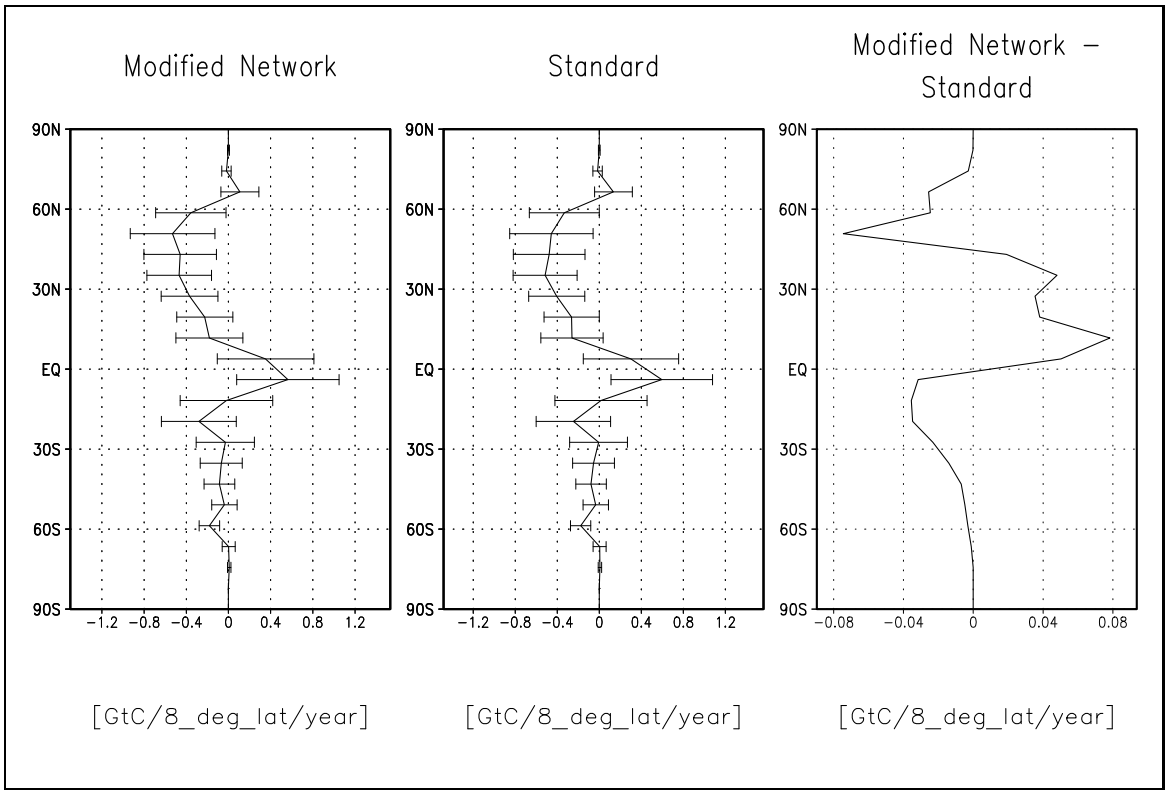

Figure 30: *A posteriori estimate of zonal and annual mean of the sum of the flux contributions from terrestrial biosphere and ocean; inversion with modified network (left), standard inversion (middle), and their difference (right); in the difference plot, positive values quantify an enhanced source or a reduced sink due to the modification.*

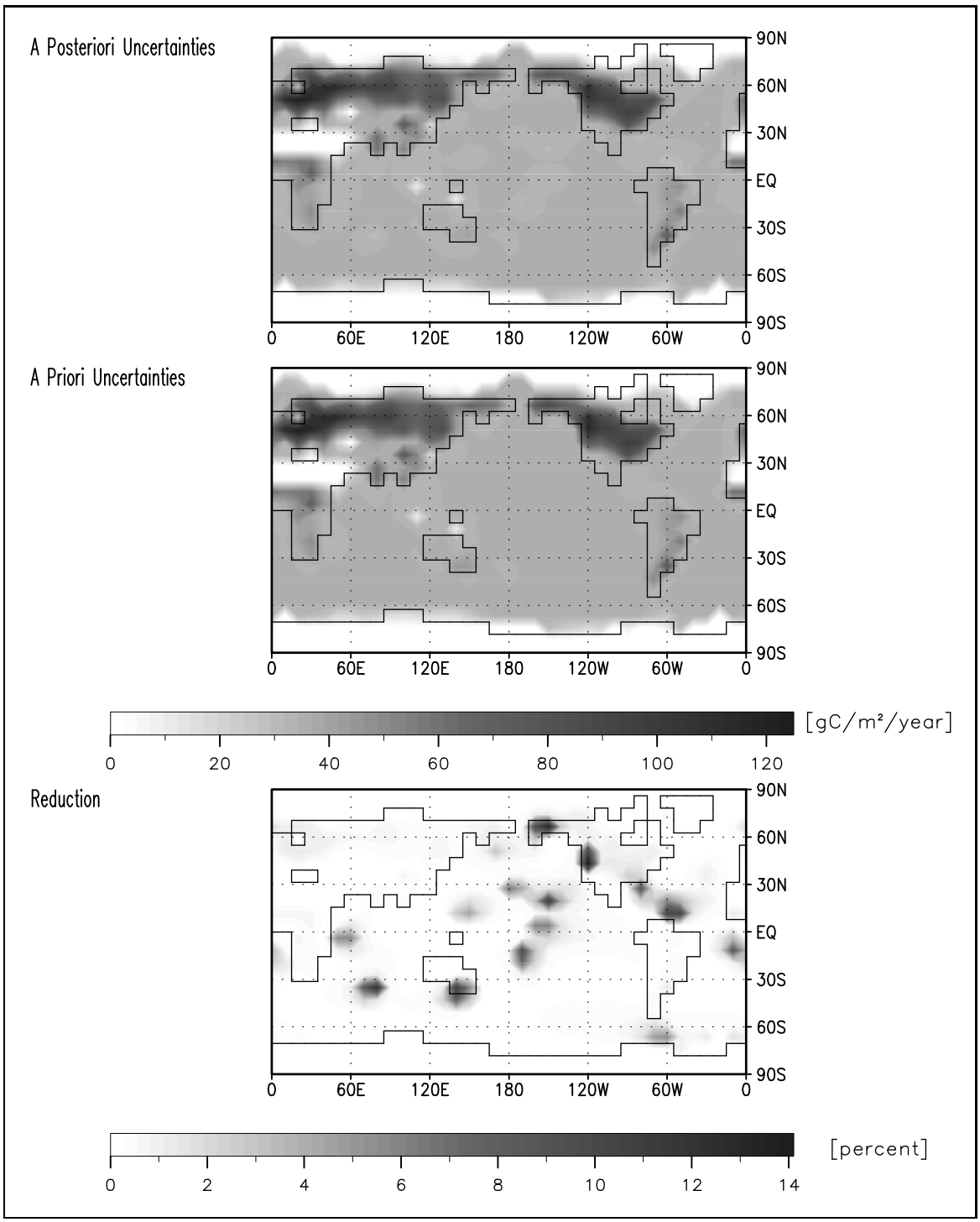

Figure 31: *A priori and a posteriori uncertainties for the annual mean of the sum of the terrestrial and oceanic flux components for modified terrestrial a priori information and the difference of their quotient from 1 in %. Values close to 100 quantify small posterior uncertainty.*

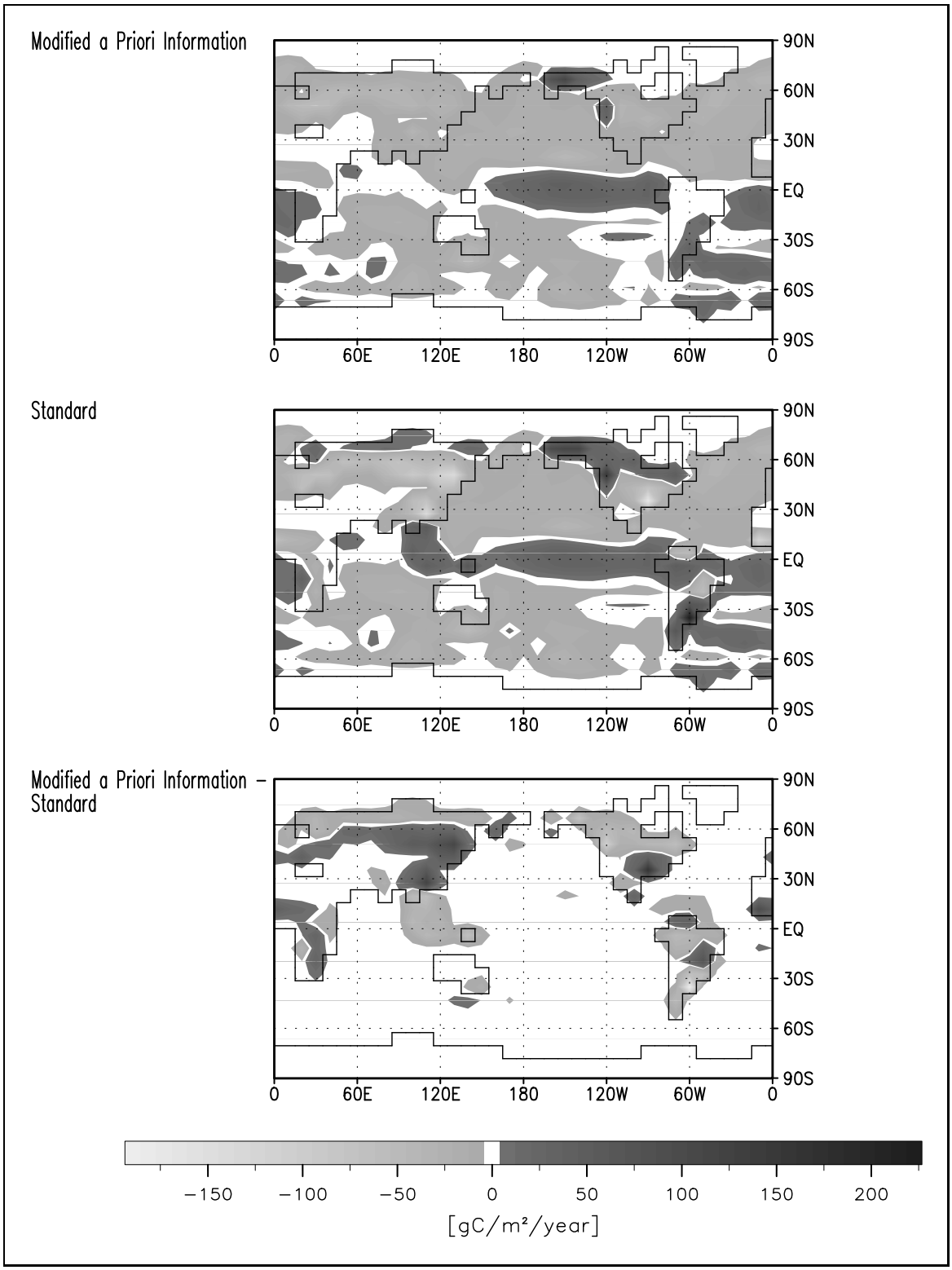

Figure 32: *A posteriori estimate of annual mean of the sum of the flux contributions from terrestrial biosphere and ocean; inversion with modified terrestrial a priori information (top), standard inversion (middle), and their difference (bottom); in the difference plot, positive values quantify an enhanced source or a reduced sink due to the modification.*

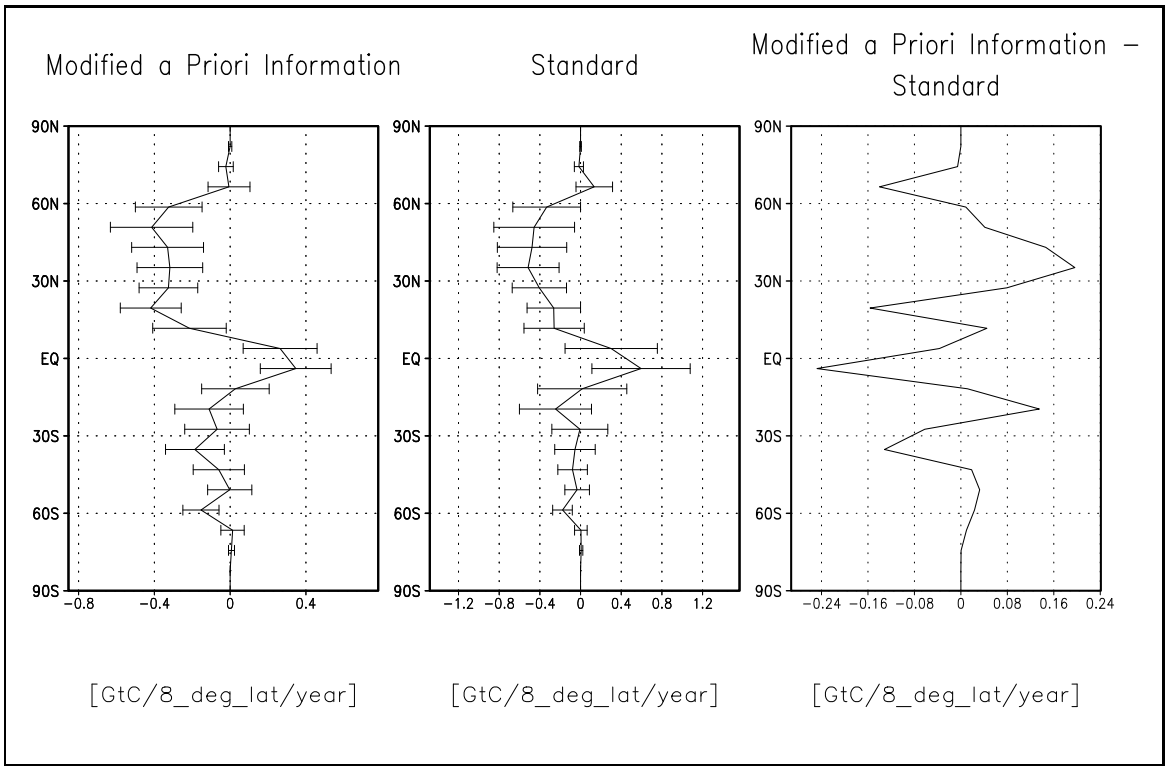

Figure 33: *A posteriori estimate of zonal and annual mean of the sum of the flux contributions from terrestrial biosphere and ocean; inversion with modified terrestrial a priori information (left), standard inversion (middle), and their difference (right); in the difference plot, positive values quantify an enhanced source or a reduced sink due to the modification.*

6 Conclusions and Perspectives

We demonstrated the benefit of the adjoint approach for the computation of the Jacobian matrix representing a three dimensional atmospheric transport model. For the models approximately 8^o by 10^o horizontal resolution and 27 stations, the computational efficiency of the adjoint was about 100 times higher compared to conventional forward modeling.

We showed a number of applications of the Jacobian including an inversion of the transport of CO_2. From atmospheric observations at 25 stations, we inferred a cyclostationary flux field on the entire TM2 grid that is consistent with the observed quasi-stationary seasonal cycle during a target period at the beginning of the 1980s. In the inversion, we included a priori estimates of the fluxes to regularize the otherwise underdetermined inverse problem. This underdeterminancy is caused by the sparse network in conjunction with the diffusive nature of the atmospheric transport and is reflected by the poor reduction of the uncertainty for estimates of single flux components. This low reduction of uncertainty, however, is inherent to the problem and not an artifact of the high resolution; it reflects the classical trade off between resolution and variance of inverse problems. Reducing the number of unknowns by prescribing patterns only achieves an apparent reduction of uncertainty, because relations among unknowns are introduced, thereby neglecting the uncertainties of these relations. For larger scale quantities such as spatial and temporal means, the reduction of uncertainty is higher.

To infer information about the processes controlling the fluxes we had to use a few shortcomings: The fossil fuel contribution has been subtracted from the observations prior to inversion, and to untangle oceanic and biospheric fluxes crude recipes have been applied. Problems of this type can be avoided by introducing, for every grid cell and month, as many unknowns as there are processes of interest. The inversion then distributes the correction of the flux onto the processes according to their respective prior uncertainties. This improved resolution of processes, however, requires the inversion of a matrix, whose size grows linearly with the number of processes.

Our posterior estimate of 1.5 ± 0.4 GtC for the total ocean uptake contradicts the estimate of less than 1 GtC by *Tans et al.* [1990]. Replacing their simple interpretation of observed air–sea partial pressure differences by oceanic a priori information from a model that includes the population dynamics of phytoplankton in conjunction with an objective search algorithm are the main factors our higher estimate can be attributed to. On the other hand our estimate is lower than the 2.3 GtC inferred by *Keeling et al.* [1989b] for 1984, although the structure of the sink supports their interpretation of the southward transport of carbon by the thermohaline circulation. Our estimate is not very sensitive to changes in the a priori information on the biospheric fluxes, changes of the network, and changes of the meteorological data that drive our transport model.

The reduction of uncertainty for the global net exchange fluxes with the ocean and the terrestrial biosphere is much lower as desirable. Measurements of additional tracers such as oxygen [*Keeling et al.*, 1996; *Stephens et al.*, submitted], ratios of carbon isotopes in CO_2 [*Ciais et al.*, 1995], or ratios of oxygen isotopes in CO_2 [*Ciais et al.*, 1997, submitted] have been reported to impose strong constraints on the partitioning between the processes. Since all these tracers are chemically inert, our matrix representation of the transport can be employed to include this additional information in the inversion procedure. In addition, a model of the processes that link these tracers' fluxes to the CO_2 fluxes is required, and the additional uncertainty introduced by the model has to be

formalized, so that it can be transformed to an uncertainty for the flux estimates.

For a few countries and continents we estimated the magnitude of the biospheric sink to explore the capacity of the observations to detect the geographic origin of a tracer. In contrast to the resolution of processes, for problems of this type, in general, no further tracer can provide additional information. The only way to reduce the uncertainties is to increase the number of observations as well as their precision. Methods for a systematic investigation of the optimal location of additional observational sites have been presented by *Rayner et al.* [1996]. In conjunction with search algorithms that need to try a high number of potential locations, for computing the atmospheric response at these locations the adjoint approach is clearly inferior to the forward approach, because the cost of the adjoint approach is proportional to the number of locations. The adjoint approach can be efficient, if the number of potential locations can be kept low, e.g. due to logistic constraints, or if a search algorithm can get along with a small number of trials.

Our sensitivity experiments confirmed that for a sparse network the a priori information on the fluxes constitutes a crucial ingredient of the inversion. For convenience we assumed a Gaussian distribution, which is quantified by mean and covariance matrix. As mean we used output of process models. For the error covariance, however, no model results were available. Hence, we invented an error covariance matrix. For simplicity of computation, we have not assumed correlations among the uncertainties of different components, although, especially on this small spatial scales, correlations are likely. Increasing correlations can be interpreted as a way to continuously reduce the degrees of freedom of the inverse problem. Hence, an increased correlation would have two effects on our inversion: First, the prior uncertainty of large scale mean fluxes such as the total ocean uptake would increase, because cancelling out of deviations from the mean with different sign becomes less likely. Second, spatial correlations would tend to couple groups of grid cells. Hence, the localized source and sink spots would get less intense and more widespread. In contrast to prescribed spatio-temporal patterns, correlated prior uncertainties can be interpreted as a means to continuously reduce the number of degrees of freedom without neglecting uncertainties. By using output from different process models, the sensitivity of the inversion to the prior estimates can be investigated. Until information on correlated uncertainties from process models is available, the sensitivity of the inversion to this ingredient can only be explored by trying different assumptions on covariance matrices.

In the present study, we characterized the sources and sinks by their net exchange fluxes with the atmosphere, rather than the processes causing the fluxes. After coupling the transport model (or its Jacobian) to process models such as the SDBM [*Knorr and Heimann*, 1995], the corresponding adjoint can be applied to estimate the internal parameters of the process models. Coupling a model of the oceanic carbon cycle to the transport matrix would allow to simultaneously fit oceanic observations such as CO_2 partial pressure and atmospheric observations. Here again formalizing the prior uncertainties in the models is important. As a by product, by running (the linearization of) the optimized process model forward, the parameters in the process model and their uncertainties could be mapped onto the exchange fluxes and their uncertainties.

We have seen that the inversion tends to compensate for biases in our model by erroneous corrections of the fluxes. Hence, improvement of the model is desirable. For the transport model, an improved version, TM3, driven by 6 hourly reanalyzed meteorological fields from the ECMWF is now available. It can be run in a finer horizontal and vertical resolution, so that a more realistic

representation of the height of the planetary boundary layer is possible. With this transport model, at least in part, the sampling procedure at the stations can be mimicked. Compared to the forward approach, on a finer grid, the computation of a matrix representation by the adjoint is even more advantageous.

In our model, we assume cyclostationarity for the fluxes and the transport. An estimate of the corresponding model error was added to the observational uncertainty. Not only would it be interesting per se to study interannual variability of the fluxes, also would a more flexible model allow to considerably reduce the uncertainty on the data side, which would improve the reduction of the fluxes' uncertainties. To consider interannual variations in the fluxes only a slight change in the setup is necessary: Instead of prescribing the same fluxes every year, interannual variation during the spin up is allowed. By the corresponding adjoint model, this more general matrix representation quantifying the impact of flux components up to 3 years ago can be derived at the same cost as the matrix for the cyclostationary case. In fact, it was not very smart to run the adjoint for the cyclostationary setup at all, because the general matrix can be easily transformed to the cyclostationary matrix. To include also the interannual variations in the transport, the setup has to be changed towards a simulation of the whole target period. For this case the cost of both the forward and adjoint approaches, increases linearly with the length of the target period. In any case, resolving interannual variations in the transport imposes the challenge to computationally handle the inversion of a matrix whose size increases quadratically with the length of the target period. As a preliminary test of the impact of the interannual variations in the transport, the inversion has been performed in the same setup but with the meteorology of a different year: The resulting changes in the posterior fluxes were slight.

In our example, we employed the Jacobian to derive an estimate of the sources and sinks of CO_2. However, the technique can be efficiently applied to other tracers in the same manner, as long as the number of observations is small compared to the number of source components of interest. Since, at our observational sites, also the concentrations of further tracers are measured, the same matrix can be used for modeling the quasi-stationary seasonal cycle resulting from those tracer's surface fluxes (Of course a different conversion factor from mass to concentration has to be taken into account). If the tracer, in addition, has sources or sinks above the ground, the transport matrix has to be complemented by further columns representing the sensitivity of the modeled concentration at the stations with respect to these additional sources or sinks. The cost for the computation of such an extended matrix is the same as for our matrix, so that compared to forward modeling the adjoint approach is even more advantageous.

The efficient computation of the transport matrix by the adjoint of TM2, which forms the basis of our approach, depends crucially on the sparsity of the network and on the linearity of the transport. For cases with as many observations as flux components or cases with important nonlinearities in the transport, the adjoint model allows an inversion without computing the full transport matrix: At the cost of 3–4 forward model runs, the adjoint can be employed to provide the gradient of the misfit between modeled and observed concentrations (Eq. (17)) with respect to all flux components. Exploiting this gradient information, most powerful algorithms [see e.g. *Gill et al.*, 1981; *Press et al.*, 1986; *Tarantola*, 1987] can be applied to iteratively minimize the misfit by variation of the fluxes. If the inverse problem is well posed, these algorithms typically achieve a strong reduction of the misfit in a few iterations. However, although this approach is rather

inexpensive, it does not yield reliable estimates of the uncertainties of the fluxes in an inexpensive way.

Adjoint models enable us to tackle efficiently the inversion of the atmospheric transport with an arbitrarily high resolution in the space of fluxes. Compared to many alternative methods adjoint models are a valuable tool for studying sources and sinks on smaller scales. They can close the gap of scales between local process studies and global budgets. Of course, essential additional ingredients are high quality atmospheric measurements of a dense network, a good model of the atmospheric transport, and accurate a priori information on the sources and sinks. Adjoint models especially provide a means of inferring anthropogenic trace gas emissions, which might be needed in the near future.

7 Acknowledgments

It has been a privilege and motivation to be part of the vivid and exciting research at the Climate Dynamics Department of the MPI in Hamburg. I thank our director, Klaus Hasselmann, for the opportunity to learn and work in this outstanding environment and for reviewing this thesis.

This work profited enormously from the steady and patient support by my supervisor, Martin Heimann. With his motivating enthusiasm for nature and his profound knowledge of our field he is an excellent coach. His guidance continuously kept this work on track.

Ralf Giering was teaching me the basics of automatic differentiation and software design. I thank Ralf for an intense collaboration, which was crucial for this project: He patiently improved his compiler, until I could automatically differentiate TM2.

I thank Michael Voßbeck, who is implementing the plot software for our inverse model with patience and industry; in particular, Michael has produced all GrADS plots of this thesis.

I thank Jörg Kaduk and Wolfgang Knorr for discussions about the terrestrial biosphere as well as Ernst Maier-Reimer, Katharina Six, and Christine Weber for explaining to me their views on the oceanic carbon cycle. Special thanks to Ernst for his careful "Nicht übertreiben, Junge!".

Thanks to the support of Klaus Hasselmann and Martin Heimann last summer I could visit our colleagues at CSIRO and CRC in Melbourne. I thank Ian Enting, Rachel Law, and Peter Rayner for hosting me. Many intense discussions in particular with Peter, who is an excellent teacher, greatly improved my understanding of the inverse problem.

I thank Rainer Wüst from the Dep. of Mathematics at Technical University Berlin. In a brilliant fashion, Rainer was teaching us the basics of mathematical physics, which I still find very useful for my present work.

Among the people that have been helpful solving scientific or technical problems are Georg Barzel, Christian Eckert, Martin Fischer, Patrick Heimbach, Georg Hoffmann, Frank Kauker, Matthias Münnich, Norbert Noreiks, Walter Sauf, Uwe Schulzweida, the staff from the DKRZ, Bernadette Walter, and Christine Weber.

I thank Ralf Giering, Martin Heimann, Sander Houweling, and Katharina Six, for their comments on the manuscript; Antje Viefhaus greatly helped to improve the grammar and spelling.

I thank my colleagues and friends Martin Fischer, Ralf Giering, Frank Kauker, and Michael Voßbeck for their company and their encouragement. Martin, Ralf, and Frank have left MPI; I miss them. Special thanks to Frank for taking care of my mobility.

Most of all, however, I thank my parents Christa & Herbert Kaminski for their life long encouragement as well as Antje Viefhaus for having spent six wonderful years with me.

Appendix

A Basic Concepts of Inverse Theory

From the Bayesian viewpoint our inverse problem consists in combining a set observations of the atmospheric CO_2 concentration and our model of the atmospheric transport to improve our state of information about the surface exchange fluxes.

In the textbook of *Tarantola* [1987], the concepts of inverse theory are presented in a beautiful way. Another good, more practical description can be found in the textbook of *Menke* [1989]. We briefly summarize the important concepts for our problem. They can be formulated conveniently in terms of joint probability distributions, that characterize the state of information on fluxes and concentrations at the same time. The appropriate vector space is $\mathbb{R}^{n_c+n_f}$, the space formed by concatenating the vector of fluxes and the vector of concentrations.

A priori, i.e. without taking the transport into account, the state of information about the system is then described by a probability density $\rho : \mathbb{R}^{n_c+n_f} \rightarrow [0,1]$, being defined so that for $f_i^l < f_i^u$ and $c_j^l < c_j^u$ the integral

$$\int_{f_1^l}^{f_1^u} \cdots \int_{f_{n_f}^l}^{f_{n_f}^u} \int_{c_1^l}^{c_1^u} \cdots \int_{c_{n_c}^l}^{c_{n_c}^u} \rho(\tilde{f},\tilde{c}) \quad d\tilde{f}_1 \ldots d\tilde{f}_{n_f} \quad d\tilde{c}_1 \ldots d\tilde{c}_{n_c}$$

yields the probability that at the same time all flux components $\tilde{f}_i$ are between f_i^l and f_i^u as well as all concentration components $\tilde{c}_i$ are between c_j^l and c_j^u. A priori, the fluxes and concentrations are independent of each other. This means there are independent probability densities ρ_f and ρ_c containing the a priori information on the fluxes and concentrations respectively, so that for any $\tilde{f}$ and $\tilde{c}$

$$\rho(\tilde{f},\tilde{c}) \quad = \quad \rho_f(\tilde{f}) \cdot \rho_c(\tilde{c}) \ .$$

The state of information about the system from our model of the atmospheric transport also defines a probability distribution in the joint space $\mathbb{R}^{n_c+n_f}$. We denote it by $\theta(\tilde{f},\tilde{c})$. Combining the a priori information to our model of the atmospheric transport yields the a posteriori probability density $\nu(\tilde{f},\tilde{c})$. *Tarantola* derives the appropriate way of combining the information contained in these two probability densities:

$$\nu(\tilde{f},\tilde{c}) \quad = \quad \frac{\rho(\tilde{f},\tilde{c})\theta(\tilde{f},\tilde{c})}{\mu(\tilde{f},\tilde{c})},$$

where μ denotes the probability density characterizing the state of null information: μ is uniform, i.e. all pairs of fluxes and concentrations are equally likely. If the transport contains any information, fluxes and concentrations are no longer independent, so that the resulting probability density for the fluxes has to be computed by

$$\nu_f(\tilde{f}) \quad = \quad \int\limits_{\mathbb{R}^{n_c}} \nu(\tilde{f},\tilde{c}) d\tilde{c} \ .$$

The a priori probability density of the fluxes is assumed to be Gaussian with mean f and covariance C_f:

$$\rho_f(\tilde{f}) \quad \sim \quad e^{-1/2\left\langle (\tilde{f}-f),\, C_f^{-1}(\tilde{f}-f)\right\rangle} \quad .$$

Furthermore the model errors are assumed to be Gaussian with mean 0 and covariance C_M, and the uncertainties in the observed concentrations are assumed to be Gaussian with mean c_{obs} and covariance C_{obs}:

$$\rho_c(\tilde{c}) \quad \sim \quad e^{-1/2\left\langle (\tilde{c}-c_{obs}),\, C_{obs}^{-1}(\tilde{c}-c_{obs})\right\rangle} \quad .$$

In our case the model for the transport is linear. It is represented by the matrix M. Evaluation of the integral in Eq. (A.1) yields that the a posteriori probability density is Gaussian as well [*Tarantola*, 1987]:

$$\nu_f(\tilde{f}) \quad \sim \quad e^{-1/2\left\langle (f-\tilde{f}'),\, C_f'^{-1}(f-f')\right\rangle} \quad . \tag{A.1}$$

Thereby the covariance is

$$C_f' \quad = \quad (M^* C_c^{-1} M + C_f^{-1})^{-1} \tag{A.2}$$

and the mean

$$f' \quad = \quad f + C_f' M^* C_c^{-1}(c_{obs} - Mf) \quad , \tag{A.3}$$

where $C_c = C_M + C_{obs}$. Note that the covariances of model errors and the observational errors do not enter the inversion procedure independently, but exclusively in their sum. Note further that the posterior covariance matrix is determined by the transport matrix and the prior covariance, however, it is independent of the mean f of the a priori distribution. According to Eq. (A.1) f' is not only the mean but also the most likely point of ν_f, being the minimum of the exponent:

$$1/2\left\langle (f' - \tilde{f}),\, C_f'^{-1}(f' - \tilde{f})\right\rangle \quad .$$

Inserting Eq. (A.3) and Eq. (A.2) one can verify that f' minimizes the cost function

$$J(\tilde{f}) := 1/2\left(\left\langle (f - \tilde{f}),\, C_f^{-1}(f - \tilde{f})\right\rangle + \left\langle (c_{obs} - M\tilde{f}),\, C_c^{-1}(c_{obs} - M\tilde{f})\right\rangle\right) \quad . \tag{A.4}$$

f' is often denoted as the solution of the inverse problem. The covariance C_f' determines the uncertainty in f'. Defining the (pseudo-) inverse

$$M^{-1} := C_f' M^* C_c^{-1} \tag{A.5}$$

Eq. (A.3) can be written in the form

$$f' - f \quad = \quad M^{-1}(c_{obs} - Mf) \quad : \tag{A.6}$$

M^{-1} transforms the misfit between observations c_{obs} and the modeled concentration $c_{mod} = Mf$ resulting from the a priori fluxes to a correction of the a priori fluxes.

In this framework, the essential point is the existance of the posterior covariance matrix. Eq. (A.2) formalizes how the a priori information on the fluxes regularizes the inverse problem:

For singular $M^* C_c^{-1} M$, addition of C_f^{-1} allows to define an inverse. If $M^* C_c^{-1} M$ is non singular, addition of C_f^{-1} makes the inversion more stable. (Stability can be quantified by any norm in the space of $n_f \times n_f$ matrices. A stable inversion is then characterized by a high norm of $M^* C_c^{-1} M + C_f^{-1}$ and, consequently, by a low norm of $C_f^{'}$.)

A concept characterizing the nature of an inverse problem is the model resolution. The model resolution quantifies the ability of the observations to constrain the posterior estimate of the mean f by Eq. (A.6). If f_0 is a known flux field, then $c_{obs} := M f_0$ would be the corresponding observation provided that the model was perfect. Inserting c_{obs} and an a priori estimate f together with their covariances into Eq. (A.6) yields

$$f^{'} - f \quad = \quad M^{-1}(c_{obs} - Mf) \quad = \quad M^{-1}M(f_0 - f) \ . \tag{A.7}$$

The matrix $R_m := M^{-1}M$ is denoted as model resolution matrix. The interpretation of Eq. (A.7) is the following: For each component the correction suggested by the inversion procedure Eq. (A.6) is a weitghted sum of the correction that would be necessary to recover f_0. Thereby the weights form the model resolution matrix. If R_m equals the identity matrix, the model resolution is perfect: By the inversion procedure the components of f_0 can be recovered independently of each other. Using the definitions of M^{-1} (Eq. (A.5)) and $C_f^{'}$ (Eq. (A.2)), the model resolution matrix can be expressed in terms of the product of posterior and prior covariance matrices

$$R_m = C_f^{'} M^* C_c^{-1} M = C_f^{'}(M^* C_c^{-1} M + C_f^{-1} - C_f^{-1}) = 1 - C_f^{'} C_f^{-1} \ . \tag{A.8}$$

The higher the reduction of uncertainty, the closer the model resolution is to zero.

References

Andres, R. J., G. Marland, T. Boden, and S. Bischoff, Carbon dioxide emissions from fossil fuel consumption and cement manufacture 1751 to 1991 and an estimate for their isotopic composition and latitudinal distribution, in *The Carbon Cycle*, edited by T. M. L. Wigley, and D. Schimel, Cambridge University Press, 1997.

Broecker, W., and T.-H. Peng, *Greenhouse Puzzles*, Eldigio Press, Lamont-Doherty Earth Observatory, Columbia University, Palisades, New York, 1993.

Brown, M., Deduction of emissions of source gases using an objective inversion algorithm and a chemical tranport model, *J.Geophys.Res.*, (D7), 12639–12660, 1993.

Brown, M., The singular value decomposition method applied to the deduction of the emissions and the isotopic composition of atmospheric methane, *J.Geophys.Res.*, (100), 425–446, 1995.

Ciais, P., et al., Partitioning of ocean and land uptake of CO_2 as inferred by $\delta^{13}C$ measurements from the NOAA climate monitoring and diagnostics laboratory global air sampling network, *J.Geophys.Res.*, (100), 5051–5070, 1995.

Ciais, P., et al., A three dimensional synthesis study of $\delta^{18}O$ in atmospheric CO_2 , Part II: Surface fluxes, *J.Geophys.Res.*, (102), 5857–5872, 1997.

Ciais, P., et al., A three dimensional synthesis study of $\delta^{18}O$ in atmospheric CO_2 , Part II: Simulations with the TM2 transport model, *J.Geophys.Res.*, submitted.

Corliss, G. F., and L. B. Rall, An introduction to automatic differentiation, in *Computational Differentiation: Techniques, and Tools*, edited by M. Berz, C. Bischof, G. Corliss, and A. Griewank, pp. 1–18, SIAM, Philadelphia, Penn., 1996.

Courtier, P., and O. Talagrand, Variational assimilation of meteorological observations with the adjoint equation – Part II. Numerical results, *Q. J. R. Meteorol. Soc.*, *113*, 1329 – 1347, 1987.

Denning, A. S., Investigations of the transport, sources, and sinks of atmospheric CO_2 using a general circulation model, Ph.D. thesis, Colorado State University, Fort Collins, Colorado, 1995.

Denning, A. S., I. Y. Fung, and D. Randall, Latitudinal gradient of CO_2 due to seasonal exchange with biota, *Nature*, (376), 240–243, 1995.

Enting, I. G., Inverse problems in atmospheric constituent studies. III: Estimating errors in surface sources, *Inverse Problems*, (9), 649–665, 1993.

Enting, I. G., and J. V. Mansbridge, Seasonal sources and sinks of atmospheric CO_2: Direct inversion of filtered data, *Tellus*, (41B), 111–126, 1989.

Enting, I. G., T. M. L. Wigley, and M. Heimann, Future emissions and concentrations of carbon dioxide: key ocean/atmosphere/land analyses, Technical Paper 31, CSIRO Division of Atmosheric Reseach, Aspendale, Victoria, Australia, 1994.

Enting, I. G., C. M. Trudinger, and R. J. Francey, A synthesis inversion of the concentration and $\delta^{13}C$ of atmospheric CO_2, *Tellus*, (47B), 35–52, 1995.

Giering, R., *Tangent linear and Adjoint Model Compiler, Users Manual*, MPI, Bundesstr. 55, 20251 Hamburg, Germany, 1996.

Giering, R., and T. Kaminski, Recipes for Adjoint Code Construction, *ACM Transactions on Mathematical Software*, in press.

Gill, P. E., W. Murray, and M. H. Wright, *Practical Optimization*, Academic Press, New York, 1981.

Globalview–CO2, *Cooperative Atmospheric Data Integration Project - Carbon Dioxide , CD-ROM*, NOAA/CMDL, Boulder, Colorado, 1996.

Griewank, A., On automatic differentiation, in *Mathematical Programming: Recent Developments and Applications*, edited by M. Iri, and K. Tanabe, pp. 83 – 108, Kluwer Academic Publishers, 1989.

Griewank, A., Achieving logarithmic growth of temporal and spatial complexity in reverse automatic differentiation, Preprint MCS–P228–0491, Mathematics and Computer Science Division, Argonne National Laboratory, 9700 S. Cass Ave., Argonne, IL 60439–4801, 1991.

Haas-Laursen, D., Regional estimates of carbon dioxide fluxes deduced with an inverse method, Ph.D. thesis, Georgia Institute of Technology, 1997.

Hartley, D., and R. Prinn, Feasibility of determining surface emissions of trace gases using an inverse method in a three-dimensional chemical transport model, *J. Geophys. Res.*, *98*, 5183–5197, 1993.

Heimann, M., The Global Carbon Cycle in the Climate System, in *Modelling Oceanic Climate Interactions*, edited by J. Willebrand, and D. E. T. Anderson, vol. I11 of *NATO ASI Series*, pp. 299–336, Springer -Verlag, Berlin-Heidelberg, 1993.

Heimann, M., The global atmospheric tracer model TM2, Technical Report No. 10, Max-Planck-Institut für Meteorologie, Hamburg, Germany, 1995.

Heimann, M., et al., Evaluation of terrestrial carbon cycle models through simulations of the seasonal cycle of atmospheric CO_2: First results of a model intercomparison study, *Global Biogeochemical Cycles*, in press.

Heimann, M., and C. D. Keeling, A Three Dimensional Model of Atmospheric CO_2 Transport Based on Observed Winds: 2. Model description and simulated tracer experiments, in *Aspects of Climate Variability in the Pacific and the Western Americas*, edited by D. H. Peterson, American Geophysical Union, Washington,D.C., 1989.

Heimann, M., and P. Monfray, Spatial and Temporal Variations of the Gas Exchange Coefficient for CO_2 : Data Analysis and Global Validation, Tech. Rep. No.31, Max-Planck-Institut für Meteorologie, Hamburg, 1989.

Heimann, M., C. D. Keeling, and I. Y. Fung, Simulating the atmospheric carbon dioxide distribution with a three-dimensional tracer model, in *The Changing Carbon Cycle; A Global Analysis*, edited by J. Trabalka, and D. Reichle, Springer, 1986.

Hein, R., and M. Heimann, Determination of global scale emissions of atmospheric methane using an inverse modelling method, in *Non-CO_2 Greenhouse Gases*, edited by J. van Ham et al., Kluver, 1994.

Hein, R., P. Crutzen, and M. Heimann, An inverse modeling approach to investigate the global atmospheric methane cycle, *Global Biogeochemical Cycles*, *11*, 43–76, 1996.

Houghton, J. T., L. M. Filho, J. Bruce, H. Lee, B. A. Callander, E. Haites, N. Harris, and K. Maskell, eds., *Climate Change 1995 - The Science of Climate Change: Contribution of Working Group I to the Second Assessment Report of the Intergovernmental Panel on Climate Change*, Cambridge University Press, Cambridge, UK, 1995a.

Houghton, J. T., L. M. Filho, B. Callander, N. Harris, A. Dattenberg, and K. Maskell, eds., *Climate Change 1994 - Radiative Forcing of Climate Change*, Cambridge University Press, Cambridge, UK, 1995b.

Houghton, R. A., et al., The flux of carbon from terrestrial ecosystems to the atmosphere in 1980 due to changes in land use: Geographic distribution of the global flux, *Tellus*, *39B*, 122–139, 1987.

Iri, M., History of automatic differentiation and error estimation, in *Automatic Differentiation of Algorithms: Theory, Implementation, and Application*, edited by A. Griewank, and G. F. Corliss, SIAM, Philadelphia, PA, 1991.

Jacob, D. J., M. J. Prather, S. C. Wofsy, and M. B. McElroy, Atmospheric Distribution of ^{85}Kr Simulated With a General Circulation Model, *J.Geophys.Res.*, pp. 6614–6626, 1987.

Juedes, D., A taxonomy of automatic differentiation tools, in *Automatic Differentiation of Algorithms: Theory, Implementation, and Application*, edited by A. Griewank, and G. F. Corliss, SIAM, Philadelphia, PA, 1991.

Kaminski, T., R. Giering, and M. Heimann, Sensitivity of the seasonal cycle of CO_2 at remote monitoring stations with respect to seasonal surface exchange fluxes determined with the adjoint of an atmospheric transport model, *Physics and Chemistry of the Earth*, *21*(5–6), 457–462, 1996.

Kaminski, T., M. Heimann, and R. Giering, A matrix representation for an atmospheric transport model computed by its adjoint, in *Proceedings of the 22nd NATO/CCMS International Technical Meeting on Air Pollution Modelling and its Application*, Plenum Press, in press.

Keeling, C. D., R. B. Bacastow, A. F. Carter, S. C. Piper, T. P. Whorf, M. Heimann, W. G. Mook, and H. Roeloffzen, A Three Dimensional Model of Atmospheric CO_2 Transport Based on Observed Winds: 1. Analysis of Observational Data, in *Aspects of Climate Variability in the Pacific and the Western Americas*, edited by D. H. Peterson, pp. 165–236, American Geophysical Union, Washington,D.C., 1989a.

Keeling, C. D., M. Heimann, and S. C. Piper, A Three Dimensional Model of Atmospheric CO_2 Transport Based on Observed Winds: 4. Analysis of the Mean Annual Gradients of CO_2, in *Aspects of Climate Variability in the Pacific and the Western Americas*, edited by D. H. Peterson, pp. 305–363, American Geophysical Union, Washington,D.C., 1989b.

Keeling, R. F., S. C. Piper, and M. Heimann, Global and hemispheric CO_2 sinks deduced from changes in atmospheric O_2 concentration, *Nature*, (381), 218–221, 1996.

Knorr, W., Satellitengestützte Fernerkundung und Modellierung des Globalen CO_2 -Austauschs der Landvegetation: Eine Synthese, Ph.D. thesis, Max-Planck-Institut für Meteorologie, Hamburg, Germany, 1997.

Knorr, W., and M. Heimann, Impact of drought stress and other factors on seasonal land biosphere CO_2 exchange studied through an atmospheric tracer transport model, *Tellus*, (47B), 471–489, 1995.

Kurz, K. D., Zur Saisonalen Variation des ozeanischen Kohlendioxidpartialdrucks, Ph.D. thesis, Max-Planck-Institut für Meteorologie, Hamburg, Germany, 1993.

Law, R., and I. Simmonds, The sensitivity of deduced CO_2 sources and sinks to variations in transport and imposed surface concentrations, *Tellus*, (48B), 613–625, 1996.

Law, R. M., et al., Variations in modelled atmospheric transport of carbon dioxide and the consequences for CO_2 inversions, *Global Biogeochemical Cycles*, (10), 783–796, 1996.

Liss, P. S., and L. Merlivat, Air–Sea Gas Exchange Rates: Introduction and Synthesis, in *The Role of Air–Sea Exchange in Geochemical Cycling*, edited by P. Buat-Ménard, vol. 185, pp. 113–127, D. Reidel Publishing Company, Hingham, 1986.

Louis, J. F., A parametric model of vertical eddy fluxes in the atmosphere, *Boundary Layer Meteorology*, (17), 187–202, 1979.

Maier-Reimer, E., Geochemical cycles in an ocean general circulation model. Preindustrial Tracer Distributions, *Global Biogeochemical Cycles*, (7), 645–677, 1993.

Marchuk, G. I., *Adjoint Equations and Analysis of Complex systems*, Kluwer Academic Publishers, Dordrecht, The Netherlands, 1995.

Masarie, K. A., and P. P. Tans, Extension and integration of atmospheric carbon dioxide data into a globally consistent measurement record, *J.Geophys.Res.*, *100*(D6), 11,593–11,610, 1995.

Menke, W., *Geophysical Data Analysis*, Academic Press, San Diego, CA, 1989.

NAGLIB, *Fortran Library Manual - Mark 13*, Numerical Algorithms Group, 1987.

Pearman, G., and P. Hyson, Activities of the global biosphere as reflected in atmospheric CO_2 records, *J.Geophys.Res.*, (C8), 4468–4474, 1980.

Press, W. H., B. P. Flannery, S. A. Teukolsky, and W. T. Vetterling, *Numerical Recipes: The Art of Scientific Computing*, Cambridge University Press, New York, 1986.

Ramonet, M., and P. Monfray, CO_2 baseline concept in 3-d atmospheric transport models, *Tellus*, (48B), 502–520, 1996.

Rayner, P. J., and R. M. Law, A comparison of modelled responses to presrcibed CO_2 sources, Technical Paper 36, CSIRO Divison of Atmospheric Research, Aspendale, Victoria, Australia, 1995.

Rayner, P. J., I. G. Enting, and C. M. Trudinger, Optimizing the CO_2 observing network for constraining sources and sinks, *Tellus*, (48B), 433–444, 1996.

Rehfeld, S., Deposition Radioaktiver Tracer in einem Transportmodell der Atmosphäre, Ph.D. thesis, Max-Planck-Institut für Meteorologie, Hamburg, Germany, 1994.

Rostaing, N., S. Dalmas, and A. Galligo, Automatic differentiation in Odyssée, *Tellus*, *45A*, 558–568, 1993.

Russel, G. L., and J. A. Lerner, A new finite-differencing scheme for the tracer transport equation, *J. Appl. Met.*, pp. 1483–1498, 1981.

Shah, P., Application of adjoint equations to estimation of parameters in distributed dynamic systems, in *Automatic Differentiation of Algorithms: Theory, Implementation, and Application*, edited by A. Griewank, and G. F. Corliss, SIAM, Philadelphia, PA, 1991.

Six, K. D., and E. Maier-Reimer, Effects of plankton dynamics on seasonal carbon fluxes in an ocean general circulation model, *Global Biogeochemical Cycles*, *10*(4), 559–583, 1996.

Stephens, B., R. F. Keeling, M. Heimann, K. D. Six, R. Murane, and K. Caldera, Testing global ocean carbon models using measurements of atmospheric O_2 and CO_2 concentration, *Global Biogeochemical Cycles*, submitted.

Talagrand, O., The use of adjoint equations in numerical modelling of the atmospheric circulation, in *Automatic Differentiation of Algorithms: Theory, Implementation, and Application*, edited by A. Griewank, and G. F. Corliss, SIAM, Philadelphia, PA, 1991.

Talagrand, O., and P. Courtier, Variational assimilation of meteorological observations with the adjoint vorticity equation – Part I. Theory, *Q. J. R. Meteorol. Soc.*, *113*, 1311 – 1328, 1987.

Tans, P. P., I. Y. Fung, and T. Takahashi, Observational constraints on the global atmospheric CO_2 budged, *Science*, (247), 1431–1438, 1990.

Tarantola, A., *Inverse Problem Theory - Methods for Data Fitting and Model Parameter Estimation*, Elsevier, Amsterdam, 1987.

Taylor, A. H., A. J. Watson, M. Ainsworth, J. E. Robertson, and D. R. Turner, A modelling investigation of the role of phytoplankton in the balance of carbon at the surface of the North Atlantic, *Global Biogeochemical Cycles*, *5*(2), 151–171, 1991.

Thacker, W. C., Automatic differentiation from an oceanographer's perspective, in *Automatic Differentiation of Algorithms: Theory, Implementation, and Application*, edited by A. Griewank, and G. F. Corliss, SIAM, Philadelphia, PA, 1991.

Thacker, W. C., and R. B. Long, Fitting dynamics to data, *J. Geophys. Res.*, *93*(C2), 1227 – 1240, 1988.

Tiedtke, M., A comprehensive mass flux scheme for cumulus parameterization in large-scale models, *Mon. Weath. Rev*, (117), 1779–1800, 1989.

Trampert, J., and R. Snieder, Model estimations biased by truncated expansions: Possible artifacts in seismic tomography, *Science*, *271*, 1257–1260, 1996.

Watson, R., M. Zinyowera, and R. Moss, eds., *Climate Change 1995 - Impacts, Adaptations and Mitigation of Climate Change: Scientific-Technical Analyses: Contribution of Working Group II to the Second Assessment Report of the Intergovernmental Panel on Climate Change*, Cambridge University Press, Cambridge, UK, 1995.

Weber, C., Zur Dynamik des interhemisphärischen CO_2-Transports im Ozean, Master's thesis, Max-Planck-Institut für Meteorologie, Hamburg, Germany, 1996.